

**UNDERSTANDING AND TARGETING ETV1 IN SARCOMA
PATHOGENESIS**

**by
Leili Ran**

A Dissertation

Presented to the Faculty of the Louis V. Gerstner, Jr.
Graduate School of Biomedical Sciences,
Memorial Sloan-Kettering Cancer Center
in Partial Fulfillment of the Requirements for the Degree of
Doctor of Philosophy

New York, NY

April 2016

Ping Chi MD/PhD

Dissertation Mentor

Date

Copyright by Leili Ran 2016

DEDICATION

This dissertation is dedicated for my parents, Huarong Ran and Xiaorong He.
Of all these years and all those decisions I have made, they are always there
for me, love me and support me.

ABSTRACT

ETV1, an *ETS* family transcription factor, has been implicated in various cancer types, including Ewing Sarcoma, melanoma and prostate cancer. I have focused my studies on the oncogenic function of *ETV1* in gastrointestinal stromal tumor (GIST) and malignant peripheral nerve sheath tumor (MPNST), both are sarcomas with unique molecular features.

The majority of GIST is molecularly characterized by *KIT/PDGFR α /BRAF* activating mutations and originating from the precursor interstitial cells of Cajal (ICCs). MPNST originates from cellular compartments of the peripheral nerves, and we and others have molecularly characterized them as losing three central tumor suppressor pathways: including *NF1*, *CDKN2A* and PRC2 (*EED* or *SUZ12*). Despite the differences in cell of origin and molecular features, both tumor types activate the MAP kinase signaling pathway; both tumor types are dependent on *ETV1* for growth, survival and tumorigenesis. Using *in vitro* human cancer derived cell line models, xenograft and genetically engineered mouse models, we have established the functional requirement of *ETV1* in both GIST and MPNST pathogenesis, as well as establishing novel models of *BRAF*-mutant GIST tumors in the *ETV1* specific ICC-lineage. These studies have established the rationale of targeting *ETV1* in GIST and MPNST pathogenesis.

To therapeutically target *ETV1*, we have taken advantage of its protein stability regulation by MAP kinase signaling pathway. We identified a novel strategy of combined KIT and MAPK pathway inhibition that can lead to synergistic growth suppression of GIST cells and eradication of GIST tumorigenesis *in vivo*. These

studies have provided the scientific rational for the ongoing clinical trial of using the combined imatinib (KIT inhibitor) and MEK162 (a MEK inhibitor) in advanced GIST patients.

Collectively, our data have defined an important role of *ETV1* in GIST and MPNST tumorigenesis. We have further showed an effective combination therapy to target ETV1 protein stability in GISTs, which may provide important insights for other *ETV1*-driven cancer types.

ACKNOWLEDGEMENT

First, I would like to thank my mentor Dr. Ping Chi for bravely taking me as her first graduate student in the lab. None of the work in this dissertation would be possible without Dr. Ping Chi's guidance and support. Dr. Ping Chi has not only taught me how to conduct research, but more importantly how to be a good scientist. She is always supportive for my career and life, as friend and family. Dr. Ping Chi has been the role model for me in the past five years, and will continue to be my role model in the future.

I would like to thank my thesis committee members, Dr. Charles Sawyers and Dr. Ingo Mellinshoff, for providing me with reagents and useful suggestions on my projects. I would also like to thank Dr. Yu Chen for his mentorship and for patiently answering my numerous scientific questions.

I would like to thank all my lab members for helping out with my experiments whenever I have a question and sharing your joys with me during lunch breaks. In particular, I would like to thank Devan Murphy and Jessica Sher for helping with my mouse experiments, Dong Gao for his suggestions with experimental design, Amanda Moore for keeping companion with me during weekends and sharing my tears during frustrating times, Shangqian Wang for always picking up bacteria cultures and virus infection plates for me.

I would like to thank everyone in the Gerstner Sloan Kettering graduate school. Specifically, I would like to thank our dean Dr. Kenneth Marias for always supporting every student, Linda Burnley for continuously improving the program, Iwona

Abramek for helping with my dissertation and classes, Maria Torres for always know my answers, Ivan Gerena for the candies. Without their efforts, we would not be able to have such a fantastic program.

I would like to thank Dr. Sarat Chandarlapaty for his supportive words and smiles. I would like to thank two friends that I am lucky to have in New York, Marie Will and Weiyi Toy. Thank you for sharing important moments and supporting me.

I would like to thank a very important person in my life, Zhen Cao. Thank you for helping me with my experiments, for guiding me when I am lost, for making me laugh and for loving me. I am grateful to my two cute cats, Boo Boo and Lulu. Thanks for the cuteness and your magic healing purrs.

At the end, I would like to thank my parents, Huarong Ran and Xiaorong He. It is their love that makes me strong.

TABLE OF CONTENTS

LIST OF TABLES	x
LIST OF FIGURES	xi
LIST OF ABBREVIATIONS	xiv
CHAPTER ONE	1
INTRODUCTION	1
<i>Malignant Peripheral Nerve Sheath tumor (MPNST)</i>	1
<i>Gastrointestinal stromal tumor (GIST)</i>	16
<i>ETS variant 1 (ETV1)</i>	35
THESIS AIMS	39
CHAPTER TWO	41
MATERIAL AND METHODS	41
<i>Generation of Compound Genetically Engineered Mouse Models (GEM)</i>	41
<i>Mouse Procedures</i>	41
<i>Human Tumor Tissue Collection</i>	43
<i>Sample Preparation and Quality Control for Genomic Analysis</i>	44
<i>RNA Sequencing and Analysis</i>	44
<i>DNA Sequencing and Analysis</i>	45
<i>SNP6.0 Arrays and Analysis</i>	46
<i>Immunoblotting, Immunofluorescence, Immunohistochemistry and Histology</i>	51
<i>Stable Gene Expression</i>	51
<i>RNA Isolation and qRT-PCR</i>	52
<i>Chromatin Immunoprecipitation (ChIP) and Sequencing</i>	53
<i>Cell Viability</i>	56
<i>Lentiviral Knockdown and CRISPR/Cas9 Mediated Knockout</i>	56
<i>Statistics</i>	57
CHAPTER THREE	59
AN ONCOGENIC ROLE FOR ETV1 IN MALIGNANT PERIPHERAL NERVE SHEATH TUMOR	59

<i>Introduction</i>	59
<i>Results</i>	60
<i>Discussion</i>	71
PRC2 IS RECURRENTLY INACTIVATED THROUGH EED OR SUZ12 LOSS IN MALIGNANT PERIPHERAL NERVE SHEATH TUMORS	74
<i>Introduction</i>	74
<i>Results</i>	74
<i>Discussion</i>	92
CHAPTER FIVE	94
A MOUSE MODEL OF GASTROINTESTINAL STROMAL TUMOR WITH <i>BRAF</i>^{V600E} MUTATION	94
<i>Introduction</i>	94
<i>Results</i>	97
<i>Discussion</i>	106
CHAPTER SIX	109
COMBINED INHIBITION OF MAP KINASE AND KIT SIGNALING SYNERGISTICALLY DESTABILIZES ETV1 AND SUPPRESSES GIST TUMOR GROWTH	109
<i>Introduction</i>	109
<i>Results</i>	112
<i>Discussion</i>	136
CHAPTER SEVEN	138
DISCUSSION AND FUTURE DIRECTIONS	138
<i>Role of ETV1 in MPNST pathogenesis</i>	138
<i>Role of ETV1 in GIST</i>	142
BIBLIOGRAPHY	145

LIST OF TABLES

Table 2.1 Whole Exome sequencing metrics	47
Table 2.2 Antibodies and dilutions for IB, IF, IHC and CHIP	50
Table 2.3 Primer sets for qRT-PCR	54
Table 2.4 Primer sets for CHIP qRT-PCR validation	55
Table 2.5 CRISPR target guides sequences	58

LIST OF FIGURES

Figure 1.1 Histology of conventional MPNSTs and differentiated MPNSTs	4
Figure 1.2 Representation of NF1 interactions with the Ras and PI3K pathways	8
Figure 1.3 Diagram outlining the stages of Schwann cell development and the periods of Cre-mediated recombination in various neurofibroma models	14
Figure 1.4 Examples of gastrointestinal stromal tumor (GIST)	19
Figure 1.5 Molecular classifications of GISTs	21
Figure 1.6 <i>KIT</i> and <i>PDGFRA</i> mutations in GISTs	25
Figure 1.7 Oncogenic signaling pathways in GISTs	28
Figure 1.8 New therapies being tested for the treatment of GISTs Drug.....	34
Figure 1.9 Model of the role of <i>ETV1</i> in ICC maintenance and GIST oncogenesis.....	38
Figure 3.1 <i>ETV1</i> is highly expressed in MPNST	62
Figure 3.2 <i>ETV1</i> is required for MPNST cell survival	63
Figure 3.3 <i>ETV1</i> suppression does not affect cell cycle in MPNST724 cells.....	64
Figure 3.4 Doxycycline-inducible shRNA can efficient knockdown <i>ETV1</i>	66
Figure 3.5 <i>ETV1</i> depletion suppresses MPNST tumor initiation and maintenance	67
Figure 3.6 MPNST tumors growing with <i>ETV1</i> shRNA escaped <i>ETV1</i> knockdown	68
Figure 3.7 <i>ETV1</i> cooperates with <i>Nf1</i> loss to drive tumorigenesis in NIH3T3	70
Figure 3.8 <i>ETV1</i> regulates important cellular context for MPNST tumorigenesis	72
Figure 4.1 The most frequent genetic alterations in MPNST (NF1 associated, sporadic, radiotherapy associated and epithelioid) and neurofibroma	76
Figure 4.2 Summary of copy number variation by SNP6.0 array of MPNSTs	77
Figure 4.3 <i>EED</i> alterations in MPNST	78
Figure 4.4 <i>SUZ12</i> structural variants in MPNST	79
Figure 4.5 MPNSTs with PRC2 loss exhibit distinct gene expression pattern from MPNSTs with wild-type PRC2, signifying activation of developmentally suppressed pathways	82
Figure 4.6 H3K27me3 immunohistochemistry correlates with PRC2 genetic status, and H3K27me3 loss characterizes progression from neurofibroma to MPNST	85
Figure 4.7 Coexistent subpopulations as calculated by EXPANDS analysis of sample 16T exome sequencing data	87
Figure 4.8 PRC2 loss promotes cell proliferation and growth in MPNST with PRC2 loss	89

Figure 4.9 RNA-seq profiles of MPNST cell lines ST88-14 and MPNST724 at the <i>SUZ12</i> locus showing the absence of <i>SUZ12</i> transcript in ST88-14 cells	90
Figure 4.10 Western blot of MPNST cells	91
Figure 5.4 Combination of homozygous <i>BRAF^{V600E}</i> and <i>p53</i> loss induced phenotypes in stomach, cecum and small intestine	95
Figure 5.1 <i>Etv1</i> is expressed in ICC-IMs and ICC-MYs that are susceptible to GIST tumorigenesis	99
Figure 5.2 <i>BRAF^{V600E}</i> activation induces a minimal hyperplasia phenotype in mouse large intestine	100
Figure 5.3 <i>BRAF^{V600E}</i> activation induced phenotypes in stomach, cecum and small intestine	101
Figure 5.5 <i>BRAF^{V600E}</i> robustly cooperates with <i>p53</i> loss in GIST tumorigenesis.....	104
Figure 5.6 Combination of heterozygous <i>BRAF^{V600E}</i> and <i>p53</i> loss induced phenotypes in stomach, cecum and small intestine	105
Figure 5.7 Dabrafenib inhibits GIST tumor growth in BRAF mutated GISTs of <i>Etv1^{CreERT2}; BRAF^{CA/+}; p53^{fl/fl}</i> mouse	107
Figure 6.1 <i>ETV1</i> is required for GIST tumor initiation <i>in vivo</i>	113
Figure 6.2 <i>Etv1</i> is required for intramuscular and myenteric ICC development	114
Figure 6.3 <i>Etv1</i> ablation with tamoxifen decreases <i>Etv1</i> and <i>Kit</i> expression in <i>Kit^{Δ558/+}; Etv1^{flox/flox}; Rosa26^{CreERT2/CreERT2}</i> mice	116
Figure 6.4 <i>ETV1</i> is required for GIST tumor proliferation <i>in vivo</i>	117
Figure 6.5 <i>ETV1</i> positively regulates <i>Kit</i> expression in murine GISTs	119
Figure 6.6 <i>Etv1</i> positively regulates <i>Kit</i> expression in murine stomach	120
Figure 6.7 <i>ETV1</i> positively regulates <i>KIT</i> expression through direct binding to <i>KIT</i> enhancers in human GIST cells and forms a positive feedback circuit in GIST oncogenesis	123
Figure 6.8 <i>ETV1</i> regulates <i>KIT</i> expression in GIST48 cells	124
Figure 6.9 Combined inhibition of MAP kinase and KIT signaling destabilizes ETV1 protein and results in enhanced growth suppression of human GIST cells	127
Figure 6.10 MAP kinase pathway inhibition decreases <i>ETV1</i> target gene expression	128
Figure 6.11 Combined inhibition of the MAP kinase and KIT signaling synergistically suppresses tumor growth in <i>in vivo</i> GIST xenograft mouse models	131
Figure 6.12 Dual lineage inhibition inhibits tumor initiation <i>in vivo</i>	132

Figure 6.13 Combined inhibition of MAP kinase and KIT signaling synergistically suppresses tumor growth in genetically engineered GIST mouse model135

Figure 7.1 Schematic model of ETV1-mutatnt KIT feed forward circuit in GIST oncogenesis....
144

LIST OF ABBREVIATIONS

- BWA:** Burrows-Wheeler aligner
- ChIP:** chromatin immunoprecipitation
- CML:** chronic myelogenous leukaemia
- CSF1R:** colony stimulating factor 1 receptor
- CSRD:** cysteine/serine-rich domain
- ES:** embryonic stem
- ETS:** erythroblast transformation-specific
- EYFP:** enhanced yellow fluorescent protein
- FLT3:** fms related tyrosine kinase 3
- GATK:** genome analysis toolkit
- GIST:** gastrointestinal stromal tumor
- GI tract:** gastrointestinal tract
- GSEA:** gene set enrichment analysis
- H3K27me3:** tri-methylation of Lys 27 of histone H3
- ICC:** interstitial cell of Cajal
- ICC-MY:** myenteric ICC
- ICC-IM:** intramuscular ICC
- IHC:** immunohistochemical
- IRB:** institutional review board
- KITLG:** KIT ligand
- LOH:** loss of heterozygosity
- MPNST:** malignant peripheral nerve sheath tumor
- MRI:** magnetic resonance imaging
- NF1:** neurofibromatosis type I and neurofibromin I

NLS: nuclear localization sequence
OCT: optimal cutting temperature
PCA: principal component analysis
PDGFR: platelet derived growth factor
PEA3: polyomavirus enhancer activator 3
PH: pleckstrin homology
PNS: peripheral nervous system
PR: partial response
PRC1: polycomb repressive complex 1
PRC2: polycomb repressive complex 2
RB: retinoblastoma
SCF: stem cell factor
SH: src-homology-2
TBD: tubulin-binding domain

CHAPTER ONE

Introduction

Malignant Peripheral Nerve Sheath tumor (MPNST)

Definition and Characteristics

Malignant Peripheral Nerve Sheath tumors (MPNSTs), often associated with peripheral nerves, are very aggressive soft-tissue tumors that account for 3-10% of all soft tissue sarcomas (Vauthey, Woodruff et al. 1995, Lawrence, Brennan et al. 1998, Grobmyer, Reith et al. 2008). The incidence of MPNST is rather low with approximately 1 per 10⁶ people per year. (Kolberg, Holand et al. 2013) In most sporadic MPNSTs, there may be a female predominance while the overall female/male ratio is about 1:1. (Cashen, Parisien et al. 2004, Anghileri, Miceli et al. 2006) The most common age at diagnosis in MPNST patients is 20-50 years, even though MPNSTs have also been reported in newborns and infants. (Ellison, Corredor-Buchmann et al. 2005, Grobmyer, Reith et al. 2008) About 10% of MPNST patients are under 20 years old (Grobmyer, Reith et al. 2008). Patients with MPNSTs commonly present with an enlarged mass, pain and neuropathic symptoms such as paraesthesia or motor weakness. Tumors arise most frequently in major nerves of the extremities, trunk, and head and neck. (Thway and Fisher 2014)

There are three subtypes of MPNSTs: neurofibromatosis type I (NF1)-associated (~50%), sporadic (~40%), and radiation-induced (~10%). NF1 is the most common and important known risk factor for MPNST. (Ducatman, Scheithauer et al. 1986) Most NF1 patients are presented with dermal neurofibromas, which rarely

undergo malignant transformation. In contrast, plexiform neurofibroma patients with NF1 have a 10% lifetime risk of undergoing malignant transformation to MPNSTs.(McGaughran, Harris et al. 1999, Walker, Thompson et al. 2005, Theos and Korf 2006, Carroll and Ratner 2008) Clinical studies of MPNST and NF1 indicated that the mean age for NF1-associated MPNST patients is younger (28.7 years old) than sporadic MPNST patients (34.0 years old). The five-year survival of NF1 patients with MPNST is 16%, compared with 53% for non-NF1 patients. (Ducatman, Scheithauer et al. 1986) NF1-associated MPNSTs tend to be large and high grade. These survival differences diminished when NF1-associated MPNSTs and sporadic MPNSTs were compared and adjusted for known prognostic factors such as size and locations in a large surgical series(Zou, Smith et al. 2009). Currently, radical surgery resection remains the primary and only curative options for all MPNSTs. However, surgical resection is frequently challenging because of the location of the tumor and the difficulty of achieving adequate negative surgical margins without significant compromise of function. MPNSTs have a high propensity to metastasize to soft tissue, bone, liver, lungs, etc. They are also known to have primary resistance to standard systemic chemotherapy and radiotherapy. Therefore, the prognosis of MPNSTs is poor with a 5-year survival rate of 30-60% and local recurrence rate of 22%.(Evans, Baser et al. 2002, Grobmyer, Reith et al. 2008, Stucky, Johnson et al. 2012, Brennan, Antonescu et al. 2013) The poor outcome of MPNST becomes a powerful impetus for efforts to understand the cell of origin and mechanism of pathogenesis of MPNSTs and to identify novel therapeutic targets in this deadly disease.

The diagnosis of MPNST has also remained challenging due to diversity of tumor morphology and lack of reliable immunohistochemical and molecular biomarkers. Histologically, MPNST shows high-grade spindle cell lesion pattern in inter-

secting fascicles, geographic regions of necrosis and wavy hyperchromatic nuclei (**Figure 1.1**). (Guo, Liu et al. 2012) However, in some cases, MPNST tumors can undergo multiple differentiations making it very difficult to discern MPNST with other tumor types. Unusual histologic features include radical arrangement of tumor cells, epithelioid differentiation with glandular structures and neuroendocrine differentiation. (Radner, Blumcke et al. 2002, Guo, Liu et al. 2012, Brennan, Antonescu et al. 2013) In addition, lack of specific immunohistochemical and molecular biomarker make it more difficult for accurate diagnosis of MPNST, especially non-NF1 associated MPNST. S-100 protein, the most commonly used marker for nerve sheath tumor of various types, does not have a consistent immunoreactivity pattern in MPNSTs. (Grobmyer, Reith et al. 2008) Recent gene expression profiling and molecular genetic analysis of MPNSTs showed further insights in the molecular diagnosis of MPNST. Works by us in the chapter 4 of this thesis and two other groups showed the first that PRC2 complex components were lost in 70-80% of all MPNSTs. (De Raedt, Beert et al. 2014, Lee, Teckie et al. 2014, Zhang, Wang et al. 2014) These observations lead the potential use of H3K27me³ absence, the ultimate result for loss of PRC2 function, as a novel reliable biomarker for accurate diagnosis.

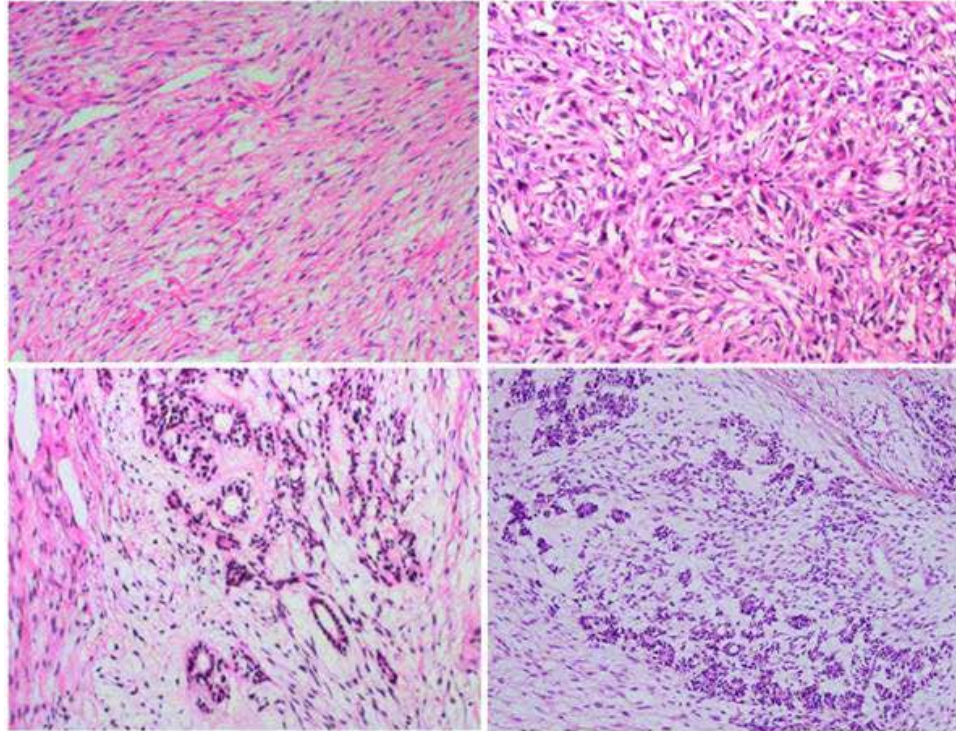


Figure 1.1 Histology of conventional MPNSTs and differentiated MPNSTs

In most regions, tumor cells are arranged in bundles with red-stained and scant cytoplasm, and spindle-shaped nuclei (top left); tumor cells grew in storiform as that in fibrous histiocytoma (top right); glandular differentiation (lower left) and neuroendocrine differentiation (lower right) (HEX100). Adapted from: Guo A, Liu A, Wei L, Song X. Malignant Peripheral Nerve Sheath Tumors: Differentiation Patterns and Immunohistochemical Features - A Mini-Review and Our New Findings. *J Cancer* 2012; 3:303-309. doi:10.7150/jca.4179. Available from <http://www.jcancer.org/v03p0303.htm>.

Neurofibromatosis Type I

Neurofibromatosis type I (Von Recklinghausen's disease, NF1) is one of the most common inherited tumor-predisposition syndromes and occurs in about 1 in every 2500 to 3000 newborns. (Gutmann 2001, Theos and Korf 2006, Le and Parada 2007) NF1 is an autosomal-dominant disorder with 100% penetrance. Despite the high penetrance, the manifestations of NF1 are quite diverse even within closely related family members. Abnormalities associated with NF1 include cafe-au-lait macules, lish nodules, bony hyperplasia, learning disabilities, cardiovascular abnormalities and a variety of tumor types such as optic glioma, astrocytomas, juvenile nonlymphocytic leukemia, pheochromocytomas and neurofibromas. (Walker, Thompson et al. 2005) As indicated by the name, nearly all NF1 patients will develop neurofibromas during their lifetime and the occurrence of multiple neurofibromas is considered to be a hallmark of NF1.

Neurofibromas, the most common type of neoplasm in NF1 patients, are benign tumors that arise within the peripheral nervous system (PNS). These lesions are composed of neoplastic Schwann cell and non-neoplastic stromal cells, including fibroblasts, mast cells and perineurial cells. Neurofibromas can be broadly subdivided into dermal/cutaneous neurofibromas and plexiform neurofibromas. (Carroll and Ratner 2008) Dermal neurofibromas originating from nerves in the skin often cause stinging, itching, pain and disfigurement. They typically arise during the second decade of life, are associated with the onset of puberty, and continue to increase in number and size throughout adulthood. However, these lesions virtually never undergo malignant transformation. Plexiform neurofibromas can grow from nerves in skin or from internal nerve bundles. They usually involve multiple nerve fascicles and can be very large. Plexiform neurofibromas

are detected at birth or seem to enlarge more rapidly during the first decade of life and are thought to be congenital defects. Plexiform neurofibromas are capable of undergoing malignant transformation, typically in the sciatic nerve, lumbosacral plexus, or brachial plexus. Despite the differences in the clinical behavior of dermal and plexiform neurofibroma, the cellular composition of all neurofibroma subtypes is identical. About 10% of NF1 patients will develop and eventually die of MPNST.(McGaughran, Harris et al. 1999, Walker, Thompson et al. 2005, Theos and Korf 2006, Carroll and Ratner 2008)

Molecular Abnormalities in NF1 and MPNST

Over the past two decades, little is known of the genetic alterations that mediate progression from neurofibroma to MPNST in NF1 patients or the molecular pathogenesis of sporadic and radiotherapy associated MPNST. Loss of *NF1* is the most common event for the pathogenesis of NF1 and MPNST. Other important genes or pathways that have been shown to be important to MPNST and NF1 include *CDKN2A*, *TP53*, *c-KIT*, *EGFR*, *PDGFR*, *SOX9*, *MET* and others. (Cairns, Polascik et al. 1995, Badache and De Vries 1998, Badache, Muja et al. 1998, Upadhyaya, Han et al. 2004, Watson, Perry et al. 2004, Dang, Nelson et al. 2005, Mantripragada, Spurlock et al. 2008, Mantripragada, Diaz de Stahl et al. 2009, Brennan, Antonescu et al. 2013) More recently, reports from chapter 5 of this thesis together with other two groups have identified the three critical pathways that is frequently loss in MPNST: *NF1* (72% of non-NF1 MPNST), *CDKN2A* (81% of all MPNST) and EED or SUZ12 in PRC2 complex (92% of sporadic, 70% of NF1-associated and 90% of radiotherapy-associated MPNSTs). (De Raedt, Beert et al. 2014, Lee, Teckie et al. 2014, Zhang, Wang et al. 2014) These three recent studies with large MPNST patient cohorts have provided important insights for accurate diagnosis of MPNST and understanding of MPNST

pathogenesis.

Neurofibromin 1 (NF1)

As seen in other tumor-predisposition syndromes, almost all NF1 patients carry constitutional mutations of the *NF1* tumor suppressor gene. The protein encoded by *NF1* gene, neurofibromin(also called neurofibromin 1 or NF1), is a large 220-250kDa protein containing three alternatively spliced exons(9a, 23a and 48a). These alternatively spliced exons have been implicated to reflect tissue-specific or differentiation-regulated RNA splicing events. The expression of isoform with exon 9a seems to be restricted to specific neuronal populations in the central nervous system, while ablation of exon 23a in mice leads to learning disabilities but no tumor development.(Gutmann, Zhang et al. 1999, Costa, Yang et al. 2001) Additional studies of these neurofibromin isoforms might shed light on the roles of Nf1 in specific tissues.

Despite the large size of NF1, little is known about its functions. Inspection of the amino acid sequence of neurofibromin revealed a RasGAP-related domain or GRD homologous to both a mammalian Ras GTPase activating protein (GAP) known as p120RasGAP and the *Saccharomyces Cerevesiae* Ras GAPs IRA1 and IRA2. This domain stimulates the intrinsic GTPase activity of the mammalian Ras homologue, accelerates the conversion of active GTP-bound Ras to inactive GDP-bound form, and thus inactivates Ras and reduces Ras-mediated growth signaling (**Figure 1.2**). NF1 has been shown to function as a GAP for Ras *in vitro* and *in vivo*.(Martin, Viskochil et al. 1990, Xu, Lin et al. 1990)

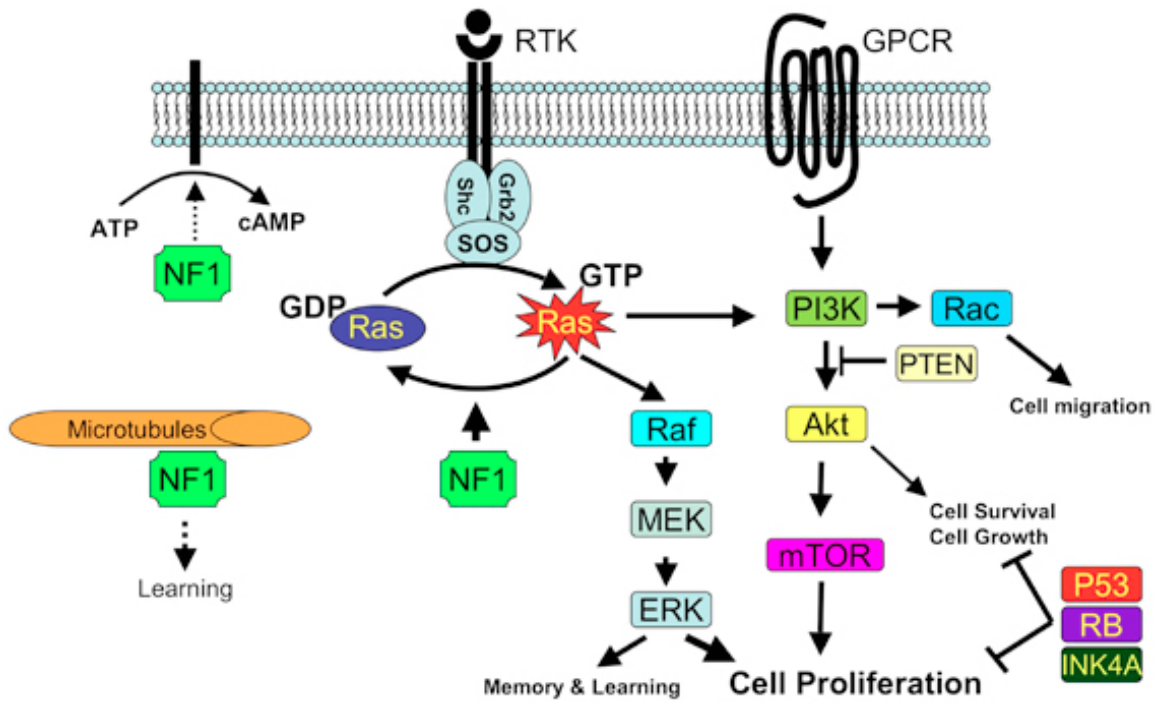


Figure 1.2 Representation of NF1 interactions with the Ras and PI3K pathways

NF1 constrains Ras activity in the normal cell. Therefore, loss of NF1 expression leads to elevated Ras activity, dysregulated cell growth and tumorigenesis. NF1 may also associate with microtubules and modulate the cAMP-PKA signaling pathway. Reprinted by permission from Macmillan Publishers Ltd: ONCOGENE, 26, 4609-16, Copyright 2007.

Furthermore, various *NF1*-deficient tumors including neurofibromas and NF1-associated MPNSTs exhibit elevated level of GTP bound Ras and reintroduction of this GRD into tumor cells decreases Ras activation and slows tumor cell proliferation.(Ballester, Marchuk et al. 1990, Martin, Viskochil et al. 1990, Xu, Oconnell et al. 1990, Guha, Lau et al. 1996) It has also been reported that the learning defects in *Nf1*^{+/-} mice can be rescued by genetic and pharmacologic manipulations that decrease Ras function. In fact, active Ras mutations are frequently seen in multiple human cancers by stimulating MAPK and/or PI3K pathways, which lead to escape of apoptosis.(Li, Cui et al. 2005, Ismat, Xu et al. 2006) Given these evidences, the *NF1* gene has been hypothesized to function as a tumor suppressor by inhibiting RAS activity as well as RAS-mediated signaling pathways.

Although most studies of NF1 function have focused on its GRD domain, there are increasing evidences indicating that neurofibromin may be involved in other cellular processes giving that mice expressing NF1 GRD only partially rescued the phenotypes seen in *Nf1*^{-/-} mice.(Ismat, Xu et al. 2006) In addition, multiple mutations outside of GRD have also been identified in NF1 patients.(Kluwe, Friedrich et al. 2003, Lee, Teckie et al. 2014) It has been suggested that several other domains exist within neurofibromin, including a tubulin-binding domain (TBD), a cysteine/serine-rich domain (CSRD), a Sec14-homology domain (Sec14), a pleckstrin homology domain (PH) and a nuclear localization sequence (NLS). (Bollag, McCormick et al. 1993, Izawa, Tamaki et al. 1996, Aravind, Neuwald et al. 1999, D'Angelo, Welte et al. 2006) However, the biological functions of these domains are largely unknown. Reports also showed that even the four alternatively spliced isoforms of NF1 can also exhibit different functions through tissue-specific and/or developmental stage-specific expression.(Gutmann, Cole et

al. 1995, Gutmann, Geist et al. 1995, Gutmann, Geist et al. 1995, Geist and Gutmann 1996, Hinman, Sharma et al. 2014) *NF1* loss is reported to increase cAMP in Schwann cells while decrease cAMP in astrocytes via unknown mechanisms. (Tong, Hannan et al. 2002, Dasgupta, Dugan et al. 2003) This finding further indicates that the biological functions of NF1 are cellular context dependent and underscores the importance of investigating the lineage-specific cellular context for MPNST and NF1.

cyclin-dependent kinase Inhibitor 2A (CDKN2A)

Locating on chromosome 9p21, CDKN2A codes for two critical cell cycle proteins: INK4A (also known as p16) and ARF (also known as p14, or p19 in mice). INK4A and ARF are generated through the use of shared coding regions and alternative reading frames in CDKN2A gene locus. Two separate promoters drive the transcription of INK4A and ARF using different exon 1 of CDKN2A gene while sharing common downstream exon 2 and 3. In addition, the open reading frame in exon 2 is also different for INK4A and ARF. (Quelle, Zindy et al. 1995) The INK4A protein can bind to and inhibit cyclin-dependent kinase 4/6 (CDK4/6), preventing phosphorylation of another tumor suppressor retinoblastoma protein (RB). Hypophosphorylated RB can then recruit the transcription factor E2F, resulting in G1 arrest during cell cycle. Loss of INK4A in cancer cells lead to hyperphosphorylation of RB, release of E2F and activation of genes that are necessary for G1 to S transition. (DePinho 1998, Sherr and Roberts 1999) ARF functions as a potent growth suppressor through regulating E3 ubiquitin ligase of p53, MDM2. Binding of MDM2 and ARF can inhibit MDM2 mediated polyubiquitylation of p53, and thus stabilize p53. Activation of p53 regulates genes that are importance for cellular stress response. Loss of ARF can result in un-regulated cellular response and resistance to apoptosis in cancer cells. Frequent homozygous deletion of

CDKN2A has been reported in many different types of cancers, including melanoma, pancreatic cancer, gastric cancer, leukemia, bladder cancer, MPNST, etc. (Kamb, Gruis et al. 1994, Nobori, Miura et al. 1994, Serrano, Goebel et al. 2000, Zhu, Montgomery et al. 2007, De Raedt, Beert et al. 2014, Lee, Teckie et al. 2014, Zhang, Wang et al. 2014, Zhen, Rabe et al. 2015)

Polycomb Repressive Complex 2 (PRC2)

Polycomb group proteins are key regulators for gene-expression during early development and differentiation through regulating chromatin structures. The two main polycomb group complexes in mammals are polycomb repressive complex 1 (PRC) and PRC2. There are four core subunits: EZH1/2, SUZ12, EED and RbAp46/48 (also known as RBBP7/4). The core components of PRC2 are conserved from *Drosophila* to mammals. Several additional proteins have recently been shown to be part of PRC2 complex, including AEBP2, PCLs and JARID2. (Nekrasov, Klymenko et al. 2007, Li, Margueron et al. 2010, Walker, Chang et al. 2010) PRC2 complex is responsible for the di- and tri- methylation of Lys 27 of histone H3 (H3K27me_{2/3}) to regulate gene silencing during development and differentiation. It is believed that the histone methylation by PRC2 mediated by the methyltransferase activity of EZH1 or EZH2. PRC2 components have been indicated in various cancers such as lymphoma, melanoma, breast cancer and prostate cancer, mostly through overexpression. (Varambally, Dhanasekaran et al. 2002, Holm, Grabau et al. 2012, Tiffen, Gallagher et al. 2015) Recently, PRC2 is reported to loss in majority of MPNSTs. (De Raedt, Beert et al. 2014, Lee, Teckie et al. 2014, Zhang, Wang et al. 2014)

Animal Models of NF1/MPNST

There have been many studies trying to develop mouse models for NF1 and

MPNST since 1994. These genetically engineered mouse models serve as great tools to investigate molecular mechanisms driving the pathogenesis of NF1 and MPNST. They also provide important insights on understanding the cell of origin, microenvironment and cell signaling for these tumors.

Early models of NF1

Copeland group and Weinberg group developed the first knockout mouse models for *Nf1* independently in 1994. (Brannan, Perkins et al. 1994, Jacks, Shih et al. 1994) Both groups showed that homozygous mice with null mutations of *Nf1* exon 31 (*Nf1*^{Δ31/Δ31} mice) were embryonic lethal due to severe cardiac failures. In the heterozygous *Nf1*^{+Δ31} mice, there are no obvious abnormalities even after 10 months follow up. Weinberg group described that the *Nf1* mutations may accelerate the development of tumor types to which these animals are already susceptible, supporting the role of *Nf1* as a tumor suppressor.

One potential explanation for the lack of neurofibroma development in the heterozygous *Nf1*^{+Δ31} mice could be that loss of the wild type allele of *Nf1* in the right cell type is the rate-limiting step for neurofibroma formation. Therefore, Cichowski and coworkers developed a chimeric mouse model where they injected *Nf1*^{-/-} embryonic stem cell into *Nf1*^{+/-} C57BL/6 blastocysts. (Cichowski, Shih et al. 1999) Most of the mice generated exhibited moderate degree of chimerism, and developed plexiform neurofibromas with 100% penetrance. In addition, these tumors presented with schwann cells, suggesting that *Nf1* LOH in Schwann cells is required for neurofibroma pathogenesis.

To test whether *Nf1* LOH in Schwann cells is sufficient for neurofibroma pathogenesis, Zhu and coworkers developed a conditional mouse model, in which *Nf1*

can be conditionally ablated in Schwann cell specific marker *Krox20* expressed cells.(Zhu, Ghosh et al. 2002) Plexiform neurofibroma with human histological features only developed in *Krox20-Cre ;Nf1^{flox/-}* by 1 year of age, while there is no significant Schwann cell hyperplasia in the *Krox20-Cre ;Nf1^{flox/flox}*. This study suggested that *Nf1* LOH in Schwann cells is sufficient for neurofibroma pathogenesis. However, it also need to cooperate with a *Nf1* haploinsufficient micro-environment, which is further supported by later studies.(Tan, Yazicioglu et al. 2003, Yang, Chen et al. 2006, Yang, Ingram et al. 2008)

Mouse models for the cell-of-origin debate

Although we have known that MPNST and NF1 are originated from the Schwann cell lineage, it is still unknown which type of Schwann cells or what stage of Schwann cell is the cell of origin for these tumors. There are different stages of Schwann cell differentiation (**Figure 1.3**). The Schwann cell lineage is believed to arise from the migrating neural crest cells in mice at around embryonic day 8.5-9, which then differentiated into Schwann cell precursors (SCPs) at around embryonic day 12-13. SCPs are differentiated into Immature Schwann cells starting at embryonic day 13 until perinatal. After birth, Immature Schwann cells are further differentiated into the two mature Schwann cell types: myelinating Schwann cells and nonmyelinating Schwann cells.(Jessen and Mirsky 2005, Carroll and Ratner 2008)

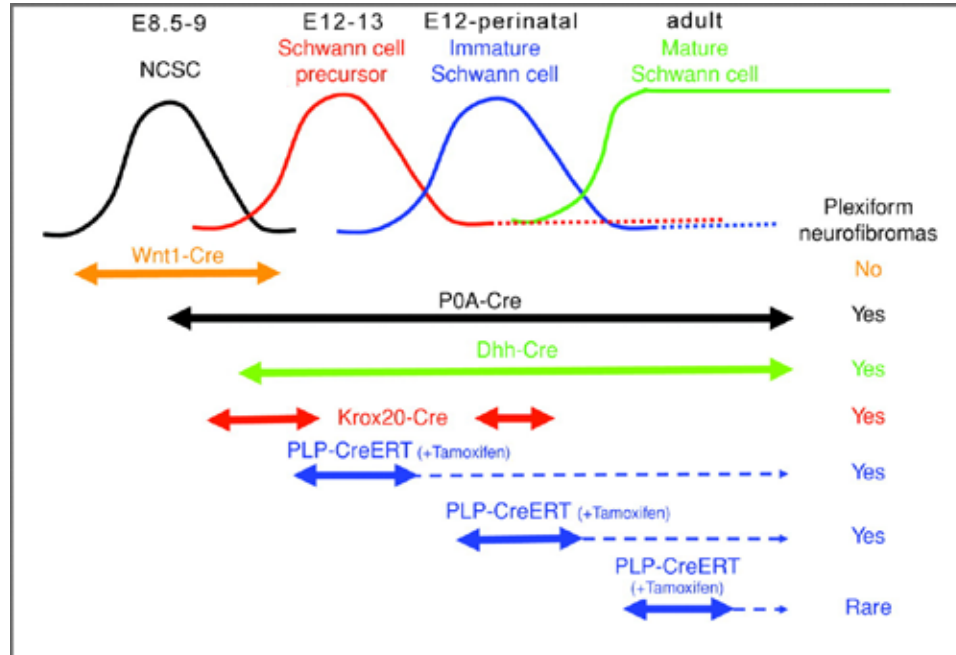


Figure 1.3 Diagram outlining the stages of Schwann cell development and the periods of Cre-mediated recombination in various neurofibroma models
 Cre-mediated recombination to ablate NF1 expression only leads to plexiform neurofibromas when the cre is activated in Schwann cell precursors or immature Schwann cells. Reprinted from Cancer Research, Copyright 2011, 71(13), 4686-95, Le LQ, Liu C, Shipman T, Chen Z, Suter U, Parada LF., Susceptible stages in Schwann cells for NF1-associated plexiform neurofibroma development., with permission from AACR.

To investigate the exact cell of origin for MPNST and NF1, *Nf1^{flox/-}* mice have been crossed with different Schwann cell lineage promoter driven cre mice. Ablation of *Nf1* at early neural crest cell stage with *Wnt1-Cre*, *Mpz-Cre*, and *Pax3-Cre* led to early death before they developed any neurofibroma. When *Nf1* was ablated at Schwann cell precursor stages with *3.9Periostin-Cre*, *P₀a-Cre* and *Dhh-Cre*, both *P₀a-Cre* and *Dhh-Cre* driven models developed neurofibroma although *3.9Periostin-Cre* driven model died within the first month due to cardiac fibroblasts malfunction. (Joseph, Mosher et al. 2008, Wu, Williams et al. 2008, Zheng, Chang et al. 2008) Interestingly, when *Nf1* was ablated with *Dhh-Cre*, neurofibroma could develop even with an *Nf1* wild type microenvironment. Le and coworkers have developed a novel mouse model for NF1 that allows timely control of *Nf1* ablation with tamoxifen (*Plp-CreERT2; Nf1^{flox/-}*). (Le, Liu et al. 2011) With this conditional knockout model for *Nf1*, Le and coworkers showed that both Schwann cell precursors and immature Schwann cells were potential cell of origin for neurofibroma (**Figure 1.3**).

Recent works have also developed *in vitro* culture of stem cell populations to understand the cell of origin for NF1/MPNST. Skin-derived precursors (SKPs) are neural crest derived precursor cells in the dermis of adult mice, which is capable of both Schwannian and melanocytic differentiation. (Le, Shipman et al. 2009) Le and coworkers showed that SKPs could develop dermal neurofibroma in the skin and plexiform neurofibroma when grafted into sciatic nerve, suggesting dermal and plexiform neurofibroma may share similar cell of origin. They have also recently identified a population of GAP43(+) PLP(+) precursors in embryonic nerve roots as the potential cells of origin for plexiform neurofibroma. (Chen, Liu et al. 2014)

Mouse models for MPNST

Although extensive efforts have been focused on developing models for plexiform neurofibroma, it is more important to model MPNST for NF1 patients since they have high risk to transform to MPNST. However, plexiform neurofibromas in mouse models rarely undergo malignant transformation to MPNSTs. This could be either because of the relative short lifespan of mice comparing to human, or because additional oncogenic events are required for the malignant transformation. Mice with germ line mutations of *Nf1* and *p53* (*Nf1*^{+/-}; *p53*^{+/-} cis) were generated either linked on the same chromosomes to allow for LOH in lesions. (Cichowski, Shih et al. 1999) As expected, 30% of these mice developed MPNST while there was no MPNST with single mutations. When germ line mutations of *Nf1* and *p53* (*Nf1*^{+/-}; *p53*^{+/-} cis) were put on opposite chromosomes, LOH of the other copy of *Nf1* and *p53* simultaneously was much harder resulting in tumors only similar to single mutations. Due to the frequent deletion of *CDKN2A* in MPNSTs, *Nf1*^{+/-} mice with simultaneous homozygous deletion of the *CDKN2A* were generated. (Joseph, Mosher et al. 2008) 26% of these mice eventually developed MPNSTs, while *Nf1*^{+/-} mice with heterozygous deletion of *CDKN2A* developed MPNSTs at a much lower frequency.

These models have important implications for understanding pathogenesis of MPNST and NF1, as well as for the development of novel therapies targeting these tumors. However, new mouse model of MPNST needs to be generated to recapitulate loss of additional oncogenic events such as PRC2 loss.

Gastrointestinal stromal tumor (GIST)

Definition and Characteristics

Gastrointestinal stromal tumor (GIST) has emerged as the most common mes-

enchymal tumor of the gastrointestinal (GI) tract, and also represents one of the most common subtypes of human sarcoma (Perez, Livingstone et al. 2006, Chi 2010). The incidence of GIST has been reported consistently between 7 to 20 per million populations per year (Goettsch, Bos et al. 2005, Nilsson, Bummig et al. 2005, Tran, Davila et al. 2005, Mucciarini, Rossi et al. 2007), with approximately 5000-6000 new cases per year in the United States (Fletcher, Berman et al. 2002). Even though GISTs have been reported in individuals of all ages, they typically occur between the ages between 40 and 80 at the time of diagnosis. (DeMatteo, Lewis et al. 2000, Singer 2001, Hayashi, Okazaki et al. 2005, Gold and DeMatteo 2006) The median age of GISTs is about 60 years (Singer 2001). There is no clear sex predilection although some reports showed slightly male predominance. (Singer 2001, Miettinen, Majidi et al. 2002)

The presentation of GISTs varies widely on symptom, location and pathology features. Most GIST patients will be symptomatic at presentation, while asymptomatic patients with small lesions are typically diagnosed incidentally during surgery, physical examination, radiologic imaging or laparotomy. (Pidhorecky, Cheney et al. 2000, Gold and DeMatteo 2006, Gupta, Tewari et al. 2008) The most common symptoms in GIST patients are abdominal mass and GI bleeding due to mucosal ulceration. Other clinical symptoms associated include fatigue, abdominal pain, dysphagia, satiety, and obstructions. (He, Wang et al. 1988, Dougherty, Compton et al. 1991, Pidhorecky, Cheney et al. 2000, Gupta, Tewari et al. 2008) GISTs are dominantly present in the stomach (60%-70%) and small intestine (20%-25%), but they can also arise in the colon (5%), esophagus (5%), and rarely in omentum, retroperitoneum and mesentery. (Haque and Dean 1992, Tworek, Appelman et al. 1997, Tworek, Goldblum et al. 1999, Tworek, Goldblum et al. 1999, Miettinen, Sarlomo-Rikala et al. 2000, Miettinen, Sarlomo-Rikala et

al. 2000, Ortiz-Hidalgo, Bojorge et al. 2000, Reith, Goldblum et al. 2000, Corless, Fletcher et al. 2004, Corless 2014)

The size of GIST tumors can range from 1cm to more than 40cm, with an average of about 5cm. (Levy, Remotti et al. 2003, Corless, Fletcher et al. 2004, Corless 2014) Morphologically, spindle-cell type and epithelioid or round cell type are the two predominant cell types in the GIST(Pidhorecky, Cheney et al. 2000, Levy, Remotti et al. 2003, Corless 2014). The spindle cells are usually composed of cigar-shaped cells with elongated nuclei and blunted ends frequently with a clear perinuclear halo and moderately abundant pink cytoplasm. The Epithelioid cells are composed of round or polygonal cells with central or slightly accentric placed nuclei and moderately abundant cytoplasm. These cells may have a variety of architectural patterns and may presents differently between different subtypes of GISTs. (**Figure 1.4**) Most of the GISTs are spindle cell tumors (70%), 20% GISTs are epithelioid cell tumors and 10% GISTs are mixture of spindle and epithelioid cells. (Eisenberg and Pipas 2012) The diversity of morphology among GISTs has made it challenging to diagnosis GIST based on histology and requires the reliable immunohistochemical markers for accurate diagnosis.

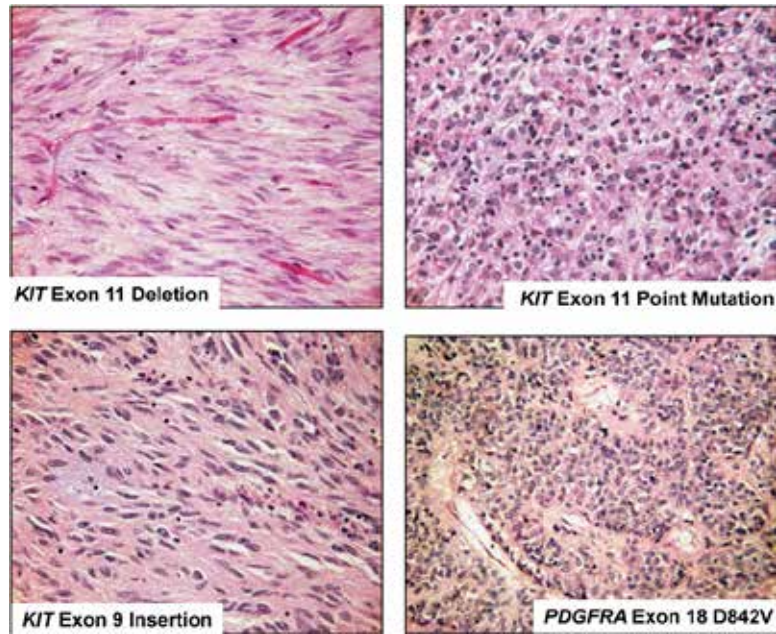


Figure 1.4 Examples of gastrointestinal stromal tumor (GIST)

Spindle cell GISTs (left panels) often harbor a mutation in KIT exon 9 and 11. Epithelioid GISTs (right panels) vary in their genotype, having either (or neither) a KIT or PDGFRA mutation. Reprinted by permission from Macmillan Publishers Ltd: MODERN PATHOLOGY, 27, S1-16, Copyright 2014.

The first immunohistochemical marker that helped GIST diagnosis is CD34, which is expressed in 60% to 70% of all GISTs. (Miettinen, Virolainen et al. 1995, Fletcher, Berman et al. 2002, Corless 2014) In 1998, two reports showed that CD117 (c-KIT protein) is expressed in most GISTs. (Hirota, Isozaki et al. 1998, Kindblom, Remotti et al. 1998) KIT was soon shown to express in ~ 95% of GISTs in follow studies, making it becomes one of the most reliable immunohistochemical markers for GIST diagnosis. (Miettinen, Sobin et al. 2000, Miettinen and Lasota 2001, Hornick and Fletcher 2002) The addition of DOG1, which is expressed in ~97% of GISTs, as another GIST immunohistochemical marker has greatly improve the accuracy of GIST diagnosis. (West, Corless et al. 2004) Combination of KIT and DOG1 together can define the diagnosis of GIST in more than 99% of cases in a recent report. (Lopes, West et al. 2010) Furthermore, 30% to 40% are positive for smooth muscle actin (SMA), approximately 5% are positive for the S100 staining, mostly absent for desmin and loss for SDHA or SDHB mutation in succinate dehydrogenase deficient GISTs. (Gold and DeMatteo 2006, Janeway, Kim et al. 2011, Corless 2014)

Oncogenic mutations in GISTs

Mutations in receptor tyrosine kinase KIT are the most common mutation in GISTs (~75%), followed by its close homolog α -receptor for platelet derived growth factor (PDGFRA) (~10%). Other driver mutations in *KIT/PDGFR*A wild type GISTs include *BRAF*, *SDHA/B/C/D*, *HRAS*, *NRAS*, *PI3KA* and *NF1* (**Figure 1.5**). (Janeway, Kim et al. 2011, Eisenberg and Pipas 2012, Corless 2014)

Genetic Type	Relative Frequency	Anatomic Distribution	Germline Examples
KIT mutation (relative frequency 75%–80%)			
Exon 8	Rare	Small bowel	One kindred
Exon 9 insertion AY502-503	10%	Small bowel and colon	None
Exon 11 (deletions, single nucleotide substitutions and insertions)	67%	All sites	Several kindreds
Exon 13 K642E	1%	All sites	Two kindreds
Exon 17 D820Y, N822K, and Y823D	1%	All sites	Five kindreds
PDGFRA mutation (relative frequency 5%–8%)			
Exon 12 (such as V561D)	1%	All sites	Two kindreds
Exon 14 N659K	<1%	Stomach	None
Exon 18 D842V	5%	Stomach, mesentery and omentum	None
Exon 18 (such as deletion of amino acids IMHD 842–846)	1%	All sites	One kindred
KIT and PDGFRA wild type (relative frequency 12%–15%)			
BRAF V600E	~7%–15%		
SDHA, SDHB, SDHC, and SDHD mutations	~2%	Stomach and small bowel	Carney–Stratakis
HRAS and NRAS mutation	<1%		
Sporadic pediatric GISTs	~1%	Stomach	Not heritable
GISTs as part of the Carney triad	~1%	Stomach	Not heritable
NF1 related	Rare	Small bowel	Numerous

Figure 1.5 Molecular classifications of GISTs

GIST, gastrointestinal stromal tumor; NF1, neurofibromatosis type I; PDGFRA, platelet-derived growth factor receptor- α ; SDH, succinate dehydrogenase. Reprinted from Hematology/Oncology Clinics of North America, 26(6), Eisenberg BL, Pipas JM., Gastrointestinal stromal tumor--background, pathology, treatment. 1239-59. Copyright 2012, with permission from Elsevier.

KIT

First discovered in 1998 by Hirota et al, 75%-80% GISTs have mutations in the receptor tyrosine kinase KIT. (Hirota, Isozaki et al. 1998) This breakthrough discovery has not only revolutionized the management of GIST, but also made GISTs become an important model in the emerging field of molecularly targeted therapies for solid tumors. *KIT* was first identified as the cellular homolog of V-Kit Hardy-Zuckerman 4 Feline Sarcoma Viral Oncogene. The human *KIT* gene maps to 4q12-13 and is composed of 21 exons. *KIT* belongs to the type III receptor tyrosine kinase family that includes platelet derived growth factor receptor α/β (PDGFRA/B), colony stimulating factor 1 receptor (CSF1R) and fms related tyrosine kinase 3 (FLT3). (Hanks, Quinn et al. 1988) *KIT*, together with the other type III receptor tyrosine kinase family members, contains an N terminal extracellular ligand binding domain, a single transmembrane domain including a juxtamembrane domain, and a cytoplasmic kinase domain. (Roskoski 2005) There are two isoforms of KIT protein, deriving from alternatively spliced *KIT* mRNA. However, the significance of these two structural variants is not fully understood.

KIT acts as the cell-surface receptor for the cytokine KIT Ligand (KITLG) or also known as Stem Cell Factor (SCF). The kinase activity of KIT is repressed by its juxtamembrane domain, which forms a hairpin loop that locks KIT in the inactive form. Upon KITLG/SCF binding, the KIT receptors start to form homodimer and transphosphorylate at specific tyrosine residues, that serves as the docking sites for the src-homology-2 (SH2) domain of downstream signaling and adaptor protein. The activation of *KIT* and downstream signaling plays an essential role for the regulation of various cellular processes, including cell survival and proliferation, hematopoiesis, stem cell maintenance, gametogenesis, Interstitial Cell of Cajal (ICC) development, mast cell development, migration and function,

and in melanogenesis.(Maeda, Yamagata et al. 1992, Huizinga, Thuneberg et al. 1995, Timokhina, Kissel et al. 1998, Kissel, Timokhina et al. 2000) *KIT* has been shown to activate Ras/ MAP kinase, Rac/Rho-JNK, PI3K/AKT, and SFK/STAT signaling networks. The activation and signaling of *KIT* in physiological status are tightly regulated by cellular context and presence of downstream signaling components, resulting in differential cascades activation in different cell types. Loss-of-function mutations of *KIT* or *KITLG* lead to deficiencies in multiple major cell systems. One of these cell systems is the pace makers cell of GI tract, Intestinal Cell of Cajals, which is the cell of origin for GIST. (Maeda, Yamagata et al. 1992, Chi 2010) In contrast, activation mutations of *KIT* have been implicated in several tumor types: seminoma(Tian, Frierson et al. 1999), mastocytosis(Nagata, Worobec et al. 1995, Longley, Tyrrell et al. 1996), acute myelogenous leukemias(Gari, Goodeve et al. 1999), GIST(Hirota, Isozaki et al. 1998) and more recently in melanomas(Willmore-Payne, Holden et al. 2005).

The most common mutations of *KIT* in GIST lie in the juxtamembrane domain that is encoded by exon 11. **(Figure 1.6)** Previous studies showed that the juxtamembrane domain might act as a negative regulator of *KIT* kinase. Mutations in exon 11 disrupt the inhibitory function of juxtamembrane domain in two-thirds of GISTs. The types of mutations in exon 11 can be in-frame deletions, insertions, substitutions or combinations thereof, with 5' end as a common hot spot. In general, activating mutations of *KIT* in exon 11 does not appear to be associated with specific clinical presentation, but the deletions are associated with a more aggressive behavior in comparison with other exon 11 mutations. More specifically, deletions of codon 557 and/558 are associated with poor prognosis. (Ernst, Hubbs et al. 1998, Lasota, Jasinski et al. 1999, Taniguchi, Nishida et al. 1999, Singer, Rubin et al. 2002, Wardelmann, Losen et al. 2003, Liu, Bai et al. 2005, Martin, Poveda et al. 2005, Andersson, Bumming et al. 2006, Cho, Kitadai et al. 2006)

The second most common mutation sites of *KIT* are located in an extracellular domain encoded by exon 9 (7% -10%). (Lux, Rubin et al. 2000) Most *KIT* exon 9 mutations are identical tandem duplication of six nucleotides, encoding for AY 502-503, potentially mimicking the extracellular conformational change upon *KIT* ligand binding. This change influences *KIT* inhibitor sensitivity during targeted therapy treatment. The locations of tumors in GISTs harboring exon 9 mutations are primary in small and large intestine, and rarely in stomach. (Lux, Rubin et al. 2000, Lasota, Kopczynski et al. 2003, Hostein, Longy et al. 2006) Other *KIT* mutations in GISTs are identified in kinase domains, such as exon 13 or 17, but at a much lower incidence. (Lasota, Corless et al. 2008)

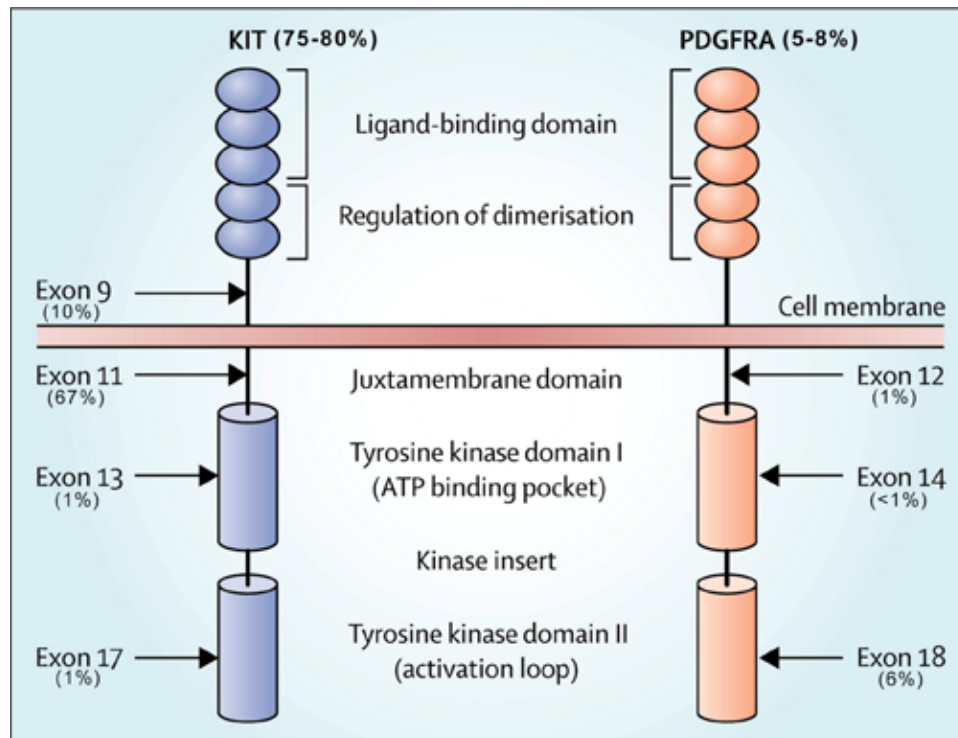


Figure 1.6 KIT and PDGFRA mutations in GISTs

Reprinted from The Lancet, 382(9896), Joensuu H, Hohenberger P, Corless CL., Gastrointestinal stromal tumour. 973-83. Copyright 2013, with permission from Elsevier.

Platelet-Derived Growth Factor Receptor α (PDGFRA)

Approximately 10% of GISTs harbor mutations in *PDGFRA* instead of *KIT* in the juxtamembrane domain (exon 12), the ATP-binding domain (exon 14), or the activation loop (exon 18). (**Figure 1.5** and **Figure 1.6**) (Heinrich, Corless et al. 2003, Hirota, Ohashi et al. 2003, Lasota, Dansonka-Mieszkowska et al. 2004) Consistent with the extensive functional overlapping between *KIT* and *PDGFRA*, *KIT* and *PDGFRA* mutations are mutually exclusive in GISTs. Mutations in *PDGFRA* resulted in ligand independent activation of the receptor, as well of the downstream pathways that are identical to those in *KIT*-mutant GISTs. However, *PDGFRA*-mutant GISTs still show distinctive clinical features from *KIT*-mutant GISTs, including gastric location, epithelioid morphology, variable *KIT* expression, different gene expression and lower potential for malignancy. (Debiec-Rychter, Wasag et al. 2004, Medeiros, Corless et al. 2004, Sakurai, Hasegawa et al. 2004, Subramanian, West et al. 2004, Wardelmann, Hrychuk et al. 2004, Wasag, Debiec-Rychter et al. 2004, Kang, Nam et al. 2005, Tzen and Mau 2005)

BRAF

BRAF gene encodes the BRAF protein, which belongs the raf family of three serine/threonine kinases. *BRAF* plays a central role in the regulation of MAP Kinase/ERKs signaling cascades. Upon growth factor stimulation, *B-RAF* is active through binding with Ras-GTP, subsequently activating MEKs and ERKs, which then can directly or indirectly activate many transcription factors to regulate gene expression. The highly regulated signaling transduction of BRAF and MAP Kinase signaling plays an important role in the regulation of gene expression, cell proliferation and survival. (Seger and Krebs 1995)

BRAF mutations have been identified in various cancer types, including melano-

ma (Davies, Bignell et al. 2002), colorectal cancer (Rajagopalan, Bardelli et al. 2002), thyroid cancer (Namba, Nakashima et al. 2003) and lung cancer (Brose, Volpe et al. 2002). Mutations of BRAF usually resulted in ligand independent activation of downstream signaling. Interesting, approximately 90% of known *BRAF* mutations are V600E mutations. (Cantwell-Dorris, O'Leary et al. 2011) Recent reports showed that *BRAF* V600E mutation is detected in about 7% to 15% of *KIT/PDGFR* wild type GISTs, leading to KIT ligand independent activation of MAP kinase signaling pathway. (Agaram, Wong et al. 2008, Agaimy, Terracciano et al. 2009, Hostein, Faur et al. 2010, Cantwell-Dorris, O'Leary et al. 2011, Miranda, Nucifora et al. 2012) Based on these studies, *BRAF*-mutated GISTs usually arise in the small intestine and stomach with spindle-cell morphology. Histologically, these GISTs do not have significant distinction with other GISTs.

Other Driver Mutations

Other oncogenic mutations reported in GISTs are *HRAS*, *NRAS* and *PIK3CA* with a very low frequency. (Miranda, Nucifora et al. 2012) GISTs can also be seen in the small intestine in 7% of neurofibromatosis type I (NF1) patients (Anderson, Sihto et al. 2005). More recently, defects in succinate dehydrogenase are reported in approximately 50% of *KIT/PDGFR* wild type GISTs through mutations or deletions of the SDH subunits *SDHA/B/C/D*. Sporadic pediatric GISTs patients are predominantly SDHB immunonegative although rarely harbor an SDH gene mutation. (Killian, Kim et al. 2013, Mason and Hornick 2013) These tumors showed a different gene expression profile and clinical features from *KIT/PDGFR*-mutant GISTs. (Prakash, Sarran et al. 2005, Agaram, Laquaglia et al. 2008) Functions of GIST-related oncogenic genes are summarized in **Figure 1.7**. (Joensuu, Hohenberger et al. 2013)

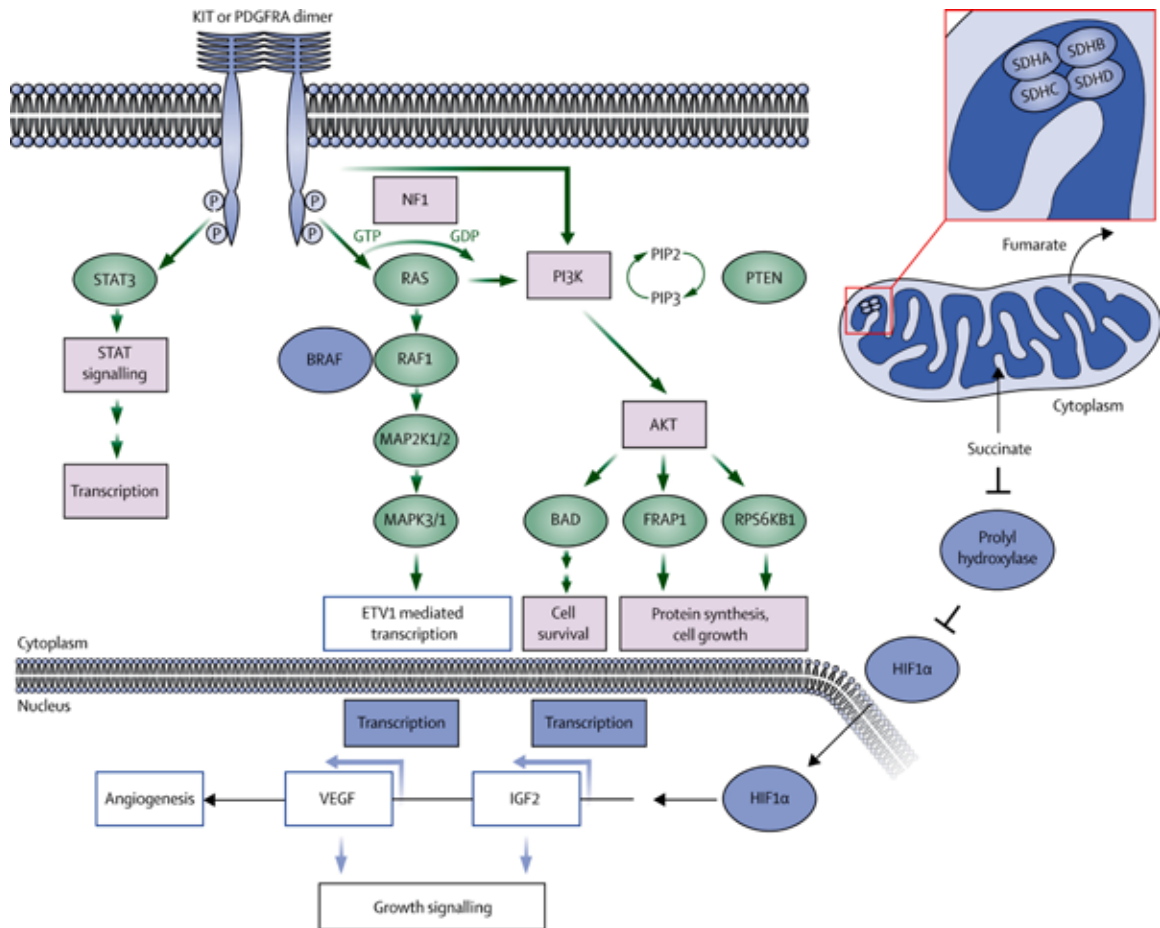


Figure 1.7 Oncogenic signaling pathways in GISTs

Summary of the signaling pathways which GIST oncogenic mutations involve. Reprinted from The Lancet, 382(9896), Joensuu H, Hohenberger P, Corless CL., Gastrointestinal stromal tumour. 973-83. Copyright 2013, with permission from Elsevier.

Animal models of GISTs

The fact that *KIT* activation mutations are the most frequent mutations in GISTs have made it is important to model GIST with *KIT* mutants. Based on this, Sommer and coworkers developed a GIST mouse model through knock in an activating mutation in the exon 11 of *KIT*, where most mutations of *KIT* lie. (Sommer, Agosti et al. 2003) The V558 deletion mutation (*Kit^{V558Δ}*) in the juxtamembrane domain of human *KIT* was selected based on a human familial GIST case. (Nishida, Hirota et al. 1998) Heterozygous mutant *Kit^{V558Δ/+}* mice developed variable distension of the distal ileum (mega-ileum) starting at 4 weeks of age and eventually died from pathology in the GI tract. All mutant mice developed neoplastic mass in the cecum indicating the penetrance of GI disease in *Kit^{V558Δ/+}* mice is 100%. Further histological and immunohistochemical analysis showed the GIST in *Kit^{V558Δ/+}* mice highly resembled human familial GISTs. Myenteric Plexus hyperplasia was also identified throughout the GI tract, which is consistent with ICC hyperplasia observed in human familial GISTs. Survival of mutant *Kit^{V558Δ/+}* mice was ≈50% at 9 months. This mouse model suggested that activation mutations of *KIT* and *KIT* signaling pathway is important and sufficient for ICC hyperplasia and GIST tumorigenesis. It also served as an important tool to further investigate *KIT* pathway activation, GIST pathogenesis, ICC biology and preclinical validation of drug treatments for the disease for many follow-up studies. (Rossi, Ehlers et al. 2006, Chi 2010, Ran, Sirota et al. 2015)

In 2005, Rubin and coworkers developed another GIST mouse model by introducing *Kit* gene K641E mutation with knock-in gene targeting strategy. (Rubin, Antonescu et al. 2005) This point mutation, locating in the kinase domain encoded by exon 13, was originally identified in both sporadic and familial human GISTs. (Yarden, Kuang et al. 1987) The *Kit^{K641E:Neo}* mice developed a dose-de-

pendent phenotype in the GI tract. Homozygous *Kit*^{K641E:Neo/K641E:Neo} developed ICC hyperplasia and GIST tumors in the cecum starting at 3 weeks of age and could only survive 3-30 weeks. Heterozygous *Kit*^{+/K641E:Neo} were viable and asymptomatic with milder ICC hyperplasia limited to colon and smaller sized GISTs in comparison with the homozygous mice. Rubin and coworkers also pointed out the distribution of GISTs in cecal is very different than is seen in humans since human large bowel GISTs are very rare. Nevertheless, the ICC hyperplasia and GISTs in *Kit*^{K641E:Neo} mice were still identical to human GISTs at histological, immunohistochemical, ultrastructural and molecular levels.

More recently, a mouse model for human multiple GIST family with *KIT*^{D820Y} mutation was generated by Nakai and coworkers with knock-in gene targeting strategy. (Nakai, Ishikawa et al. 2008) Similar to the other two mouse models, this *Kit*^{D818Y} mutation in mice is the homologous to the human *KIT*^{D820Y} mutation identified in two families of GISTs. (Hirota, Nishida et al. 2002, O'Riain, Corless et al. 2005) Homozygous *Kit*^{D818Y/D818Y} mice developed severe GI symptoms at early age including ICC hyperplasia along the GI tract and large tumor in the cecal. The heterozygous showed similar phenotypes as the previous *Kit*^{V558Δ/+} mice with ICC hyperplasia and cecum tumors. The penetrance of GI disease in *Kit*^{D818Y} mice is also 100%. Hyperplasia ICCs and GISTs were reminiscent of human GISTs. This mouse model is the third reported mouse model for understanding *KIT* signaling in GIST pathogenesis.

Despite the development of multiple *KIT*-mutant GIST mouse model, there is no other mouse model available to study other oncogenic mutations in GIST such as PDGRA, BRAF or SDH.

Treatment of GIST with Tyrosine Kinase Inhibitor (TKI) therapy

TKI therapy in GIST

Historically the prognosis of GISTs has remained poor due to its intrinsic resistance to conventional chemotherapy and radiation therapy. Surgery was the only effective therapy for GISTs with limited value since many patients still eventually die of disease recurrence after surgical resection. It is only until 1998 with the landmark discovery of KIT mutation in GISTs by Hirota and coworker that the management of GISTs was revolutionized soon after with tyrosine kinase inhibitor imatinib.

Imatinib was originally developed as a selective kinase inhibitor for BCR-ABL oncoprotein in chronic myelogenous leukaemia (CML) in 1990s. Due to the structural similarity between ABL, KIT and PDGFR, Imatinib could also specifically and effectively inhibit KIT and PDGFR. Imatinib is a 2-phenyl amino pyrimidine derivative that functions by occupying ATP-binding active site of KIT, leading to decreased activity. Based on these facts, clinical trials were soon conducted in GISTs with Imatinib treatment and showed significant improvement from conventional treatments. Imatinib achieves partial responses or stable disease in nearly 75-80% of patients with advance GISTs. (Demetri, von Mehren et al. 2002, Verweij, Casali et al. 2004, Blanke, Rankin et al. 2008, Van Glabbeke and MetaGIST 2010) Only few GIST patients are insensitive to imatinib (so-called "primary resistance"). The median survival for GIST patients is now nearly 5 years compared to 9-20 months in the pre-imatinib era. (De Giorgi and Verweij 2005)

Resistance to TKI therapy

Despite the early clinical success, imatinib resistance has become one of the

biggest challenges for the modern management of GIST patients. GIST patients can be intrinsically resistance to imatinib (primary resistance) or acquired secondary mutation while getting imatinib treatment (secondary resistance). Studies now show that the response rates of GIST patients to imatinib dependent on the genotype of *KIT* or *PDGRA* mutations in the tumors. (Heinrich, Corless et al. 2003) GISTs with exon 11 *KIT* mutations have a partial response (PR) rate of ~ 85%, while GISTs exon 9 *KIT* mutations have a PR rate of ~ 45%. The probability of primary resistance to imatinib for *KIT* exon 11 and *KIT* exon 9 is 5% and 16%, respectively. In addition, only a subset of *PDGRA*-mutant showed responses to imatinib. *In vitro* studies showed that the most common D842V *PDGFRA* mutation in GIST is strongly resistance to imatinib treatment.(Heinrich, Corless et al. 2003, Corless, Schroeder et al. 2005) Understandably, GIST patients without *KIT/PDGFRA* mutations showed no response to imatinib. Different TKIs or targeted therapies are needed to treat these GISTs that are primary resistant to imatinib.

After the initial response to imatinib, majority of GIST patients develop disease progression within 2 years of imatinib treatment, and eventually die of their diseases.(Verweij, Casali et al. 2004, De Giorgi and Verweij 2005, Blanke, Rankin et al. 2008, Van Glabbeke and MetaGIST 2010) The secondary resistance to imatinib is most commonly acquired through additional mutations of *KIT* or *PDGFRA* in the same gene and allele as the primary oncogenic driver mutations. However, these acquired mutations can be quite heterogeneous. For example, there may be different secondary mutations in different tumor portions in the same patients. (Lim, Huang et al. 2008) There are also other potential mechanisms to acquire secondary resistance including increase cycline D1/JUN levels, overexpression of IGF1R or up-regulation of AXL. (Sabah, Cummins et al. 2006, Mahadevan,

Cooke et al. 2007, Tarn, Rink et al. 2008, Sakurama, Noma et al. 2009)

Many efforts have been take to overcome imatinib resistance in GIST patients. It is recommended to increase the dose of imatinib before switching therapy, which may benefit a small portion of resistant patients (20-30%). (Blanke, Rankin et al. 2008) Unfortunately, this strategy will not benefit the vast majority of patients, leading to the developing of various alternative TKIs such as sunitinib, vatalanib (**Figure 1.8**).(Corless, Barnett et al. 2011) Studies have also tried to find alternative target for effective treatment in imatinib resistant GIST patients, such as PI3K-mTOR pathway, VEGFR, HSP90. More recently, combination therapy is rising as a promising treatment regiment to achieve more effective treatment.

Drug	Targets	Trial information
<i>Tyrosine kinase inhibitors</i>		
Imatinib	KIT and PDGFRA	FDA approved
Sunitinib	KIT, PDGFRA and VEGFR	FDA approved
Nilotinib	KIT and PDGFRA	Phase III (ClinicalTrials.gov ID: NCT00785785)
Dasatinib	KIT and PDGFRA	Phase II (NCT00568750)
Sorafenib	KIT, PDGFRA and VEGFR	Phase II (NCT01091207)
Regorafenib	KIT, PDGFRA and VEGFR	Phase III (NCT01271712)
Vatalanib	KIT, PDGFRA and VEGFR	Phase II (NCT00117299)
Masitinib (AB1010)	KIT and PDGFRA	Phase III (NCT00812240)
Pazopanib	KIT, PDGFRA and VEGFR	Phase II (NCT01323400)
Crenolanib	PDGFRA	Phase II (NCT01243346)
<i>HSP90 inhibitors</i>		
STA-9090	HSP90	Phase II (NCT01039519)
AT-13387	HSP90	Phase II (NCT01294202)
AUY922	HSP90	Phase II (NCT01404650)
<i>Monoclonal antibodies</i>		
IMC-3G3 (Olaratumab)	PDGFRA	Phase II (NCT01316263)
Bevacizumab	VEGFR	Phase III (NCT00324987)
<i>mTOR inhibitor</i>		
Everolimus	mTOR	Phase II (NCT00510354)
<i>Other</i>		
Perifosine	AKT (PI3K pathway)	Phase II (NCT00455559)

Figure 1.8 New therapies being tested for the treatment of GISTs Drug

FDA, US Food and Drug Administration; GISTs, gastrointestinal stromal tumors; HSP90, heat shock protein 90; PDGFRA, platelet-derived growth factor receptor- α ; VEGFR, vascular endothelial growth factor receptor. Reprinted by permission from Macmillan Publishers Ltd: NATURE REVIEWS CANCER, 11, 865-78, Copyright 2011.

ETS variant 1 (ETV1)

Introduction

ETV1 (all called ER81 for ETS-related 81) belongs to the polyomavirus enhancer activator 3 (PEA3)-subfamily of erythroblast transformation-specific (ETS)-family of transcription factors. There are two other members in the PEA3 subfamily: *ETV4* (also called E1AF or PEA3) and *ETV5* (also called ERM for ETS-related molecule). Multiple isoforms of *ETV1* have been identified although no clear-cut differences were observed. (Coutte, Monte et al. 1999) *ETV1*, together with *ETV4* and *ETV5*, has been shown to regulate many target genes through an ETS DNA binding domain that binds to a consensus 5'-CGGA[AT]-3' sequence. (Wei, Badis et al. 2010)

Physiological roles

ETV1 has been implicated in various essential developmental processes through activating or repressing target gene expressions in different cellular contexts. Arber and coworkers described that *Etv1* was expressed in developing proprioceptive neurons and motor neurons. (Arber, Ladle et al. 2000) *Etv1* mutant exhibited severe motor discoordination while the specification of motor neurons and induction of muscle spindles were not affected. It suggested that *ETV1* was important for the development of functional sensory-motor circuitry in the spinal cord. *ETV1* has also been implicated to be critical for the differentiation of dopamine neurons in the central nervous system, which regulate a variety of complex behaviors. (Flames and Hobert 2009) Flames and coworkers found that *ETV1* is expressed in dopaminergic neurons in the mouse olfactory bulb. Ablation of *ETV1* in *ETV1* mutant mice resulted in decreased number of these neurons. Sedy and coworkers showed that *ETV1* is expressed in the inner core cells of the Pacinian corpuscle, a class of mechanoreceptors. (Sedy, Tseng et al. 2006) Deletion of *ETV1*

lead to severe deficit of Pacinian corpuscles, indicating *ETV1* is required for in the assembly of Pacinian corpuscles and the survival of the sensory neurons that innervate them. More recently, *ETV1* has been described as a lineage survival factor for the cell of origin of GISTs, subclasses of interstitial cells of Cajal (ICCs). (Chi, Chen et al. 2010) Ping and coworkers showed that *Etv1* was specifically expressed in two subtypes of ICCs that could develop GISTs, the myenteric ICCs (ICC-MY) and intramuscular ICCs (ICC-IM). *Etv1* knockout mice failed to develop ICC-MYs and ICC-IMs, but not the other two types of ICCs that did not express *Etv1*. These data together indicated that *ETV1* could be the lineage-specific survival factor for ICC-GIST lineage.

Role of *ETV1* in cancers

Other than its physiological functions for development and lineage specification, *ETV1* also contribute to the pathogenesis of various cancer types through different mechanisms. *ETV1* was first identified as the fusion partner for EWS gene in Ewing Sarcoma patients. (Jeon, Davis et al. 1995) EWS was previously shown to translocate and fuse with *ETS* transcription factor, *FLI1* (~85%) and *ERG* (~10%). (Zucman, Melot et al. 1993) Jeon and coworkers further identified the fusion of EWS with a portion of *ETV1* containing the ETS DNA binding domain. (Jeon, Davis et al. 1995) However, the frequent of EWS-*ETV1* translocations are relatively rare in comparison with EWS-*FLI1* and EWS-*ERG* translocations.

Genomic rearrangement of *ETV1* and other *ETS* transcription factors with androgen-regulated gene *TMPRSS2* were also found in approximately 70% of prostate cancers. (Tomlins, Rhodes et al. 2005, Mehra, Tomlins et al. 2007) *TMPRSS2:ERG* was most frequently occurred in prostate cancers (~54%) and *TMPRSS2:ETV1* was observed in ~2% of prostate cancer patients. These trans-

locations induced the androgen-dependent overexpression of *ETS* proteins in prostate cancers, which is important for the prostate cancer pathogenesis.

ETV1 is also amplified in ~13% of primary melanomas and ~18% of metastatic melanomas.(Jane-Valbuena, Widlund et al. 2010) Amplification of *ETV1* led to aberrant overexpression of *ETV1* in melanoma cells. Deregulation of *ETV1* is required for growth and proliferation of melanomas cells with *ETV1* amplification, suggesting an oncogenic role of *ETV1* in MPNST. In addition, Jané-Valbuena and coworkers also showed that *ETV1* overexpression could cooperate with oncogenic *NRAS* for tumorigenesis in mice, which is consistent with the cooperation between *ETV1* and MAPK signaling in GISTs.(Chi, Chen et al. 2010, Jane-Valbuena, Widlund et al. 2010)

Recently, Chi and coworkers described a novel mechanism of *ETV1* activation as an oncogenic transcription factor in GISTs.(Chi, Chen et al. 2010) They first demonstrated that *ETV1* was highly expressed in GISTs while there were no significant genetic alterations in these tumors. *ETV1* was readily expressed in the cell of origin for GISTs, the ICCs. Normal level of *KIT* activation of *KIT* ligand could stabilize *ETV1* protein through MAPK signaling pathway, resulting in the physiological *ETV1* transcriptome critical for ICC development. Ablation of *ETV1* resulted in decreased ICC survival and defects in ICC development. In the context of GIST where activation mutations of *KIT* were presented, *ETV1* protein was augmented due to increased stability by up-regulated MAPK signaling. Collectively, these data suggested that *ETV1* could be a lineage survival factor to cooperate with oncogenic *KIT* mutation during GIST pathogenesis (**Figure 1.9**).

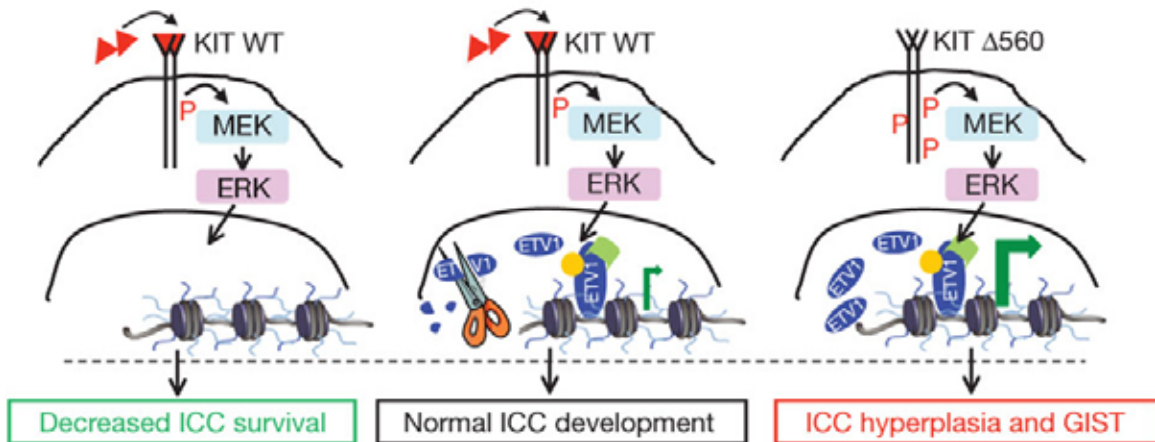


Figure 1.9 Model of the role of ETV1 in ICC maintenance and GIST oncogenesis

Binding of KIT ligand to KIT during normal ICC development results in physiological ETV1 transcriptome, which is critical for ICC development. Ablation of ETV1 leads to decreased ICC survival (left). In GIST, activating KIT mutations lead to hyperactivated MAPK signaling, which stabilizes ETV1 and leads to augmented ETV1 transcriptome that promote GIST tumorigenesis (right). Reprinted by permission from Macmillan Publishers Ltd: NATURE, 467, 849-53, Copyright 2010.

Thesis Aims

The objective of this work was to 1) understand the roles of *ETV1* for the pathogenesis of two types of aggressive sarcomas: Gastrointestinal Stromal Tumors (GISTs) and Malignant Peripheral Nerve Sheath Tumors (MPNSTs); 2) identify effective therapeutic strategies to target *ETV1* and *ETV1*-mediated oncogenic signaling in GISTs and MPNSTs.

In Chapter 3, we showed that *ETV1* is universally highly expressed in MPNST patient tumors and MPNST cell lines. *ETV1* is essential for the survival of MPNST cells *in vitro* and the tumorigenesis *in vivo*. Moreover, overexpression of *ETV1* in combination with loss of *NF1*, the most commonly mutated gene in MPNSTs, transformed mouse fibroblast NIH3T3 cells and promoted tumor formation in mice. Transcriptome profiling and global analyses of *ETV1*-binding sites suggest that *ETV1* regulates various essential pathways in MPNST, including cell cycle and hypoxia regulatory pathways. These observations implicated highly expression of *ETV1* might cooperate with *NF1* loss to drive MPNST tumorigenesis.

In Chapter 4, using comprehensive genomic approaches, we identified loss-of-function somatic alterations of the Polycomb repressive complex 2 (PRC2) components (*EED* or *SUZ12*) in 92% of sporadic, 70% of *NF1*-associated and 90% of radiotherapy-associated MPNSTs. MPNSTs with PRC2 loss showed complete loss of trimethylation at lysine 27 of histone H3 (H3K27me3) and aberrant transcriptional activation of multiple PRC2-repressed homeobox master regulators and their regulated developmental pathways. Introduction of the lost PRC2 component in a PRC2-deficient MPNST cell line restored H3K27me3 levels and

decreased cell growth. Additionally, we identified frequent somatic alterations of *CDKN2A* (81% of all MPNSTs) and *NF1* (72% of non-*NF1*-associated MPNSTs), both of which significantly co-occur with PRC2 alterations. The highly recurrent and specific inactivation of PRC2 components, *NF1* and *CDKN2A* highlights their critical and potentially cooperative roles in MPNST pathogenesis.

In Chapter 5, we generated the mouse model for *BRAF^{V600E}* mutated GISTs with mouse models of *Etv1* driven conditional cre (*Etv1-Cre^{ERT2}*) and cre-activated *Braf^{V600E}*. We confirmed the specific expression of *Etv1* in GIST origin ICCs with lineage tracing strategy. Activation of *Braf^{V600E}* in *Etv1* expressed ICCs resulted in hyperplasia in stomach and large intestine. Combination of *Braf^{V600E}* and tumor suppressor *p53* loss led to multiple GISTs in the large intestine. We further showed that *BRAF^{V600E}* inhibitor Dabrafenib could significantly inhibit *Braf^{V600E}*-mutated GIST tumor growth. This work provided the first mouse model to understand the pathogenesis of *Braf^{V600E}*-mutated GIST and investigate therapeutic treatments for this subtype of GIST patients.

In Chapter 6, we demonstrated that ETV1 is required for GIST initiation and proliferation *in vivo* with using mouse models of *Kit* activation and *Etv1* ablation, validating it as a therapeutic target. We further uncovered a positive feedback circuit where MAP kinase activation downstream of KIT stabilizes the ETV1 protein, and ETV1 positively regulates *KIT* expression. Combined targeting of ETV1 stability by imatinib and MEK162 resulted in increased growth suppression *in vitro* and complete tumor regression *in vivo*. The combination strategy to target ETV1 may provide an effective therapeutic strategy in GIST clinical management.

CHAPTER TWO

Material and Methods

Generation of Compound Genetically Engineered Mouse Models (GEM)

All mouse studies are approved by MSKCC IACUC under protocol 11-12-029. The *Kit*^{Δ558V/+} knock-in mouse was a generous gift from Dr. Peter Besmer, the *Etv1*^{-/-} mice was a generous gift from Dr. Thomas Jessell, the *Etv1*^{flox/flox} mice was a generous gift from Dr. David Ladle (Wright State University) and the *Rosa26*^{CreERT2} mice was a generous gift from Dr. Andrea Ventura. (Arber, Ladle et al. 2000, Patel, Kramer et al. 2003, Sommer, Agosti et al. 2003, Ventura, Kirsch et al. 2007) The *Etv1*^{-/-}; *Kit*^{Δ558V/+}, *Etv1*^{+/+}; *Kit*^{Δ558V/+}, *Etv1*^{flox/flox}; *Rosa26*^{CreERT2/CreERT2} and *Etv1*^{flox/flox}; *Kit*^{Δ558V/+}; *Rosa26*^{CreERT2/CreERT2} mice were generated through standard mouse breeding within the MSKCC animal facility. The *BRaf*^{CA}, *Etv1*^{CreERT2} and *Rosa26-EYFP*^{LSL} mice were purchased from The Jackson Laboratory.

Mouse Procedures

For the GI tract of mice at different postnatal age (Postnatal day 7 to 6 months old), the stomach, small intestine, large intestine, cecum or cecal GIST tumors are dissected and separated and embedded in paraffin or snap frozen for subsequent analyses. For tamoxifen or corn oil treatment of *Etv1*^{ff}; *Kit*^{V558Δ/+}; *Rosa26*^{CreERT2/CreERT2} mice, tamoxifen (Toronto Research Chemicals) was dissolved in at 20 mg/ml in corn oil and injected intraperitoneally to 6-week old mice at a dose of 4 mg every other day for 3 doses. Mice were euthanized 2 weeks after the first tamoxifen dose.

For drug treatment studies in *Kit*^{V558Δ/+} mice, approximately 8-10 weeks *Kit*-

V558Δ/+ mice were treated in 4 cohorts by oral gavage, 1) Vehicle: water; 2) Imatinib: 50 mg/kg BID; 3) MEK162 30 mg/kg, BID; 4) Imatinib+MEK162: Imatinib 50 mg/kg BID + MEK162 30 mg/kg BID. Cecal tumors were isolated and weighed after 5 days of treatment and subjected for paraffin embedding and analyzed by H&E, Trichrome stain and IHC of Ki67. For short-term treatment, the protein and RNA were isolated from cecal tumors after 1.5 day treatment for immunoblots and qRT-PCR analyses, respectively. To generate lysates for western blots, tissue was homogenized in SDS lysis buffer using the FastPrep-24 system with Lysing Matrix A (MP Biomedicals).

For xenograft studies, 5×10^6 GIST882, 2×10^6 GIST-T1 or 5×10^6 MPNST724 cells resuspended in 100 μ l of 1:1 mix of growth media and Matrigel (BD Biosciences) were subcutaneously injected into CB17-SCID mice (Taconic). For GIST tumor chunk xenograft, GIST tumors were chopped into small pieces ($\sim 8\text{mm}^3$), then subcutaneously grafted into CB17-SCID mice (Taconic). Tumor sizes were measured weekly starting 2-8 weeks after xenografting depends on tumor growth rate. For short-term treatment, xenografts were explanted after 2 days of drug treatment for histology analysis; protein and RNA were isolated for immunoblots and qRT-PCR analyses, respectively. For long term treatment, xenograft were treated twice daily until the end of experiments. For GIST882 treatment from the same day of implantation, GIST882 cells expressing firefly luciferase were grafted. Tumor growth was monitored by bioluminescence imaging of anesthetized mice by retro-orbitally injecting d-luciferin and imaging with the IVIS Spectrum Xenogen machine (Caliper Life Science). To generate lysates for western blotting, tissue was homogenized in SDS lysis buffer using the FastPrep-24 system with Lysing Matrix A (MP Biomedicals).

Human Tumor Tissue Collection

Biospecimens were collected during surgical resection from patients with pathologic diagnosis of MPNSTs or neurofibromas. Material was collected under institutional review board (IRB)-approved protocols (IRB 06-107) at MSKCC. All patients provided informed consent. Pathologic diagnosis was confirmed by at least two pathologists using diagnostic formalin-fixed and paraffin-embedded sections to select cases with an estimated tumor content of >70%. The majority of the tumors were collected from different patients. In some cases, more than one tumor was selected from the same patient, and these tumors were resected from distinct anatomical locations in different surgeries.

For the discovery cohort, the goal was to obtain normal DNA and tumor DNA for whole-exome sequencing and SNP6.0 array analysis and to obtain tumor RNA for RNA-seq analysis. A total of 15 fresh-frozen paired MPNST tumor–normal samples were identified. Tumor and adjacent normal tissue specimens were embedded in optimal cutting temperature (OCT) medium, and a histological section was obtained for review. Cryomolds of both tumor and normal tissues were macrodissected to minimize contamination before RNA and DNA preparation. Sample processing was designed to secure samples and minimize the availability of identifying information. Specimens with insufficient tissue amount or severely degraded nucleic acids were excluded.

The IMPACT assay is a hybridization capture, next-generation sequencing platform amenable to DNA from both fresh-frozen and formalin-fixed, paraffin-embedded samples for targeted sequencing. The panel includes *NF1*, *SUZ12*, *EED*, *CDK-N2A* and *TP53*. (Won, Scott et al. 2013) We validated the somatic mutational findings from the discovery cohort by performing IMPACT assays on the same DNA

isolated from tumor tissue. In addition, we performed IMPACT assays on DNA from formalin-fixed, paraffin-embedded samples derived from a second cohort of 37 MPNSTs and 7 neurofibromas from individuals with NF1 who were diagnosed with concurrent MPNST.

Sample Preparation and Quality Control for Genomic Analysis

RNA was extracted from tumor and normal tissues using a modification of the protocol for the DNA/RNA AllPrep kit (Qiagen). DNA from fresh-frozen tissues was extracted from tumor and normal tissue specimens using the DNeasy Blood and Tissue kit (Qiagen). DNA from formalin-fixed, paraffin-embedded samples was isolated using the QIAamp DNA FFPE Tissue kit (Qiagen). DNA from each specimen was initially quantified using the NanoDrop UV spectrophotometer and was further quantified with the Bioanalyzer assay (Agilent Technologies).

RNA Sequencing and Analysis

The isolated RNA was processed using the TruSeq RNA Sample Prep kit (15026495, Illumina) according to the manufacturer's protocol. Briefly, RNA was polyA selected and reverse transcribed, and the cDNA obtained underwent end repair, A-tailing, ligation of the indexes and adaptors, and PCR enrichment. Libraries were sequenced on the Illumina HiSeq 2500 platform with 51-bp paired-end reads to obtain a minimum yield of 40 million reads per sample. Sequence data were processed and mapped to the human reference genome (hg19) using STAR (v2.3). (Dobin, Davis et al. 2013, Anders and Huber 2010, Anders, Pyl et al. 2015) Variance in expression levels was calculated for all genes across samples, and the 75th percentile was set as a cutoff. PCA was performed on the set of genes with variance greater than this cutoff. We used ANOVA to define differentially expressed genes between samples with PRC2 loss and wild-type

PRC2. Genes that showed a >8-fold difference in expression and a corrected FDR of <0.05 (479 genes) were used for clustering and gene ontology analysis. Hierarchical clustering was performed using Pearson correlation in GENE-E software, and heat maps were displayed using GENE-E. Gene ontology analysis was performed using DAVID to discover enriched pathways and gene ontologies.(Huang, Sherman et al. 2009) GSEA to discover gene sets enriched among upregulated genes in samples with PRC2 loss was performed using the JAVA GSEA 2.0 program.(Subramanian, Tamayo et al. 2005) The gene sets used were Broad Molecular Signatures Database gene sets c2 (curated gene sets), c5 (gene ontology gene sets), c6 (oncogenic signatures) and c7 (immunologic signatures) as well as the additional sets 'PRC2_Module' and 'ES_Core', totaling 6,886 gene sets.(Kim, Woo et al. 2010)

We have also performed at least three sets of independent *ETV1* shRNA knockdown experiments in GIST882, GIST48 and GIST-T1 cells and assayed the effects of *ETV1* suppression on *KIT* expression by qRT-PCR and pooled all experiments for analysis. To determine the transcriptional effect of Cre-mediated *Etv1* exon 11 excision in murine cecal tumors, we performed RNA-Seq ([GSE64608](#)) and analysis as described in the previous paragraph. For *ETV1* shRNA knockdown RNA-seq in MPNST cell lines, MPNST724, ST88-14 and SNF96.2 cells were knockdown with *ETV1* shRNA or scramble shRNA. The knockdown efficiency for *ETV1* were validated by qRT-PCR and sequenced and analyzed as described in this section.

DNA Sequencing and Analysis.

Whole-exome sequencing of DNA from fresh-frozen tissue used 1,000 ng (or 500 ng in select cases) of DNA from either tumor or normal samples. DNA was sub-

jected to shearing, end repair, phosphorylation and ligation to barcoded sequencing adaptors according to the manufacturer's guidelines. Ligated DNA was size selected for fragments between 200 and 400 bp in length. These fragments were multiplexed and underwent exonic hybrid capture with SureSelect V4+UTRs exome bait (Agilent Technologies). Captured DNA was sequenced on the Illumina HiSeq 2500 platform with 75-bp paired-end reads. Raw sequences were aligned to the human genome reference sequence (hg19) using Burrows-Wheeler Aligner (BWA).(Li and Durbin 2010)? Total read count and coverage depth are shown in **Table 2.1**. Aligned data were further processed by removing duplicates using Picard followed by indel realignment and base quality score recalibration with the Gnome Analysis Toolkit (GATK).(McKenna, Hanna et al. 2010) Single-nucleotide somatic mutations and somatic indels were called by taking the union of the calls made by MuTect, Strelka and VarScan and applying a set of heuristic filters as described in the VarScan 2 report.(Koboldt, Zhang et al. 2012, Saunders, Wong et al. 2012, Cibulskis, Lawrence et al. 2013) Mutations were further filtered to remove variants that were present in dbSNP137 but not in the Catalogue of Somatic Mutations in Cancer (COSMIC, v64).(Bindal, Forbes et al. 2011) The data were further analyzed and visualized using the cBioPortal.(Cerami, Gao et al. 2012) For IMPACT assays, library construction and sequencing were performed by the MSKCC Genomics Core Facility. Alignment and SNV and indel calling were performed as described above. Copy number analysis was performed as previously described.(Won, Scott et al. 2013)

Table 2.1 Whole Exome sequencing metrics

Sample	Total Somatic Mutations	Non-synonymous Somatic Mutations	Num Reads (10 ⁵)	Uniquely Aligned Reads (10 ⁵)	% Uniquely Aligned Reads	On Target Bases (10 ⁹)	% On or Near Bait	Mean Coverage	% Target Bases at 10x	% Target Bases at 20x
2N			258	254	98.3%	11.9	81.1%	169	99.2%	98.0%
2T	194	26	179	176	98.3%	8.3	81.8%	117	98.4%	95.4%
4N			253	247	97.8%	11.1	79.1%	158	99.1%	97.7%
4T	296	54	259	255	98.3%	11.2	77.5%	158	99.1%	97.7%
7N			196	193	98.5%	8.9	80.9%	126	98.4%	96.1%
7T	280	49	153	151	98.6%	6.9	80.5%	98	97.5%	92.3%
8N			207	204	98.5%	10.1	83.4%	143	98.3%	96.2%
8T	223	32	190	187	98.5%	9.1	82.4%	129	97.4%	94.0%
9N			273	270	99.0%	14.5	88.9%	206	98.9%	97.8%
9T	350	56	196	194	99.1%	10.5	89.3%	149	98.1%	95.5%
10N			98	97	98.7%	5.3	89.2%	75	96.4%	89.6%
10T	126	11	145	144	98.8%	7.9	89.6%	112	97.8%	94.1%
11N			158	156	98.5%	7.9	86.2%	112	97.6%	94.3%
11T	352	60	172	167	97.3%	6.9	69.3%	98	97.3%	92.6%
12N			246	242	98.6%	12.6	86.0%	178	98.4%	96.9%
12T	303	55	283	279	98.6%	14.3	86.5%	203	98.6%	97.2%
13N			155	151	97.2%	6.5	71.0%	91	97.8%	93.0%
13T	552	55	442	433	98.0%	19.9	75.1%	282	99.3%	98.6%
14N			193	188	97.7%	8.2	74.1%	116	98.1%	95.1%
14T	617	46	487	472	97.0%	16.4	59.9%	232	98.3%	96.9%
15N			140	137	97.9%	6.4	79.3%	91	97.5%	92.5%
15T	129	20	92	90	97.6%	4.0	73.7%	57	94.7%	83.6%
16N			467	458	98.0%	21.5	78.1%	305	99.1%	98.5%
16T	637	121	231	224	96.9%	9.2	69.0%	130	98.8%	96.6%
18N			238	236	99.4%	12.5	90.1%	285	61.7%	61.3%
18T	93	13	105	103	98.3%	4.8	77.8%	68	96.5%	88.2%
19N			201	198	98.3%	9.9	82.5%	140	98.7%	96.5%
19T	284	51	315	309	98.3%	15.2	81.5%	215	99.2%	98.2%
20N			132	130	98.0%	6.3	78.9%	89	97.0%	91.1%
20T	145	1	202	196	97.2%	7.6	67.2%	108	97.9%	94.7%

SNP6.0 Arrays and Analysis.

A total of 500 ng of DNA from each tumor or normal tissue sample was hybridized to the Affymetrix SNP6.0 array using protocols from the Genomics Core Laboratory at MSKCC. Allele-specific copy number for each tumor-normal pair of arrays was calculated using TumorBoost in the Aroma package.(Bengtsson, Neuvial et al. 2010)

Cell lines, Antibodies and Reagents

The GIST48 and GIST882 cell lines were obtained from the laboratory of Dr. Jonathan A. Fletcher (Dana-Farber Cancer Institute). The GIST882 cell line, obtained from an imatinib naive patient, harbours a homozygous exon 13 *KIT* mutation (K642E) and was maintained in RPMI supplemented with 15% FBS, 10 mM HEPES pH 7.5. The GIST48 cell line, obtained from an imatinib-resistant patient, harbours a homozygous exon 11 *KIT* mutation (V560D) and a secondary heterozygous Exon 17 *KIT* mutation (D820A) and was maintained in Ham's F10 media supplemented with 15% FBS, 0.5% MITO + Serum Extender (BD Biosciences), and 30 mg^l⁻¹ bovine pituitary extract (BD Biosciences). The GIST-T1 cell line was obtained from Dr. Takahiro Taguchi.(Taguchi, Sonobe et al. 2002) The GIST-T1 cell line harbors 57-nucleotide (V570-Y578) in-frame deletion in *KIT* exon 11 and was maintained in RPMI supplemented with 10% FBS, 10mM HEPES pH 7.5. The MPNST724 and ST88-14 human MPNST cell lines were obtained from the laboratory of Dr. Jonathan A. Fletcher (Dana-Farber Cancer Institute) and by testing have been determined to be mycoplasma free. MPNST 724 and ST88-14 were grown in RPMI supplemented with 10% FBS and RPMI supplemented with 15% FBS, respectively. The MPNST cell lines: 920107.2, 871023.1, 900312.3, 911031.6 and 900105.1 were obtained from MSKCC private collection and tested mycoplasma free. They were grown in advanced DMEM with 15% FBS. The

SNF96.2 MPNST, U2OS osteosarcoma, LNCaP prostate cancer and NIH-3T3 mouse embryonic fibroblast cells were obtained from the American Type Culture Collection and cultured as recommended. All cell lines have been authenticated and tested negative for mycoplasma infection by MycoAlert Plus MycoPlasma Detection Kit (Lonza).

Antibodies in **Table 2.2** were used for immunoblot (IB), immunofluorescence (IF), immunohistochemistry (IHC) and ChIP.

The MEK162 (a MEK inhibitor) and imatinib (a KIT inhibitor) were supplied by Novartis. Dabrafenib was purchased from Active Biochem.

Table 2.2 Antibodies and dilutions for IB, IF, IHC and ChIP

Antibody	Manufacturer	Catalog	Immunoblot	Immunofluorescence	Immunohistochemistr	ChIP
KIT	Cell Signaling Technology	3074	1:1000		1:50	
mouse KIT	Cedarlane	CL8936ap		1:100		
ETV1	Abcam	ab81086	1:500	1:100		1ug
Ano1	LSBio	LS-C88846			1:50	
Acln	abcam	ab49900	1:5000			
Ki67	Abcam	ab16667			1:500	
H3K4me1	Abcam	ab8895				1ug
H3K4me3	Abcam	ab8580				1ug
phosphorylated KIT	Cell Signaling Technology	3037	1:1000			
phosphorylated ERK1/2	Cell Signaling Technology	4370	1:5000	1:400	1:400	
ERK1/2	Cell Signaling Technology	4695	1:5000			
phosphorylated AKT	Cell Signaling Technology	4060	1:1000			
AKT	Cell Signaling Technology	4685	1:1000			
phosphorylated S6	Cell Signaling Technology	2317	1:1000			
S6	Cell Signaling Technology	4856	1:1000		1:400	
cleaved caspase-3	Cell Signaling Technology	9661	1:1000		1:400	
GAPDH	Abcam	ab9385	1:5000			
GFP/YFP	ThermoFisher Scientific	A-21311		1:1000		
S100	DAKO	Z0311			1:2000	
EZH1	Abcam	ab13665	1:1000			
EZH2	Cell Signaling Technology	5246	1:1000			
EED	Abcam	ab4469	1:1000			
SUZ12	Cell Signaling Technology	3737	1:1000			
H3K27ac	Abcam	ab4729	1:1000			1ug
H3K27me3	Cell Signaling Technology	9733	1:1000			1ug
H3K27me3	Millipore	07-449			1:250	

Immunoblotting, Immunofluorescence, Immunohistochemistry and Histology

For immunofluorescence of cryostat sections of the mouse gastrointestinal tract, mouse stomach, small intestine, caecum and large intestine were dissected and fixed in 4% paraformaldehyde for 2h followed by an overnight incubation in 30% sucrose. They were then embedded in OCT, flash frozen and cut into 5- μ m sections using a cryostat. Tissue sections were blocked for 1 hour using 5% goat serum, incubated with primary antibodies at 4 °C overnight and secondary antibody for 2h at room temperature. For immunofluorescence of infected cell lines, cells were fixed in 4% paraformaldehyde for 10 min, permeabilized in 0.1% Triton X-100 and blocked for 1 h using 10% goat serum. Cells were then incubated for 2 h in primary antibody followed by secondary antibody. Slides were mounted using Prolong Gold with DAPI (Invitrogen). Photographs were taken on a Nikon microscope using a Roeper Scientific camera. Slides were mounted using Prolong Gold (Invitrogen) and images were taken on a Nikon Eclipse TE2000-E microscope using a Photometric Coolsnap HQ camera. Images were taken with $\times 20$ (numerical aperture 0.75) or $\times 60$ (numerical aperture 1.4) objectives. Monochrome images taken with DAPI, FITC and Texas Red filter sets were pseudo-colored blue, green and red, respectively, and merged using ImageJ. The exposure, threshold and maximum were identical between experimental and control sample images. Tissue paraffin embedding, sectioning and H&E staining were performed by the Histoserv, Inc. Immunohistochemistry was performed by the MSKCC HOPP automatic staining facility using a Ventana BenchMark ULTRA automated stainer.

Stable Gene Expression

cDNAs for human wild-type *MEK1*, wild-type *MEK2*, *MEK1^{L115P}* mutant, *ME-*

K2^{L119P} mutant were cloned into lentiviral based vector pLX301(Addgene). Lentivirus was produced in 293FT cells by standard methods using amphotropic packaging vector. GIST-T1 cells were infected and selected with 2 μ g/ml puromycin for 5 days at 48 hours post infection for subsequent biochemical and drug treatment studies.

To determine the effect of *ETV1* overexpression on *KIT* transcript levels, cDNA of human *ETV1* was cloned into MSCV-based retroviral vector pMIG (Addgene). Retrovirus was produced in 293FT cells by standard methods using amphotropic packaging vector. GIST882 and GIST-T1 cells were infected with empty vector or pMIG-ETV1.

cDNAs for wild-type human EED and SUZ12 in pDONR vectors were obtained from Harvard PlasmidID and cloned into an murine stem cell virus (MSCV)-based retroviral vector with a sequence encoding a Flag-HA (FH) tag (Addgene plasmid 41033) using Gateway technology.(Sowa, Bennett et al. 2009) To generate cell lines stably expressing these constructs, MPNST724 and ST88-14 cells were infected with empty vector, MSCV-FH-EED or MSCV-FH-SUZ12 and selected using puromycin (2 μ g/ml for 72 h).

RNA Isolation and qRT-PCR

For tissue culture cells, RNA was isolated using E.Z.N.A total RNA kit (Omega). For xenograft and mouse models, explanted tissue samples were grounded in 1000 μ l Trizol (Invitrogen) using a PowerGen homogenizer (Fisher Scientific), followed by addition of 200 μ l chloroform. The samples were then centrifuged at 10,000g for 15 min. The upper phase was mixed with an equal volume of 70% ethanol, and the RNA was further purified using E.Z.N.A total RNA kit (Omega).

For qRT-PCR, RNA was reverse transcribed using High-Capacity cDNA Reverse Transcription Kit (ABI) and PCR was run using Power SYBR Master Mix (ABI) on a Realplex machine (Eppendorf). Expression was normalized to the ribosomal protein RPL27. The primer pairs in **table 2.3** were used.

Chromatin Immunoprecipitation (ChIP) and Sequencing

Chromatin isolation from samples performed as previously described.(Chi, Chen et al. 2010) Briefly, cells were crosslinked for 15min in 1% paraformaldehyde, washed and lysed. Chromatin was sheared using Bioruptor (Diagenode) to fragments of approximately 150 base pairs and was incubated with antibodies, washed and eluted. The eluted chromatin was reverse-cross-linked, and DNA was column purified. The purified ChIP DNA was either analyzed with qRT-PCR directly for quantitative analysis, or was blunt-ended, ligated to Solexa adaptors, amplified with 18 cycles of PCR and sequenced on a Solexa Genome Analyser. We performed independent quantitative PCR validation of separate ChIP samples using **Table 2.4**.

Table 2.3 Primer sets for qRT-PCR

<i>ETV1</i>	Forward	CTACCCCATGGACCACAGATTT
	Reverse	CTTAAAGCCTTGTGGTGGGAAG
<i>KIT</i>	Forward	GGGATTTTCTCTGCGTTCTG
	Reverse	GATGGATGGATGGTGGAGAC
<i>DUSP6</i>	Forward	TGCCGGGCGTTCTACCTGGA
	Reverse	GGCGAGCTGCTGCTACACGA
<i>RPL27</i>	Forward	CATGGGCAAGAAGAAGATCG
	Reverse	TCCAAGGGGATATCCACAGA
<i>FOXN4</i>	Forward	CGTACAGCTGTCTGATCGCC
	Reverse	GGAGCCGCTCATCTTGTCT
<i>IGF2</i>	Forward	TCGCCGAACCAAAGTGGATT
	Reverse	GGGGCAGAGATAGTGGGAGA
<i>TLX1</i>	Forward	AGGCGCTCAAATGACCGAT
	Reverse	ACAAGCCGTTACCTCCACTT
<i>PAX2</i>	Forward	CAGGAATGGTGCCTGGGAG
	Reverse	TTAGTAAGGCGGGGTTGCTG

Table 2.4 Primer sets for CHIP qRT-PCR validation

KIT enhancer1	Forward	GAAGCAAACCCCAGGCTGTA
	Reverse	TTTGCCAACTGTTGCTTCGG
KIT enhancer2	Forward	GGGAAGCACGAAAAACACC
	Reverse	TCGAAGACTTGTCCCTTGGC
KIT enhancer3	Forward	TGGTTTCCTCGTCACAGATCC
	Reverse	GGAAGAAAGGAGCAGCGGAA
PSA promoter	Forward	TGGGCGTGTCTCCTCTGC
	Reverse	CCTGGATGCACCAGGCC
FOXN4	Forward	TCAGAAATGCCACAAGCCCT
	Reverse	CAGTGTTTGTGTGTTGCGGG
IGF2	Forward	GGGGCAGAGATAGTGGGAGA
	Reverse	TCTGTTTCTCTCCGTGCTGT
TLX1	Forward	GACCAGATCCTCAACAGCCC
	Reverse	TATTCTCCGTCCTGGAGGC
PAX2	Forward	GGCTTGCAGAACAAATGCCA
	Reverse	TCTGGAGTTCTCCCTCCCTG

Next-generation sequencing was performed on either an Illumina Genome Analyzer II or a HiSeq2000 with 50-bp single reads. Reads were aligned to the human genome (hg 19) using the Bowtie alignment software within the Illumina Analysis Pipeline and duplicate reads were eliminated for subsequent analysis. Peak calling was performed using MACS 1.4 comparing immunoprecipitated chromatin with input chromatin. On the basis of RefSeq gene annotation, the resultant peaks were separated into promoter peaks (located within ± 2 kb of a transcription start site), promoter distal peaks (located from -50 kb of a transcription start to $+5$ kb of a transcription end) and otherwise intergenic peaks. The ChIP-seq profiles presented were generated using Integrated Genome Browser software of SGR format files.

Cell Viability

Growth curve analysis of the infected cells was performed using Alamar blue cell viability reagent (DAL1100, Life Technologies). For drug treatment experiments, cells were seeded with desired concentration in 96-well plate on day 0 and treated with drugs after 12h to allow cell attach. Triplicate wells were cultured until day 7 and viability was assessed.

Lentiviral Knockdown and CRISPR/Cas9 Mediated Knockout

pLKO.1 constructs against *ETV1* (shETV1: TRCN0000013925, targeting CGACCCAGTGTATGAACACAA in exon 7) were purchased from Open Biosystems and pLKO.1 shScr (targeting CCTAAGGTTAAGTCGCCCTCG) was purchased from Addgene. Lentiviruses were generated by co-transfecting the shETV1 hairpin constructs with psPax2 and pVSVG (Addgene) into 293FT cells (Invitrogen) using Lipofectamine 2000 (Invitrogen). GIST882, GIST48 and GIST-T1 cells were infected shSCR or shETV1 lentivirus. RNA was collected 72

hours post infection and analyzed for *KIT* mRNA by RT-PCR.

In order to knock out *ETV1* in human GIST cell lines, we designed 3 pairs of single guide RNA (sgRNA) sequences for human *ETV1* using the design tool from Feng Zhang Lab and cloned the targeting sequences into the lentiCRISPRv2 vector obtained from Addgene. Lentiviruses for *ETV1* sgRNAs or vector control were generated in 293FT cells by standard methods using amphotropic packaging vector. GIST48 cells were infected with lentivirus for 48 hours and selected with 2 μ g/ml puromycin for 7 days. *KIT* mRNA and protein level were analyzed 16 days post infection. The target guides sequences are shown in **table 2.5**.

Statistics

Fleiss' κ statistic was used to assess the strength of co-occurrence for *NF1* mutation, *PRC2* component mutation and *CDKN2A* mutation. The R package irr was used to calculate the statistic and *P* value.(Fleiss 1971) All statistical comparisons between two groups were performed by Graphpad Prism software used a two-tailed unpaired *t* test.

Table 2.5 CRISPR target guides sequences

sgETV1-1	Forward	CACCGTGAAGAGGTGGCCCGACGTT
	Reverse	AAACAACGTCGGGCCACCTCTTCAC
sgETV1-2	Forward	CACCGCAGCCCTTTAAATTCAGCTA
	Reverse	AAACTAGCTGAATTTAAAGGGCTGC
sgETV1-3	Forward	CACCGGATCCTCGCCGTTGGTATGT
	Reverse	AAACACATACCAACGGCGAGGATCC

CHAPTER THREE

An Oncogenic Role for *ETV1* in Malignant Peripheral Nerve Sheath Tumor

Introduction

Malignant Peripheral Nerve Sheath Tumors (MPNSTs) is a type of highly aggressive soft-tissue sarcomas, accounting for 3-10% of all soft tissue sarcomas. (Vauthey, Woodruff et al. 1995, Lawrence, Brennan et al. 1998, Grobmyer, Reith et al. 2008) There are three subtypes of MPNSTs: neurofibromatosis type I (NF1)-associated (~50%), sporadic (~40%), and radiation-induced (~10%). NF1 is the most common known risk factor for MPNSTs. The prognosis of MPNSTs is very poor with a 5-year survival rate of 30-60% due to primary resistance to standard chemotherapy and radiotherapy. (Evans, Baser et al. 2002, Grobmyer, Reith et al. 2008, Stucky, Johnson et al. 2012, Brennan, Antonescu et al. 2013)

Molecular events contributing to MPNST pathogenesis remained largely unknown until recent comprehensive oncogenomic studies with large number of patient samples. (De Raedt, Beert et al. 2014, Lee, Teckie et al. 2014, Zhang, Wang et al. 2014) It is now known that *neurofibromin 1 (NF1)* loss-of-function mutations or deletions are identified in 72% of non-NF1 associated MPNSTs, together with germline-line mutations in NF1-associated MPNSTs. Alterations of tumor suppressor genes *CDKN2A* and *TP53* are reported in 81% and 33% of MPNSTs, respectively. 92% of sporadic, 70% of NF1-associated and 90% of radiotherapy-associated MPNSTs harbor loss-of-function somatic mutations of polycomb repressive complex 2 (PRC2) components (*EED* or *SUZ12*). Additional oncogenic alterations have also been implicated in MPNSTs, including *KIT*,

PDGFR and *SOX9*. However, the mechanisms through which these oncogenic mutations contribute to MPNST are poorly elucidated.

Here we show that *ETV1*, an *ETS* family transcription factor, is highly expressed in MPNST patient tumors and cell lines. Knockdown of *ETV1* results in growth inhibition of MPNST cells and tumorigenesis in xenograft mouse model. Moreover, overexpression of *ETV1* protein in combination with *NF1* loss leads to malignant transformation of NIH3T3 cells and tumorigenic growth in SCID mice, suggesting their potential cooperative roles in MPNST pathogenesis. Transcriptome profiling and global analysis of *ETV1*-binding sites show that *ETV1* regulates core sets of genes that are important for oncogenesis. These observations suggest an oncogenic role for *ETV1* in MPNST pathogenesis.

Results

ETV1 is highly expressed in MPNSTs

Previous studies indicate that chromosome 7p is frequently amplified in MPNSTs. (Yang, Ylipaa et al. 2011) *ETV1*, located on chromosome 7p21, has also been indicated to highly expressed in MPNST. (Miller, Rangwala et al. 2006) We have mined the publically available expression datasets and found that *ETV1* is significantly highly expressed in MPNST compared to many other sarcoma tumor types (**Figure 3.1A**). (Henderson, Guiliano et al. 2005) *ETV1*, an *ETS* family transcription factor, has been reported as potent oncogene in Ewing sarcoma, melanoma, prostate cancer and gastrointestinal stromal tumors. (Mertens, Antonescu et al. 2009, Chi, Chen et al. 2010, Jane-Valbuena, Widlund et al. 2010, Yang, Ylipaa et al. 2011) Quantitative RT-PCR showed that *ETV1* messenger RNA is highly expressed in the majority of MPNST tumor samples (17/18) and all MPNST cell lines (8/8) in comparison to the U2OS osteosarcoma cell line and the LNCaP

prostate cancer cell line known to overexpress ETV1 through translocation (**Figure 3.1B**). (Tomlins, Laxman et al. 2007) Immunoblot analysis further confirmed the increased level of ETV1 protein in MPNST cell lines and one MPNST patient tumor (**Figure 3.1C**). Together these data show that *ETV1* is highly expressed in MPNST both at the mRNA and the protein levels.

ETV1 is required for MPNST cell survival

To evaluate the role of ETV1 for MPNST pathogenesis, we used two independent short hairpin RNA (shRNA) constructs that effectively reduced *ETV1* mRNA and protein levels, as well as a negative control constructs containing scramble shRNA (**Figure 3.2A, B**). Infection with both shRNAs resulted in marked growth inhibition of all three MPNST cell lines, whereas control scramble shRNA did not affect cell growth. Consistent with the level of *ETV1* knockdown, ETV1 sh2 showed more significant growth suppression than ETV1 sh1 in MPNST724 and ST88-14 cells (**Figure 3.2C**). To eliminate the possibility that the growth inhibition effects observed were resulted from off-target effects of ETV1 shRNAs, we also tested the shRNA in U2OS cells that were previously shown not depend on *ETV1* for survival. (Chi, Chen et al. 2010) The growth of U2OS cells was largely unaffected although ETV1 sh2 showed slight toxicity. Moreover, ETV1 knockdown induced significant apoptosis in all three MPNST cell lines as indicated by active cleaved caspase 3 (**Figure 3.2B**). Cell cycle analysis showed that suppression of ETV1 did not affect cell proliferation of MPNST cells (**Figure 3.3** and data not shown), suggesting that *ETV1* was not required for cell growth. Collectively, these observations indicate that *ETV1* is required for MPNST cell survival.

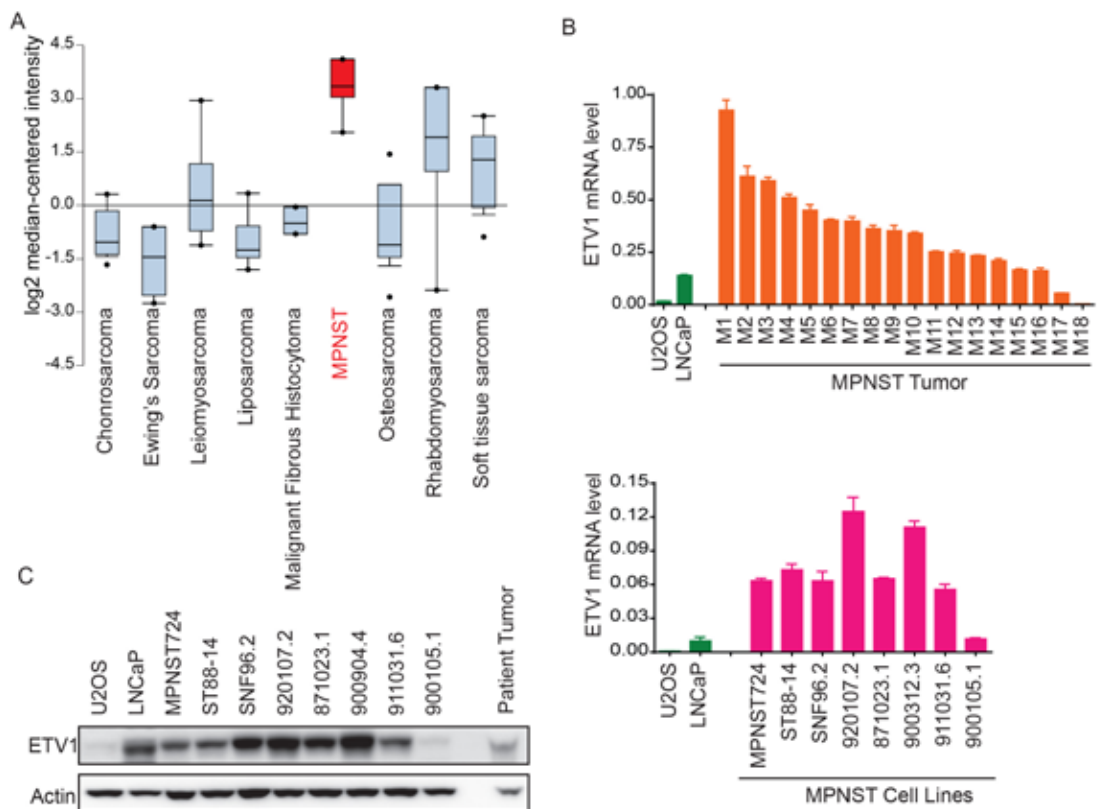


Figure 3.1 *ETV1* is highly expressed in MPNST

A, Expression of *ETV1* in multiple tumor types from the ExpO data set. Box, 25th–75th percentile; error bar, 10th–90th percentile; dots, outliers. **B**, *ETV1* mRNA levels by qRT-PCR of MPNST patient tumors (top), MPNST cell lines (bottom) and non-MPNST samples, whose details are described in Methods. Mean \pm s.e.m., $n = 3$. **C**, Immunoblotting of selected tumor tissues and cell lines from **B**.

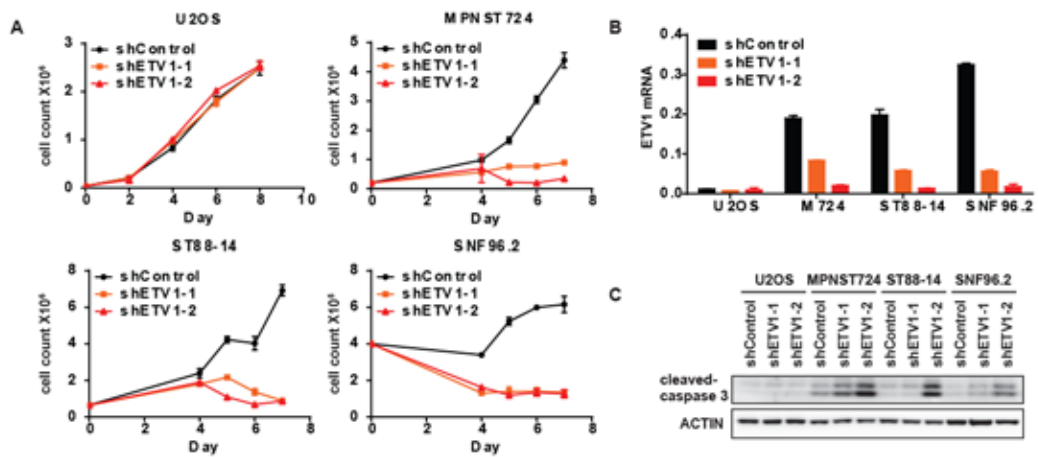


Figure 3.2 *ETV1* is required for MPNST cell survival

A, Growth curves of MPNST and U2OS cells after shRNA-mediated *ETV1* suppression compared with control. Mean \pm s.e.m., $n = 3$. **B**, *ETV1* mRNA levels by qRT-PCR of cells after 48 hours of shRNA knockdown in **A**. Mean \pm s.e.m., $n = 3$. **C**, Immunoblotting of *ETV1* and cleaved-caspase 3 protein for cells in **B**.

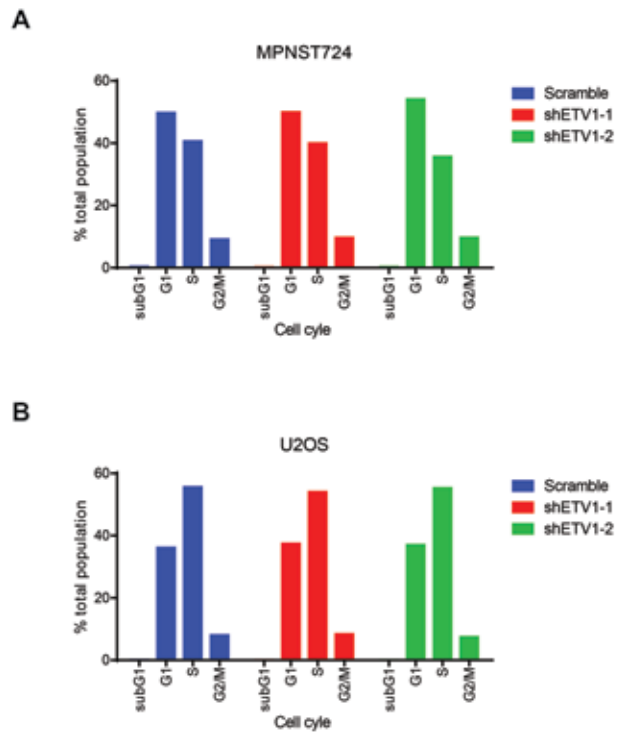


Figure 3.3 *ETV1* suppression does not affect cell cycle in MPNST724 cells
A, Cell cycle analysis of MPNST724 cells 48 hours after infecting with shRNA.
B, Cell cycle analysis of U2OS control cells 48 hours after infecting with shRNA.
 Mean \pm s.e.m., $n = 3$.

ETV1 depletion attenuates MPNST tumorigenesis

Next, we assessed the requirement of *ETV1* for MPNST tumorigenesis *in vivo*. We subcloned the more potent shRNA sequence ETV1 sh2 to a doxycycline (dox)-inducible shRNA system, enabling knockdown *ETV1* with doxycycline treatment (**Figure 3.4A**). Stable cell lines containing dox-inducible shRNA targeting *ETV1* or scramble were generated in MPNST724 cells. Using this system, *ETV1* mRNA and protein level were effectively decreased with doxycycline (**Figure 3.4B**). MPNST724 cells with scramble shRNA or ETV1 sh2 shRNA were subsequently injected into immunodeficient SCID mice and tumor growth were measured (**Figure 3.5A**). To evaluate the importance of *ETV1* for MPNST tumor initiation, SCID mice were fed with doxycycline-containing water from same day as the cell grafted. Compare to scramble shRNA controls, tumor appearance for cells with *ETV1* sh2 shRNA was delayed compared to MPNST scramble shRNA (**Figure 3.5B**). Mice were also allowed to establish tumors without doxycycline treatment for 2 months. When *ETV1* was depleted with doxycycline after tumor established, tumor growth rate was significantly decreased compared to controls (**Figure 3.5C**). When tumors were exacted at the end of experiments, those tumors that did grow out showed comparable ETV1 protein expression with control tumors, indicating they have escaped *ETV1* knockdown (**Figure 3.6**). These data show that *ETV1* is required for MPNST tumor establishment and maintenance *in vivo*.

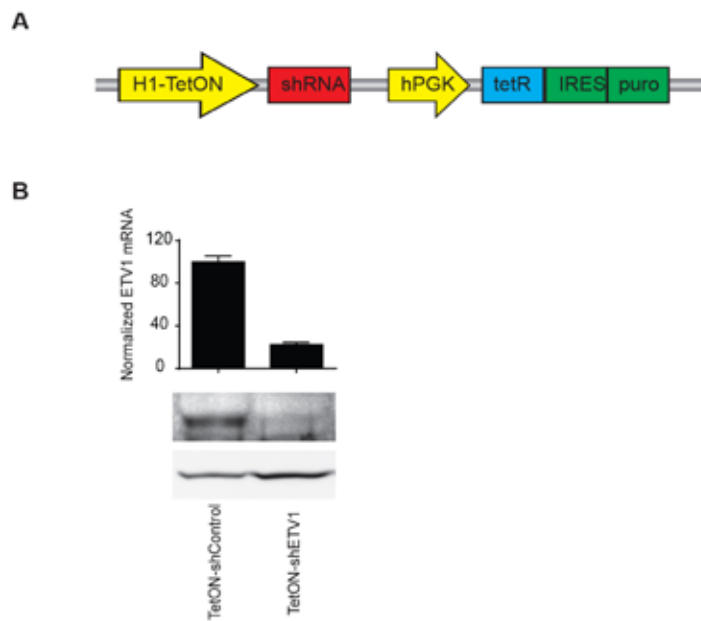


Figure 3.4 Doxycycline-inducible shRNA can efficient knockdown *ETV1*
A, Schematic showing the doxycycline-inducible shRNA construct. **B**, *ETV1* mRNA levels by qRT-PCR and immunoblotting of ETV1 protein of cells after shRNA knockdown for 48 hours.

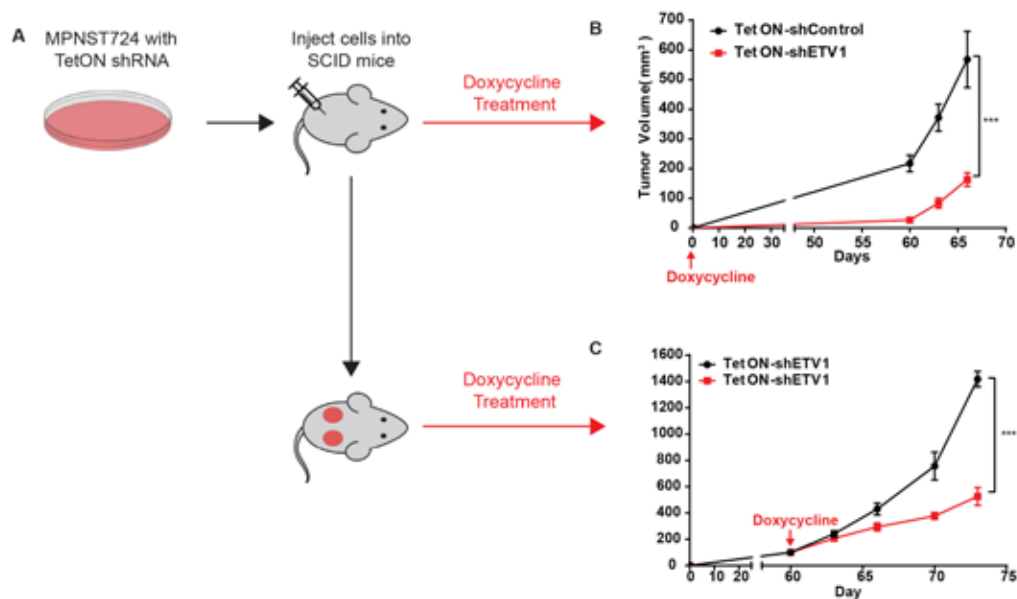


Figure 3.5 *ETV1* depletion suppresses MPNST tumor initiation and maintenance

A, Schematic of experimental design for xenografts in **B** and **C**. **B**, Tumor growth of MPNST724 xenograft with doxycycline-inducible shRNA targeting scramble or *ETV1*. Mice were fed with doxycycline water at the same day of grafting. Mean \pm s.e.m., $n = 8$. **C**, Tumor growth of MPNST724 xenograft with doxycycline-inducible shRNA targeting scramble or *ETV1*. Mice were fed with doxycycline 60 days after grafting. Mean \pm s.e.m., $n=8$.

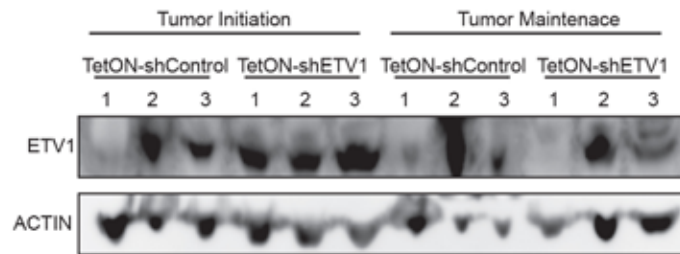


Figure 3.6 MPNST tumors growing with *ETV1*shRNA escaped *ETV1* knock-down
 Immunoblotting of ETV1 protein in xenograft tumors at the end of experiments.

ETV1 overexpression cooperates with *NF1* loss in tumorigenesis

Loss-of-function mutations in *NF1* are identified in the majority of MPNSTs. We evaluated the potentially cooperativity between *NF1* loss and *ETV1* overexpression with the NIH3T3 oncogene transformation system. *ETV1* or empty vector control were expressed in NIH3T3 cells, *Nf1* were then knockout with clustered regularly-interspaced short palindromic repeats (CRISPR) system. Immunoblot confirmed that ETV1 protein was overexpressed and *Nf1* protein was depleted in NIH3T3s (**Figure 3.7A**). Cells harboring different plasmid combination were grafted into immunodeficient SCID mice to allow tumor formation. As expected, *Nf1* knockout NIH3T3 cells were transformed and grew tumors in SCID mice, while *ETV1* overexpression was not able to transform NIH3T3 cells and no tumor formed (**Figure 3.7B**). *ETV1* overexpression strongly cooperated with *Nf1* knockout to promote tumor growth at faster rate than *Nf1* knockout alone, suggesting *ETV1* overexpression might cooperate with *NF1* loss in MPNST pathogenesis.

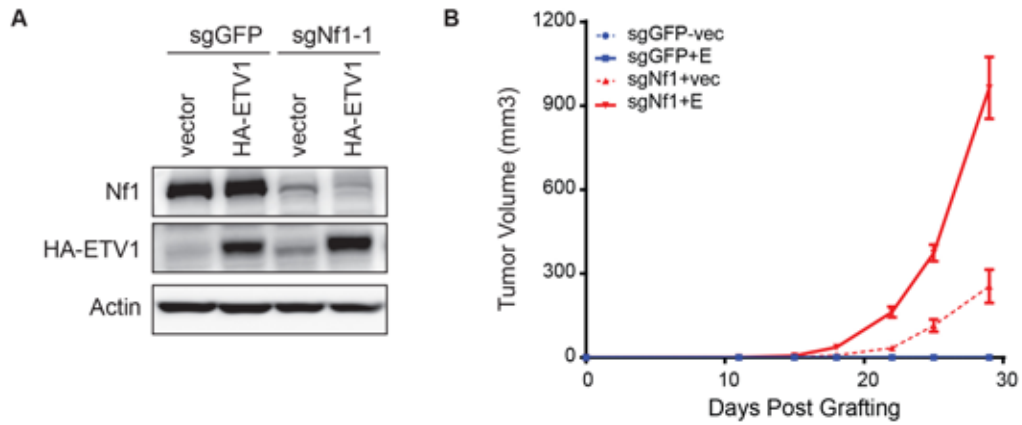


Figure 3.7 *ETV1* cooperates with *Nf1* loss to drive tumorigenesis in NIH3T3
A, Immunoblotting of Nf1 and ETV1 in NIH3T3 cells. **B**, Tumor growth of NIH3T3 xenografts. Mean \pm s.e.m., $n = 10$.

ETV1 regulate context for MPNSTs

To gain insights into the role of *ETV1* in MPNST pathogenesis, we performed RNA-sequencing for MPNST cells after *ETV1* knockdown with shRNA to identify *ETV1* target genes in MPNST. Ranked gene list based on the average gene expression change after *ETV1* knockdown was generated to minimize cell-line-specific and off-target effects (**Figure 3.8A**). Chromatin immunoprecipitation and deep sequencing (ChIP-seq) was also performed in three MPNST cells to identify *ETV1* genome-wide binding sites. Gene Set Enrichment Analysis (GSEA) showed that *ETV1*-regulated gene sets in cancer types such as GIST (**Figure 3.8B**) and Ewing sarcoma (data not shown), suggesting that *ETV1* could regulate a common set of gene targets between different cancer types during tumorigenesis. In addition, multiple cancer-related pathways were significantly enriched indicating that *ETV1* might play an important role in MPNST pathogenesis (**Figure 3.8C, D**). Moreover, among the genes that were highly down-regulated by *ETV1* knockdown, many were directly regulated by *ETV1* as indicated by *ETV1* binding peaks in ChIP-seq analysis (**Figure 3.8E-G**). Our data suggest that *ETV1* might regulate an important cellular context for MPNST pathogenesis.

Discussion

In this study, we identified overexpression of *ETV1* in majority MPNST patients and cell lines. Subsequent studies showed that *ETV1* is required for MPNST cell survival and tumorigenesis. Combination of *ETV1* overexpression with aberrant MAP kinase signaling through *Nf1* knockout showed synergistically oncogenic potential in NIH3T3 mouse fibroblast cells. Transcriptome and cistrome analysis suggested a potential oncogenic context that is defined by *ETV1* for MPNST pathogenesis. Taken together, our observations strongly suggest an important oncogenic role for *ETV1* in MPNST.

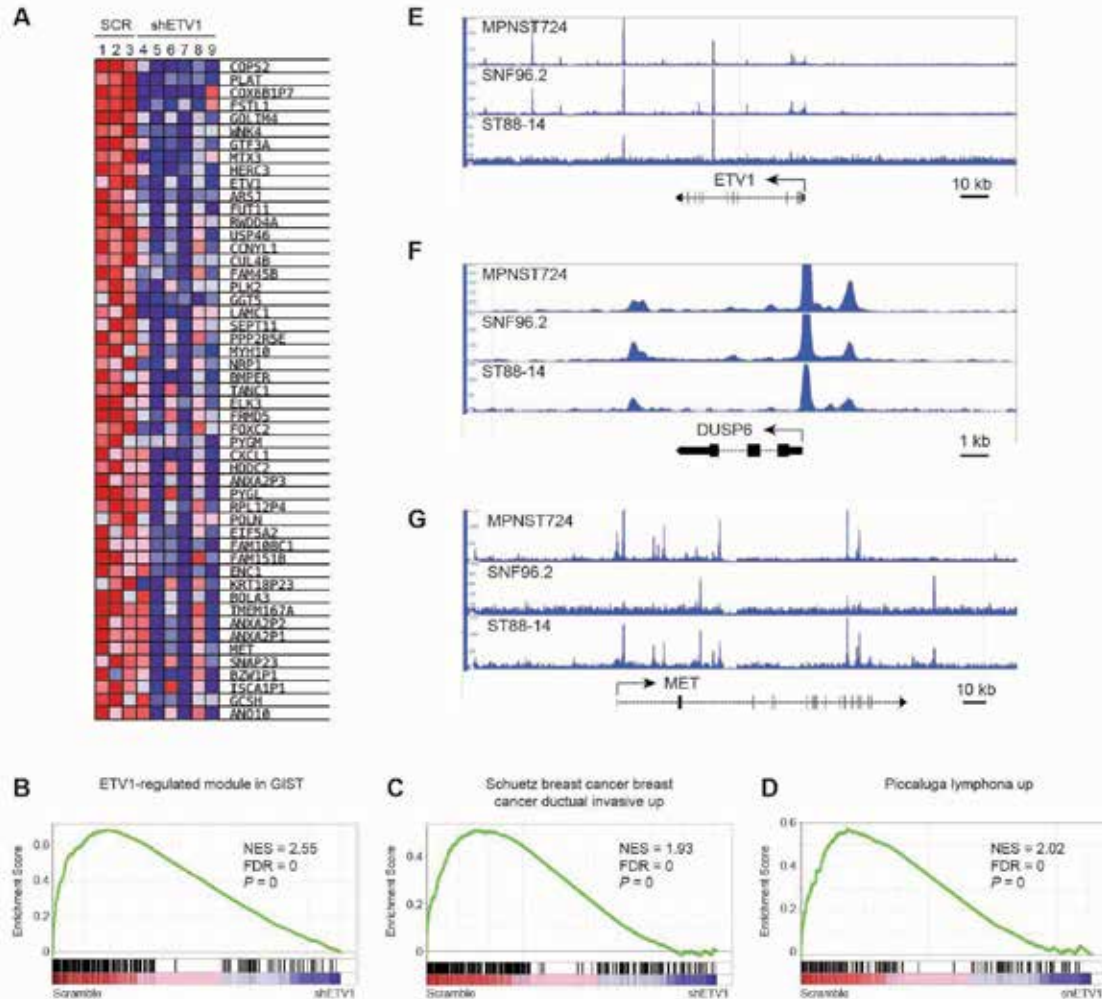


Figure 3.8 *ETV1* regulates important cellular context for MPNST tumorigenesis

A, Heatmap of expression of the top 50 genes with average down-regulation greater than 2-fold. **B-D**, GSEA plots of the shETV1 ranked list using ETV1-regulated module in GIST (**B**), breast cancer invasive gene module (**C**) and lymphoma related module (**D**). NES, normalized enrichment score. FDR, false discovery rate. **E-G**, ETV1 reads of ETV1 target genes, ETV (**E**), DUSP6 (**F**) and MET (**G**) in three MPNST cell lines.

Recent studies have pointed to the important role of ETV1 in cancer pathogenesis in Ewing sarcoma, melanoma, prostate cancer and gastrointestinal stromal tumors. We have described the oncogenic role of ETV1 into MPNST pathogenesis, expanding our understanding for *ETV1* and the mechanism through which ETV1 contribute tumorigenesis in different cellular context. With further integrated analysis of different cancer types together, we might be able to define a core oncogenic signature of *ETV1* or *ETS* transcription factors in these cancer types.

Cooperativity between *ETV1* and MAP kinase signaling is shown to be critical for *ETV1*-driven pathogenesis in melanoma with *RAS/RAF* mutations, in gastrointestinal stromal tumors with activated *KIT* mutations, or here in MPNST with *NF1* loss. Up-regulated MAP kinase signaling stabilizes ETV1, resulting in deregulated *ETV1* protein and *ETV1*-mediated oncogenic signaling. In gastrointestinal stromal tumors, ETV1 further forms a positive feedback loop with KIT mutation through direct regulation of KIT transcription.(Chi, Chen et al. 2010) Loss of *NF1* and *ETV1* overexpression in MPNST further emphasizes the importance of cooperation between oncogenic driver and signaling.

The dependencies of *ETV1* for survival and tumorigenesis in MPNST indicate that *ETV1* is a potential drug target for MPNST. Despite the difficulty to direct targeting transcription factors, ETV1 protein is tightly regulated by MAP kinase signaling which allows indirect-targeting of ETV1 with MAP kinase signaling inhibition.(Chi, Chen et al. 2010, Vitari, Leong et al. 2011, Ran, Sirota et al. 2015) Thus, effective MAP kinase signaling inhibition with single agent or combination agents could be helpful for MPNST management. Moreover, small molecule inhibitors of ETV1 are under development, and could be a novel therapeutic agent for MPNST if proven to be effective in MPNST as well.(Rahim, Minas et al. 2014)

CHAPTER FOUR

PRC2 is Recurrently Inactivated Through EED or SUZ12 Loss in Malignant Peripheral Nerve Sheath Tumors

Introduction

MPNSTs arise from peripheral nerves and associated cellular components and represent a highly aggressive subtype of soft tissue sarcoma (Brennan, Antonescu et al. 2013). MPNSTs metastasize early and are often resistant to radiotherapy and chemotherapy. Conventional MPNSTs present in three distinct clinical settings: sporadically, in association with neurofibromatosis type I (NF1-associated) or prior radiotherapy (radiotherapy-associated), respectively accounting for approximately 45%, 45% and 10% of cases (Rodriguez 2012, LaFemina 2013). Histologically, MPNSTs are characterized by intersecting fascicles of monotonous spindle cells with hyperchromatic nuclei and high mitotic counts with focal areas of necrosis, but accurate diagnosis remains challenging due to the lack of specific immunohistochemical (IHC) and molecular biomarkers (Rodriguez 2012, Antonescu, Scheithauer et al. 2013). Among NF1-patients, loss of the non-mutant allele is thought to be the key driver in benign NF1-associated neurofibromas (Taylor 2011). Little is known of the genetic alterations that mediate progression from neurofibromas into MPNST in NF1-patients or of the molecular pathogenesis of sporadic and radiotherapy-associated MPNSTs.

Results

To investigate the molecular basis of MPNSTs, we performed whole-exome sequencing (WES), DNA copy-number and loss-of-heterozygosity (LOH) profiling

and whole-transcriptome sequencing (RNA-seq) of a discovery cohort consisting of normal-tumor paired tissues of 15 MPNSTs from 12 patients (6 NF1-associated, 4 sporadic, 4 radiotherapy-associated and 1 epithelioid MPNSTs). Epithelioid MPNST is a rare histological variant of MPNST, composed of exclusively epithelioid malignant cells with diffuse immunoreactivity for the S100 protein, and is not associated with NF1 (Antonescu 2013).

We identified four frame-shift and one splice-site mutations in *EED* (**Figure 4.1A, C** and **Figure 4.2**). RNA-seq validated aberrant *EED* splicing in the splice-site mutated sample (**Figure 4.3A**). All five samples showed LOH of the *EED* locus, three samples (11T, 12T, 14T) by heterozygous deletion of the normal allele (**Figure 4.2B**) and two samples (15T, 16T) by copy-neutral LOH (**Figure 4.3B**). This data suggests that samples with *EED* mutation have complete loss of *EED* function.

We further identified two homozygous and five heterozygous deletions of *SUZ12* (**Figure 4.1A,C, Figure 4.2** and **Figure 4.4A**). We examined RNA-seq profiles of the *SUZ12* transcript among the five heterozygous loss samples. Two samples, 9T and 12T (with *EED* mutations encoding p.His213fs), expressed full-length *SUZ12* transcript, indicating that the remaining *SUZ12* copy is intact (**Figure 4.2B** and data not shown). Remarkably, the other three samples display structural alterations of *SUZ12* transcript, starting at exon 6, exon 10 and exon 4 in 2T, 7T and 13T, respectively (**Figure 4.4B-D**).

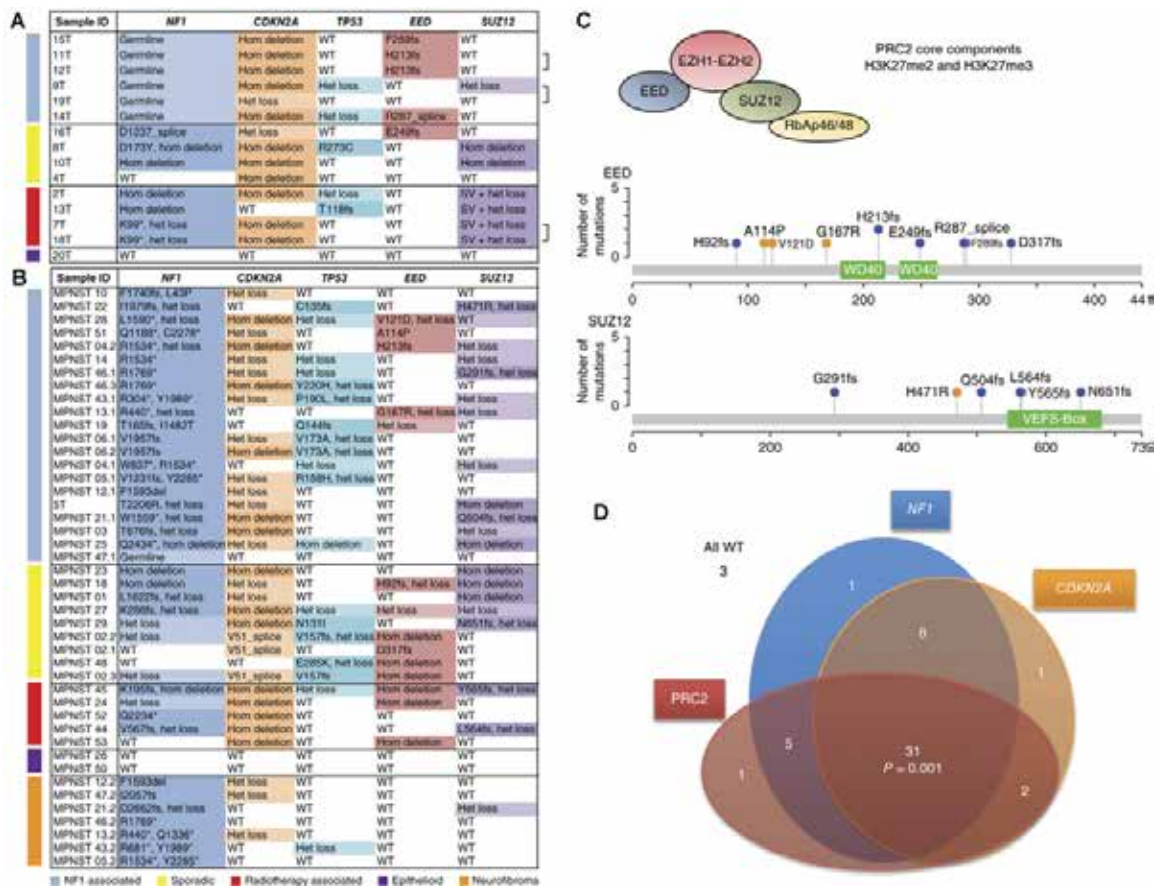


Figure 4.1 The most frequent genetic alterations in MPNST (NF1 associated, sporadic, radiotherapy associated and epithelioid) and neurofibroma
A,B, Nonsynonymous single-nucleotide variants (SNVs) and copy number variants (CNVs) in 15 MPNSTs with matched normal samples identified by whole-exome sequencing, SNP6.0 array analysis and RNA-seq **A** and in 37 MPNSTs and 7 neurofibromas identified by targeted sequencing (IMPACT) **B**. Brackets indicate two different tumor samples from the same individual. WT, wild type; hom, homozygous; het, heterozygous; SV, structural variation (light shading indicates heterozygous loss and dark shading indicates homozygous loss). **C**, Schematics of the nonsynonymous SNVs observed in the PRC2 core components EED and SUZ12 in 15 MPNST samples analyzed by whole-exome sequencing and 37 MPNST samples analyzed by custom IMPACT. **D** Schematic of the overlap of mutations affecting *NF1*, PRC2 components (*EED* or *SUZ12*) and *CDKN2A* in all MPNSTs (NF1 associated, sporadic, radiotherapy associated and epithelioid). With Fleiss' κ statistics, three-way comparison of *NF1*, *CDKN2A* and PRC2 component (*EED* or *SUZ12*) genetic alteration suggested that they significantly co-occur: $\kappa = 0.21$, $P = 0.001$.

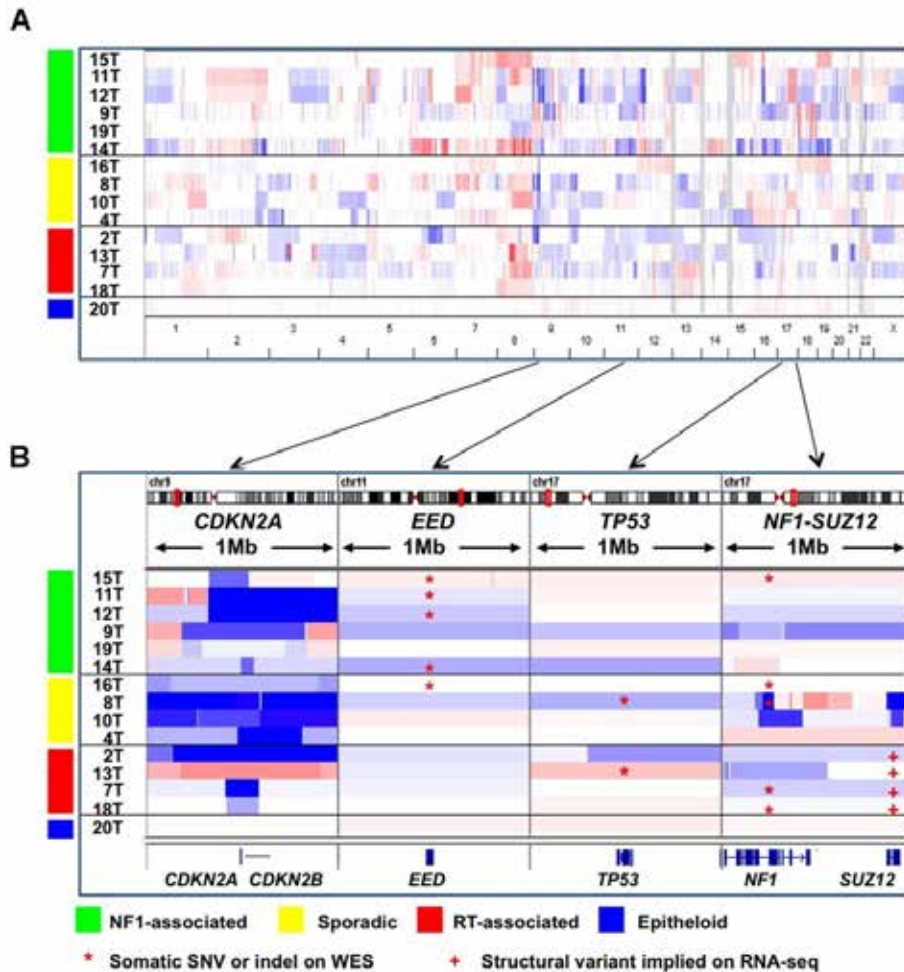


Figure 4.2 Summary of copy number variation by SNP6.0 array of MPNSTs
A, Whole-genome view of copy number variations (CNVs) using an integrative genome browser (IGV) in the 15 MPNST samples. The clinical subtype of MPNST is shown on the left: NF1 associated (green), sporadic (yellow), RT associated (red) and epithelioid (blue). **B**, Zoomed-in view of 1-Mb windows around *CDKN2A*, *EED*, *TP53* and *NF1-SUZ12*. Somatic single-nucleotide variations (SNVs) and indels are annotated by red asterisks. Transcript alterations seen on RNA-seq likely due to DNA structural variations are annotated by red plus signs.

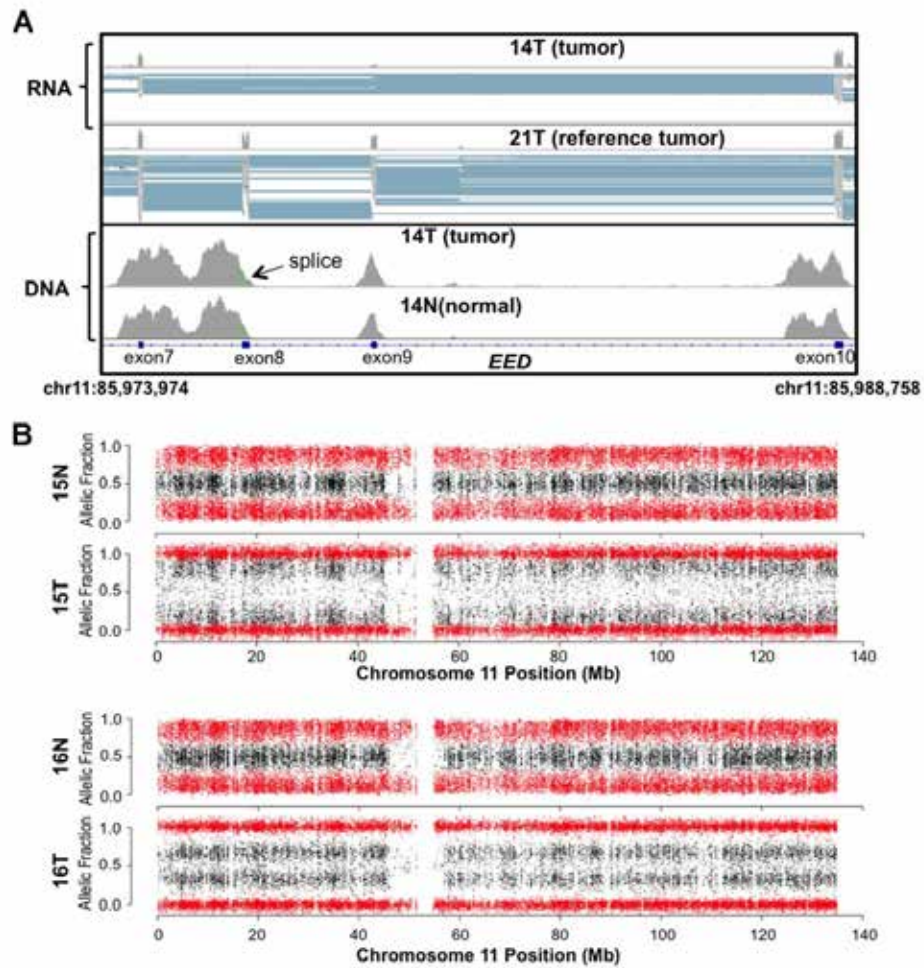


Figure 4.3 *EED* alterations in MPNST

A, Example of an *EED* splice-site mutation in sample 14T. DNA sequencing shows a donor splice-site mutation of exon 8 of the remaining intact allele. (The green line indicates an SNV relative to the reference genome, and all other SNVs represent SNPs found in both germline and tumor samples.) RNA-seq analysis shows that the *EED* transcript aberrantly splices from exon 7 into exon 10, skipping exons 8 and 9. The normal RNA splicing pattern of a reference *EED*-intact tumor (sample 21T) is shown as a reference. **B**, Scatter plot of the allelic fraction of SNPs from the SNP6.0 array analysis of chromosome 11 for tumors 15T and 16T. The data show that the entire chromosome 11 in both tumors has undergone copy-neutral LOH.

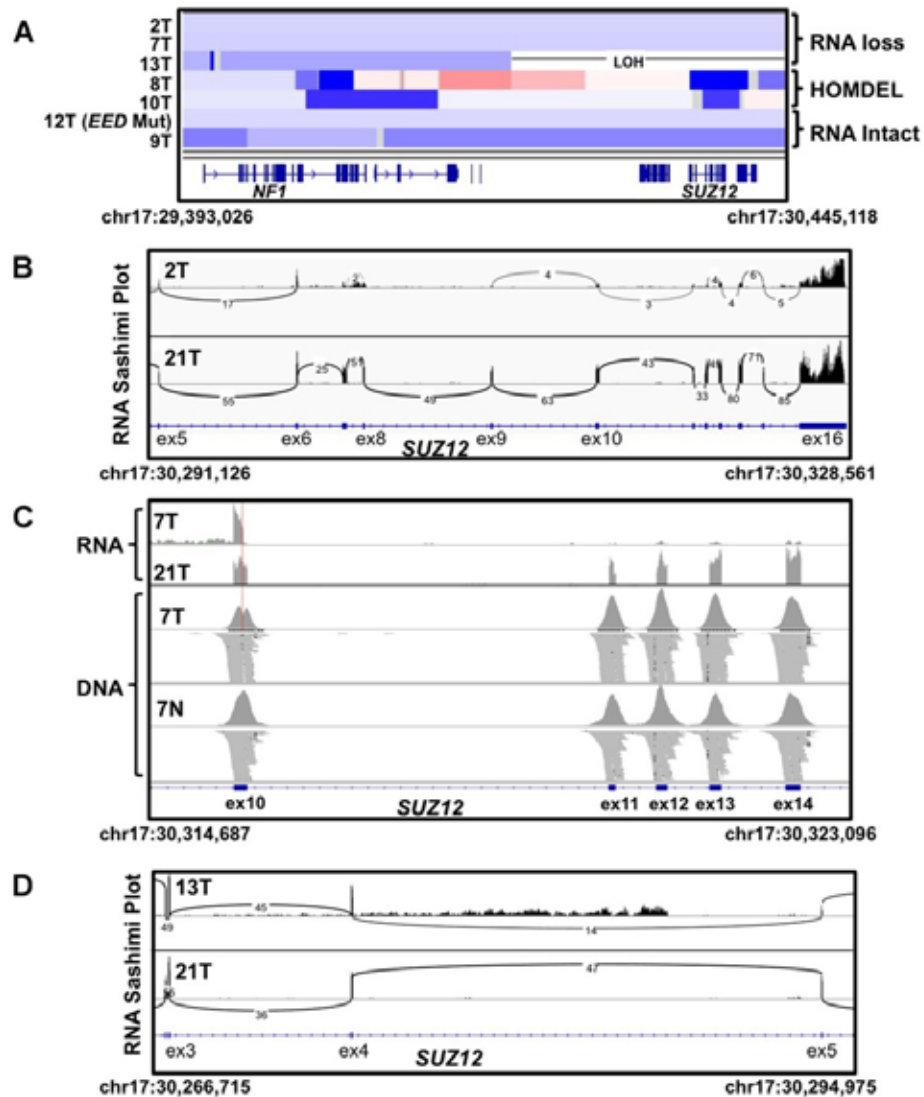


Figure 4.4 *SUZ12* structural variants in MPNST

A, Copy number view of *SUZ12* in seven MPNST samples that have either copy number loss of copy-neutral LOH. Samples 2T, 7T and 13T have structural variants of the remaining allele. Samples 8T and 10T have homozygous deletion. Samples 12T and 9T have intact wild-type RNA. **B**, Sashimi plot showing that sample 2T has *SUZ12* transcript truncation after exon 6 (sample 21T with intact transcript is shown as a reference). **C**, RNA-seq view of sample 7T showing loss of the transcript in the middle of exon 10. DNA sequencing shows that there is a translocation at this position (21T is shown as a reference). **D**, Sashimi plot showing that sample 13T has *SUZ12* transcript truncation after exon 4 with reads mapping to intron 4 (21T is shown as a reference).

These are likely due to local genomic rearrangements of the remaining copy, which were not identified by standard WES analysis. Indeed, for 7T and 18T, derived from two tumors from the same patient, there is a DNA break in exon 10 upon manual examination of WES data (**Figure 4.4C**). We designated these cases as having structural variation and heterozygous loss at the *SUZ12* locus, and, intriguingly, all constituted in radiotherapy-associated MPNSTs (**Figure 4.1A**).

EED and SUZ12 are the core components of PRC2, and together with EZH1/EZH2, establish and maintain the di- and tri-methylation of lysine 27 of histone H3 (H3K27me2 and H3K27me3)(Margueron and Reinberg 2011). *EED* and *SUZ12* genetic alterations were mutually exclusive and were collectively found in 80% (12/15) of all MPNSTs (**Figure 4.1A, C**). We did not observe any genetic alterations in other PRC2 core members, including *EZH1* and *EZH2*.

We found recurrent nonsense mutations and Homozygous deletion in *NF1* in 87.5% (7/8) of sporadic and radiotherapy-associated MPNSTs (**Figure 4.1A** and **Figure 4.2**). These data, in combination with the germline mutations in *NF1* in NF1-associated MPNSTs, suggest that NF1 is a uniquely important tumor suppressor in MPNSTs. Alterations of the *CDKN2A* locus and of *TP53* have been reported in MPNSTs(Menon, Anderson et al. 1990, Kourea, Orlow et al. 1999, Nielsen, Stemmer-Rachamimov et al. 1999, Perrone, Tabano et al. 2003)).

We observed homozygous deletion and heterozygous loss of the *CDKN2A* locus in 73% (11/15) and 13% (2/15) of MPNSTs, respectively. We also observed non-synonymous mutations and heterozygous loss in *TP53* in 13% (2/15) and 20% (3/15) of MPNSTs. We did not identify other recurrent somatic alterations with relatively high frequency.

Next, we used a targeted sequencing approach (IMPACT(Won, Scott et al. 2013), to characterize a validation cohort of formalin-fixed, paraffin-embedded samples consisting of 37 MPNSTs and 7 neurofibromas from 32 individuals (**Figure 4.1B**). Combining the discovery and validation cohorts, we observed PRC2 mutations in 70% (19/27) of NF1-associated, 92% (12/13) of sporadic and 90% (8/9) of radiotherapy-associated MPNSTs (**Figure 4.1A-D**). Genetic alterations in *NF1* were identified in 82% (18/22) of sporadic and radiotherapy-associated MPNSTs. Genetic alterations in *CDKN2A* and *TP53* were found in 81% (42/52) and 42% (22/52) of all MPNSTs, respectively (**Figure 4.1A, B**). There is a significant co-occurrence of *NF1*, *CDKN2A* and PRC2 genetic alterations (Fleiss' κ statistics, $k = 0.21$, $P = 0.001$)(Fleiss 1971), suggesting that these are three critical pathways in pathogenesis of conventional MPNSTs. In the seven NF1-associated neurofibromas, we observed few PRC2 and *CDKN2A* alterations suggesting they may be associated with malignant progression to MPNST. None of the three epithelioid MPNSTs had genetic alterations in the three critical pathways, suggesting that they represent a distinct entity.

To understand the effect of PRC2 loss, we performed gene expression analysis in 16 MPNSTs. In principal component analysis (PCA), all samples with *EED* mutations or *SUZ12* homozygous deletion clustered together and were separated from the others by the first principal component (PC1) (**Figure 4.1A** and **Figure 4.5A**). Of the five samples with heterozygous loss of *SUZ12*, three with structural variation of the remaining *SUZ12* copy (2T, 7T, 13T) and one with an *SUZ12* mutation encoding p.His213fs (12T) clustered with the group with PRC2 loss and one with an intact *SUZ12* transcript (9T) clustered with the group with wild-type PRC2. These observations highlight the complexity in identifying structural variations that accurately determine PRC2 status in cases of heterozygous *EED* loss.

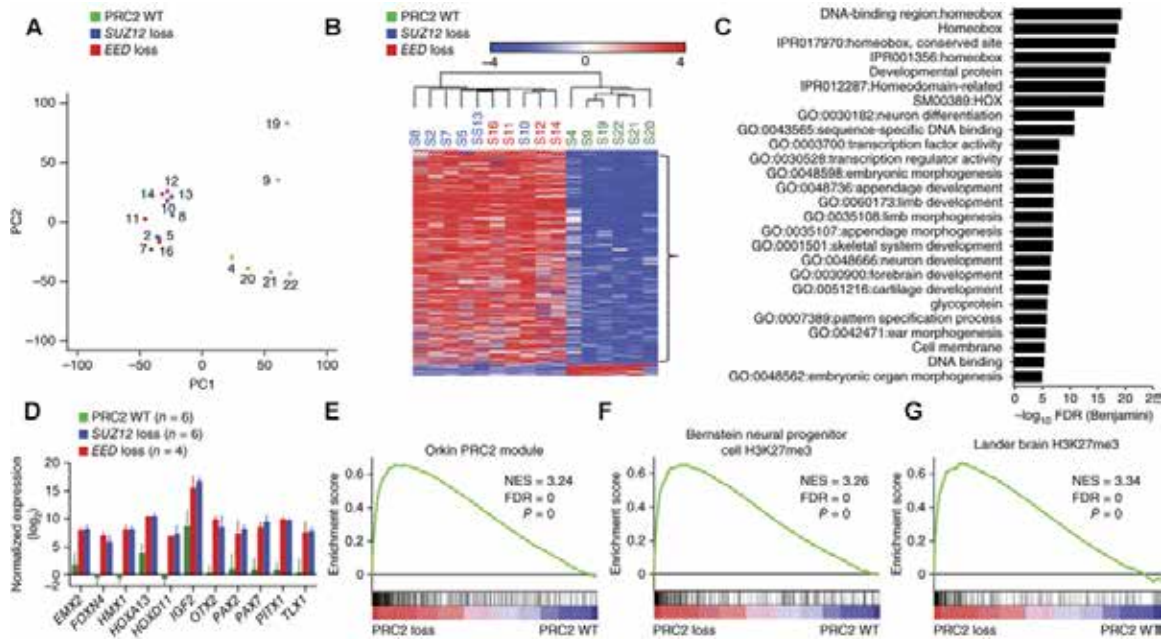


Figure 4.5 MPNSTs with PRC2 loss exhibit distinct gene expression pattern from MPNSTs with wild-type PRC2, signifying activation of developmentally suppressed pathways

A, PCA of the MPNST whole-transcriptome data showed that the samples with wild-type PRC2 and those with PRC2 component (*SUZ12* and *EED*) loss segregate by principal component 1 (PC1). Each sample is colored on the basis of its corresponding PRC2 mutational status derived from whole-exome sequencing data, except for samples 21 and 22, which are colored on the basis of manual examination of the RNA-seq data for mutations in PRC2 components. **B**, Heat map of genes with significantly different expression in MPNSTs with PRC2 loss and those with wild-type PRC2 identified by RNA-seq. Clustering was based on the 479 most differentially expressed genes with a false discovery rate (FDR) of <0.05 and a fold change in expression of >8.0. Samples are colored on the basis of PRC2 mutational status. The key shows mean log₂-transformed normalized fold change. **C**, GO analysis of the differentially upregulated genes in MPNSTs with PRC2 loss in comparison to those with wild-type PRC2. **D**, Gene expression by RNA-seq of a representative group of developmental master regulators and imprinted genes in MPNSTs with PRC2 loss and those with wild-type PRC2. Error bars, s.e.m. (**E-G**) GSEA plots of the ranked list of differentially expressed genes in MPNSTs with PRC2 loss and those with wild-type PRC2 generated using three gene sets: PRC2 module (**E**), and H3K27me3 targets in brain (**G**), and neural precursor cells (**F**). NES, normalized enrichment score.

To explore the transcriptional consequence of PRC2 loss, we generated a gene set composed of genes that were differentially expressed in MPNSTs with loss of PRC2 and those with wild-type PRC2. Hierarchical clustering of these genes robustly separated the MPNSTs with loss of PRC2 and those with wild-type PRC2. The vast majority of differentially expressed genes (455/479; 95%) were upregulated in MPNSTs with PRC2 loss, consistent with the role of PRC2 in transcriptional repression (**Figure 4.5B**). In Gene ontology (GO) analysis, known PRC2 suppressed targets, including homeobox transcription factors and genes associated with development and morphogenesis, were highly enriched among genes upregulated in PRC2-loss MPNSTs (**Figure 4.5C**). The expression of several prototypical PRC2-suppressed genes confirmed this difference (**Figure 4.5D**). In Gene Set Enrichment Analysis (GSEA), the most significantly enriched gene sets upregulated in MPNSTs with PRC2 loss included the 'PRC2 module' defined by genes bound by PRC2 components in mouse embryonic stem (ES) cells (Kim, Woo et al. 2010) (**Figure 4.5E**) and H3K27me3 target genes in neural precursor cells (Mikkelsen, Ku et al. 2007) (**Figure 4.5F**) and brain tissue (Meissner, Mikkelsen et al. 2008) (**Figure 4.5G**). These data indicate that loss of function in PRC2 results in distinct transcriptome changes, including activation of developmentally regulated master regulators and imprinted genes (for example, *IGF2*).

We evaluated H3K27me3 levels by immunohistochemistry in formalin-fixed, paraffin-embedded samples of MPNST and neurofibroma. Whereas MPNSTs with wild-type PRC2 showed robust staining for H3K27me3, MPNSTs with PRC2 loss showed complete loss of H3K27me3 in tumor cells and preservation of H3K27me3 staining in stromal cell (**Figure 4.6A**). Positive and negative immunostaining for H3K27me3 were highly concordant with a genetic status of wild-type PRC2 and homozygous PRC2 loss, respectively (**Figure 4.6B**). However, heterozygous loss of PRC2 components was not predictive of H3K27me3 staining in immunohistochemistry (**Figure 4.6B**). Among the samples with heterozygous loss for which associated RNA-seq data were available, clustering by transcriptional pattern matched H3K27me3 immunohistochemistry results. This finding suggests that DNA sequencing (exome or IMPACT) alone cannot predict PRC2 functional status in all MPNSTs and that H3K27me3 immunohistochemistry might be more accurate.

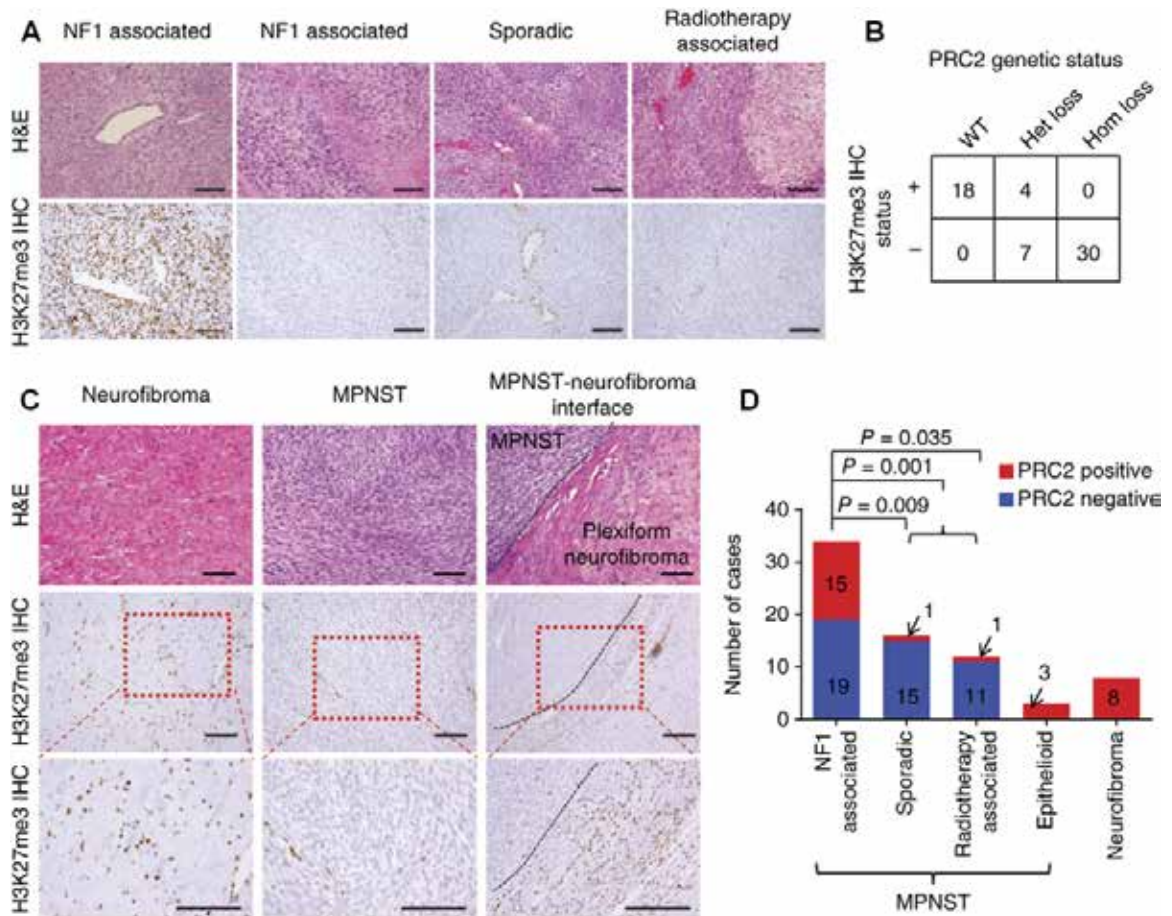


Figure 4.6 H3K27me3 immunohistochemistry correlates with PRC2 genetic status, and H3K27me3 loss characterizes progression from neurofibroma to MPNST

A, Representative hematoxylin and eosin (H&E) staining and H3K37me3 immunohistochemistry (IHC) images of NF1-associated, sporadic and radiotherapy-associated MPNSTs. Scale bars, 100 μ m. **B**, Correlation of PRC2 genetic status by whole-exome sequencing, RNA-seq and custom targeted sequencing and H3K27me3 immunohistochemistry status. **C**, Representative hematoxylin and eosin staining and H3K27me3 immunohistochemistry images of neurofibroma, NF1-associated MPNST and the interface of plexiform neurofibroma transitioning into MPNST. Scale bars, 100 μ m. **D**, Distribution of PRC2 loss and PRC2 presence by H3K27me3 immunohistochemistry in NF1-associated, sporadic, radiotherapy-associated and epithelioid MPNSTs and in neurofibromas. Fisher's exact test was used to calculate P values.

All neurofibromas (7/7), which were wild type for PRC2 except for one sample with heterozygous loss of *SUZ12*, retained H3K27me3 immunostaining (**Figure 4.1B** and **Figure 4.6C, D**). In specimens that contained the interface of MPNSTs arising from preexisting benign plexiform neurofibromas, we observed a transition from robust H3K27me3 staining in the plexiform neurofibroma to a clear loss of this staining in the MPNST. These data suggest that PRC2 loss is involved in the malignant progression of benign plexiform neurofibroma into MPNST. Indeed, 56% (19/34) of the NF1-associated MPNSTs had lost H3K27me3 (**Figure 4.6D**). Curiously, a significantly greater percentage (>90%) of sporadic and radiotherapy-associated MPNSTs had lost H3K27me3 staining (**Figure 4.6D**), suggesting that the progression of disease and sequence of genetic inactivation of *NF1*, *CDKN2A* and PRC2 components might be different in MPNSTs that arise in distinct clinical settings. Unlike NF1-associated MPNSTs that universally arise from preexisting neurofibromas, sporadic and radiotherapy-associated MPNSTs rarely have identifiable preexisting benign nerve sheath tumors. (Antonescu, Scheithauer et al. 2013) In one sporadic MPNST sample (16T), the presence of nonsynonymous mutations in both *NF1* (encoding a p.Asp1237_splice alteration) and *EED* (encoding p.Glu249fs) allowed us to use the prevalence of these mutations to infer the sequence of genetic events (Andor, Harness et al. 2014). The largest subpopulation of cells (84%) contained the *NF1* mutation, whereas a smaller subpopulation (57%) contained the *EED* mutation, suggesting that the *NF1* mutation occurred first during progression of this sporadic MPNST (**Figure 4.7**). The sequence of *NF1*, PRC2 component and *CDKN2A* inactivation described here is largely correlative. The precise sequence of events will require experimental validation with sequential inactivation of each pathway in cell line and mouse models.

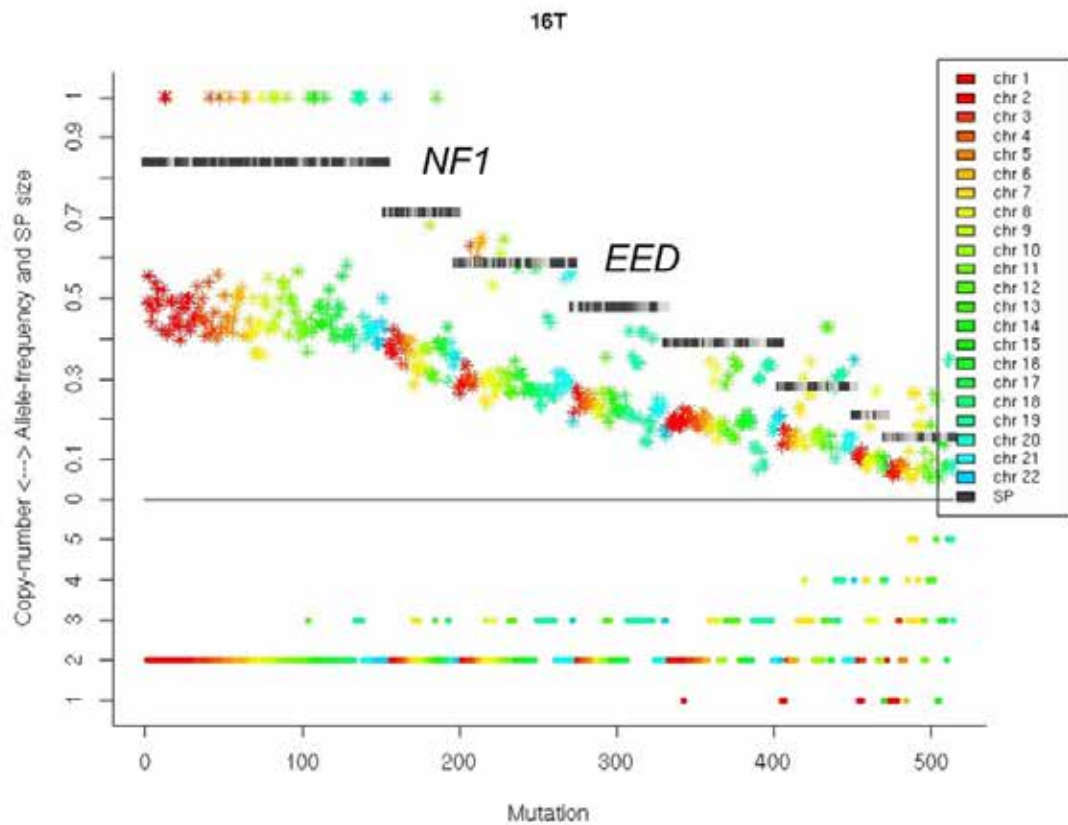


Figure 4.7 Coexistent subpopulations as calculated by EXPANDS analysis of sample 16T exome sequencing data

Eight subpopulations (SPs) were detected within the tumor, with the most prevalent being present in 84% of the tumor and containing the *NF1* D1237_splice mutation. Subpopulation 3 is present in 57% of the sample and contains the *EED* mutation encoding p.Glu249fs, suggesting that the *NF1* mutation occurred first in the progression of this sporadic MPNST. For each of 526 somatic mutations (x axis), the squares designate the SP to which the mutation has been assigned, the circles represent the copy number of the genomic locus of the mutation, and the asterisks represent the allele frequency of the mutation. Colors represent the chromosome where the mutation is located. SPs are sorted from most prevalent to least prevalent.

To determine whether PRC2 loss is required for MPNST oncogenesis, we screened available human MPNST cell lines using immunoblotting for H3K27me3. We identified one MPNST cell line (ST88-14; derived from an NF1-associated MPNST) that had lost H3K27me3 marks. RNA-seq analysis showed that ST88-14 cells had lost expression of *SUZ12*, and immunoblotting confirmed loss of the SUZ12 protein (**Figure 4.8A, B** and **Figure 4.9**). We next introduced Flag-HA-tagged wild-type SUZ12 (FH-SUZ12) or EED (FH-EED) into the ST88-14 cell line and into an MPNST cell line with wild-type PRC2 (MPNST724) that maintained H3K27me3 levels (**Figure 4.8A, B**). FH-SUZ12 but not FH-EED restored H3K27me3 levels in ST88-14 cells and substantially decreased cell growth (**Figure 4.8A-C**). In MPNST724 cells, there was a mild increase in H3K27me3 levels with the introduction of either FH-SUZ12 or FH-EED (**Figure 4.8A**), but neither had any effect on cell growth (**Figure 4.8C**). These data suggest that PRC2 loss contributes to oncogenesis at least in part by promoting cell proliferation and growth.

We next examined the transcriptional and chromatin changes in ST88-14 and MPNST724 cells after the introduction of FH-SUZ12, focusing on several known PRC2-regulated genes (*FOXN4, IGF2, PAX2* and *TLX1*) that are significantly upregulated in MPNST samples with PRC2 loss in comparison to MPNST samples with wild-type PRC2 (**Figure 4.5C**). At baseline, ST88-14 cells exhibited increased expression of *FOXN4, IGF2, PAX2* and *TLX1* accompanied by loss of PRC2 components (SUZ12 and EZH2) and the PRC2-repressive mark (H3K27me3) and reciprocal gain of the activation marks trimethylation at lysine 4 of histone H3 (H3K4me3) and acetylation of lysine 27 of histone H3 (H3K27ac) at their promoters (**Figure 4.8D** and **Figure 4.10**).

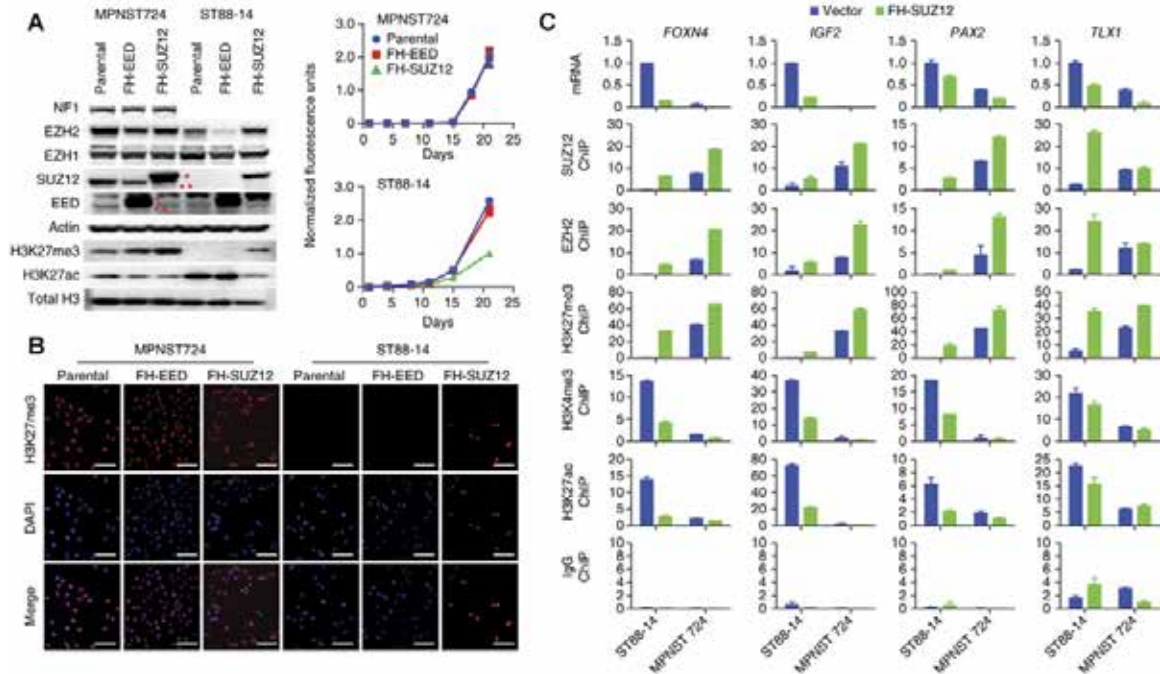


Figure 4.8 PRC2 loss promotes cell proliferation and growth in MPNST with PRC2 loss

A, Immunoblots demonstrating SUZ12 loss and corresponding loss of H3K27me3 in ST88-14 cells, a cell line derived from NF1-associated human MPNST, in comparison to a cell line derived from sporadic human MPNST, MPNST724, with intact PRC2 and retained H3K27me3 levels. Introduction of exogenous Flag-HA-tagged SUZ12 (FH-SUZ12) but not Flag-HA-tagged EED (FH-EED) in ST88-14 cells restores H3K27me3 protein levels. *, exogenous FH-SUZ12 or FH-EED; **, endogenous SUZ12 or EED. **B**, Immunofluorescence of H3K27me3 demonstrating the restoration of H3K27me3 levels at the cellular level by introducing FH-SUZ12 in the ST88-14 MPNST cell line with SUZ12 loss. Scale bars, 100 μ m. DAPI, 4',6-diamidino-2-phenylindole. **C**, Representative growth curves for the MPNST724 and ST88-14 cell lines demonstrating that the introduction of FH-SUZ12 but not FH-EED in *SUZ12*-deficient ST88-14 cells leads to growth retardation, whereas it had no effect in MPNST724 cells. Similar results have been obtained in at least three independent experiments. **D**, ST88-14 and MPNST724 cells were infected with vector control virus or virus expressing FH-SUZ12. Plots of expression determined by quantitative RT-PCR (expressed as $2^{-\Delta\Delta C_t}$) and promoter localization determined by chromatin immunoprecipitation (ChIP) and quantitative PCR (expressed as percent input) of SUZ12, EZH2, H3K27me3, H3K4me3, H3K27ac and IgG control for the *FOX N4*, *IGF2*, *PAX2* and *TLX1* genes are shown. Error bars, s.e.m. $n = 3$ technical replicates.

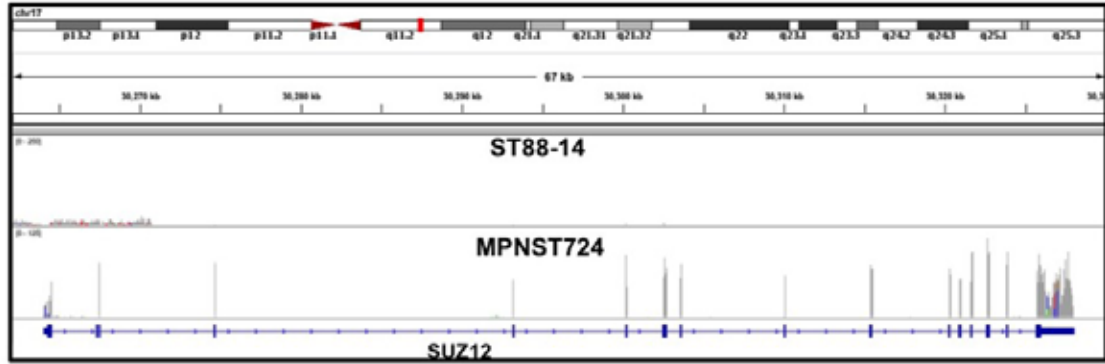


Figure 4.9 RNA-seq profiles of MPNST cell lines ST88-14 and MPNST724 at the *SUZ12* locus showing the absence of *SUZ12* transcript in ST88-14 cells

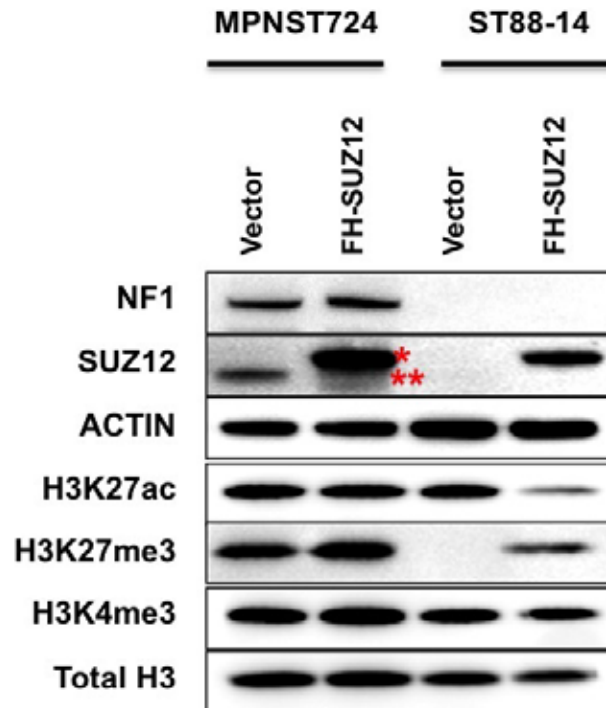


Figure 4.10 Western blot of MPNST cells

Western blot of NF1, SUZ12 and various chromatin marks with introduction of Flag-HA-tagged SUZ12 (FH-SUZ12) and control vector (Flag-HA-tagged GUS) in PRC2-wild-type MPNST724 and SUZ12-deficient ST88-14 human MPNST cells.

*, exogenous Flag-HA-tagged SUZ12; **, endogenous SUZ12.

After the introduction of FH-SUZ12 in ST88-14 cells, FH-SUZ12 localized to the promoters of these genes. This localization was accompanied by increased levels of EZH2 and H3K27me3 and decreased levels of H3K4me3 and H3K27ac at the promoter regions, as well as by decreased transcript levels of these PRC2 target genes. These data suggest that PRC2 loss has a direct impact on transcriptional regulation, and introduction of the missing PRC2 component has the ability to at least partially restore PRC2 function.

Discussion

MPNSTs often exhibit divergent differentiation including rhabdomyoblasts, glandular, squamous and neuroendocrine elements (Antonescu 2013). Our study identified a high frequency of loss-of-function genetic alterations in *NF1*, *CDKN2A* and PRC2 components (*EED* or *SUZ12*), demonstrating that MPNSTs share common molecular pathogenic pathways despite clinical and histological diversity. PRC2 loss activates multiple developmentally suppressed pathways, which might explain the frequent observation of divergent differentiation in MPNST. The high frequency of PRC2 loss suggests that PRC2 mutational status and, more specifically, H3K27me3 immunohistochemistry could be used as biomarkers for the more acute diagnosis of MPNST.

PRC2 was initially thought to be oncogenic: PRC2 components have higher expression in dividing cells and are important to maintain stemness. *EZH2* is overexpressed in a variety of cancers (Varambally, Dhanasekaran et al. 2002, Simon and Lange 2008), and activating *EZH2* mutations are found in a subset of lymphomas (Morin, Johnson et al. 2010). Paradoxically, recent work suggests that PRC2 can be tumor suppressive in distinct contexts with loss-of-function genetic alterations found in up to 25% in myeloid disorders and T-cell acute lymphoblas-

tic leukemia (ALL) (Ernst, Chase et al. 2010, Nikoloski, Langemeijer et al. 2010, Ntziachristos, Tsirigos et al. 2012) and 42% in early T-cell ALL (Zhang, Ding et al. 2012). Notably the majority of the loss-of-function alterations are found in *EZH2* (Ernst, Chase et al. 2010, Nikoloski, Langemeijer et al. 2010, Ntziachristos, Tsirigos et al. 2012, Zhang, Ding et al. 2012). Cellular studies and mouse models show that *Ezh1* can maintain suppression of Polycomb-regulated genes in the setting of *Ezh2* loss, and combined *Ezh1* and *Ezh2* loss or individual loss of *Eed* or *Suz12* depresses Polycomb-regulated genes and causes *Cdkn2a*-mediated growth arrest (Margueron, Li et al. 2008, Shen, Liu et al. 2008, Ezhkova, Lien et al. 2011, Xie, Xu et al. 2014). These findings suggest that MPNST is unique in that complete loss of PRC2 function is important for tumorigenesis, and loss of *CDKN2A* may be a critical cooperative event in addition to *NF1* loss.

Reprinted from Lee W, Teckie S, Wiesner T, Ran L, Prieto Granada CN, Lin M, Zhu S, Cao Z, Liang Y, Sboner A, Tap WD, Fletcher JA, Huberman KH, Qin LX, Viale A, Singer S, Zheng D, Berger MF, Chen Y, Antonescu CR, Chi P. (2014) PRC2 is recurrently inactivated through EED or SUZ12 loss in malignant peripheral nerve sheath tumors. *Nat Genet.*, **46**, 1227-32.

CHAPTER FIVE

A Mouse Model of Gastrointestinal Stromal Tumor with *BRAF*^{V600E} Mutation

Introduction

Gastrointestinal Stromal Tumor (GIST) is the most common type of sarcomas in the gastrointestinal tract (GI tract), with approximately 5000-6000 new cases per year in the United States (Perez, Livingstone et al. 2006). GISTs have been shown to arise from the pacemaker cells of GI tract, the Interstitial Cells of Cajal (ICCs). Most of GISTs harbor gain-of-function mutations in the receptor tyrosine kinases (RTK) *KIT* (75-80%) and *PDGFRA* (8-10%). (Corless 2014) Mutations in *KIT* and *PDGFRA* lead to ligand-independent activation of downstream signaling, which is critical for the pathogenesis of GISTs. Several mouse models were developed to investigate the mechanism of GIST development driven by *KIT* signaling, and preclinical evaluation of GIST therapeutic strategies. (Sommer, Agosti et al. 2003, Rubin, Antonescu et al. 2005, Nakai, Okada et al. 2008) Other oncogenic mutations reported in *KIT/PDGFRA* wild-type GISTs include *BRAF*, *SDHA/B/C/D*, *HRAS*, *NRAS*, *PIK3CA* and *NF1*. (Corless 2014) However, little is known about how these oncogenic mutations contribute to GIST pathogenesis. There is no animal model developed for GISTs driven by oncogenic mutations other than *KIT* mutations.

Recent studies have discovered activating mutations of *BRAF* in about 3-13% of *KIT/PDGFRA* wild-type GISTs. (Agaram, Wong et al. 2008, Agaimy, Terracciano et al. 2009, Martinho, Gouveia et al. 2009, Tos, Montesco et al. 2010, Daniels,

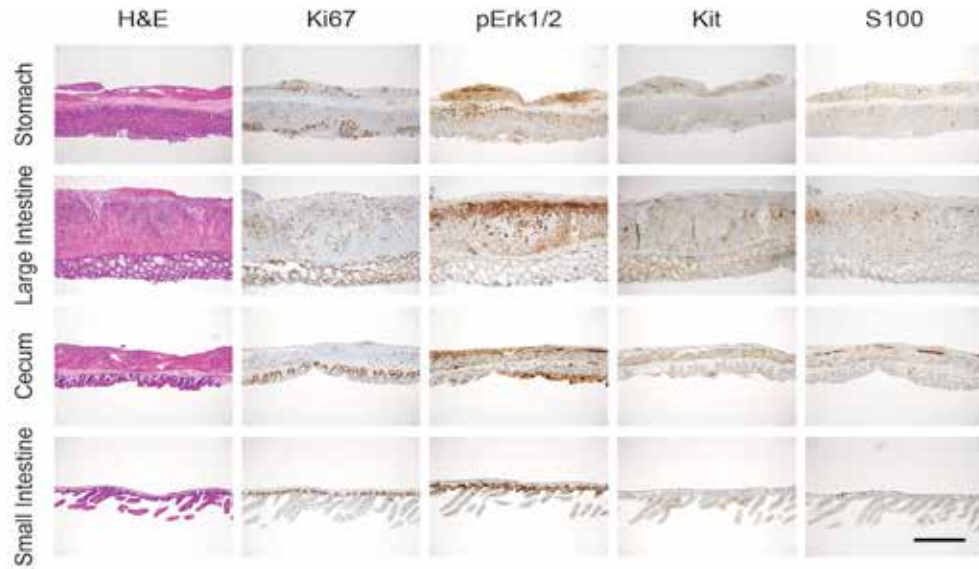


Figure 5.4 Combination of homozygous *BRaf*^{V600E} and *p53* loss induced phenotypes in stomach, cecum and small intestine

Representative H&E histology and IHC of Ki67, phospho-Erk1/2, Kit and S100 of the stomach, large intestine, cecum and small intestine from 2-month-old *Et-v1*^{CreERT2}; *BRaf*^{CA/CA}; *p53*^{fl/fl} mice after 2 weeks of tamoxifen injection. Scale bar, 400 μ m.

Lurkin et al. 2011) BRAF, protein encoded by *BRAF* gene, belongs to the raf/mil family of serine/threonine protein kinases. It plays an important role in cell division, differentiation, and secretion through the MAP kinase/ERK signaling pathways. Activation mutations of BRAF have been implicated in a wide range of cancers, such as malignant melanoma, colorectal carcinoma and Papillary Thyroid Carcinoma.(Davies, Bignell et al. 2002) Similar to these tumors, *BRAF*-mutated GISTs are located within exon 15 V600E hot spot. *BRAF*-mutated GISTs most commonly arise in the small intestine with high risk of malignancy. These tumors share similar histological and clinical parameters with the non-*BRAF*-mutated GISTs counterparts. There is also no significant difference in term of the MAP kinase/ERK or AKT signaling pathway activation between *BRAF*-mutated GISTs and KIT/PDGFR α mutated GISTs.(Hostein, Faur et al. 2010) However, the role of *BRAF* mutation in GIST pathogenesis remains unclear.

Previously, we have described that *ETV1*, an *ETS* family transcription factor, is a master regulator of the lineage specification and development of GIST precursor ICCs.(Chi, Chen et al. 2010, Ran, Sirota et al. 2015) *ETV1* is specifically expressed only to the two subsets of ICCs that give rise to GISTs, (myenteric and intramuscular ICCs). Consequently, germline knockout of *ETV1* resulted in defective development of these two ICC subsets, and failure to initiate GISTs in *Kit*^{A558V/+} knock-in mouse model. We further showed that *ETV1* and *KIT* form a positive feedback circuit through MAP kinase signaling to regulate target gene expression: *ETV1* was stabilized by MAP kinase signaling downstream of mutant *KIT*, *ETV1* directly and positively regulated *KIT* expression. These observations suggest that cooperation between *ETV1* and MAP kinase signaling is important for GIST tumorigenesis. *ETV1*-expression compartments are the cells of origin for GIST.

Here, we report a conditional mouse model of human *BRaf*^{V600E}-mutated GISTs using *Etv1*-promoter-driven cre recombinase to specifically activate *BRaf*^{V600E} allele (*BRAF*^{CA}) in GIST precursor ICCs. The mice carrying *BRaf*^{CA} allele express normal BRaf prior to cre-mediated recombination, but after which BRaf^{V600E} is expressed. (Dankort, Filenova et al. 2007) Homozygous (*Etv1*^{CreERT2}; *BRaf*^{CA/CA}) and heterozygous mice (*Etv1*^{CreERT2}; *BRaf*^{+ /CA}) exhibited hyperplasia in stomach and large intestine starting at 6 months from the first cre-activation, and low frequency of GIST tumors in the large intestine after 12 months from the first cre-activation. The small intestine and cecum did not show any significant hyperplasia. Combination of *BRaf*^{V600E} and *p53* loss led to highly lethal hyperplasias in GI tract of double homozygous *Etv1*^{CreERT2}; *BRaf*^{CA/CA}; *p53*^{fl/fl} mice, and all mice died within two weeks after the first tamoxifen injection. *BRaf*^{V600E} heterozygous *Etv1*^{CreERT2}; *BRaf*^{CA/+}; *p53*^{fl/fl} mice developed multiple GISTs in the large intestine and significant hyperplasia-like lesions in the stomach starting at 6-8 weeks after the first tamoxifen injection. The penetrance of GIST disease in *Etv1*^{CreERT2}; *BRaf*^{CA/CA}; *p53*^{fl/fl} is 100%.

Results

To access whether *Etv1* is expressed in the Interstitial Cell of Cajals (ICCs), we used the Cre/LoxP lineage tracing system to mark *Etv1* expressed cell in GI tract. Specifically, in *Etv1*-expressing cells from *Rosa26-EYFP*^{LSL/+}; *Etv1*^{CreERT2/+} mice, expression of the enhanced yellow fluorescent protein (EYFP) is activated through the action of Cre recombinase to remove a transcriptional “stop” sequence after tamoxifen injection. As a result, *Etv1* expressed cells would be light up with EYFP expression after tamoxifen injection. Different ICCs in the stomach, small intestine, large intestine and cecum were identified by positive membrane expression of Kit protein. Consistent with prior observation, EYFP was detected

in the subtypes of ICCs susceptible to oncogenesis, ICC-MYs and ICC-IMs, as early as one week after the first tamoxifen injection (**Figure 5.1**). (Chi, Chen et al. 2010) For example, EYFP was only expressed in the Myenteric ICCs (ICC-MYs) and Intramuscular ICCs (ICC-IMs), but not submucosal ICCs (ICC-SMPs) in the large intestine (**Figure 5.1**). In addition, the EYFP expression could be maintained at least 8 weeks after the first tamoxifen injection (Data not shown). These observations indicate *Etv1^{creERT2/+}* could sustainably and specifically activate cre recombinase controlled gene expression in *Etv1*-expressed ICCs. *Etv1^{creERT2/+}* allele was subsequently used to activate *BRaf^{V600E}* mutation in these oncogenic ICCs.

To gain insight into the role of *BRaf^{V600E}* mutation in GIST oncogenesis *in vivo*, we utilized the *BRaf^{CA}* mice that harbor a germline conditional *BRaf^{V600E}* allele, the expression of which is initiated at physiological level under the control of *BRaf* endogenous promoter by the action of cre recombinase (Dankort, Filenova et al. 2007, Hauschild, Grob et al. 2012). We crossed *BRaf^{CA}* mice with *Etv1^{creERT2}* mice to conditionally activate *BRaf^{V600E}* specifically in *Etv1* expressed ICCs. Hyperplasia were observed in the large intestine and stomach of *Etv1^{creERT2}; BRaf^{CA/CA}* mice starting from 6 months from the first tamoxifen application (**Figure 5.2** and **Figure 5.3**), and GIST tumors formed in one mice after 12 months from the first tamoxifen application. Similarly, hyperplasia was also identified at in *Etv1^{creERT2}; BRaf^{CA/+}* mice (**Figure 5.2 A** and **Figure 5.3**). The penetrance of GIST hyperplasia was high in both *Etv1^{creERT2}; BRaf^{CA/CA}* and *Etv1^{creERT2}; BRaf^{CA/+}* mice (**Figure 5.2B**). There was no discernable hyperplasia detected in the GI tract of *Etv1^{creERT2}* mice (**Figure 5.2** and **Figure 5.3**), indicating that GIST hyperplasia was require the conversion from the wild type *BRaf* to *BRaf^{V600E}* and this was dose dependent.

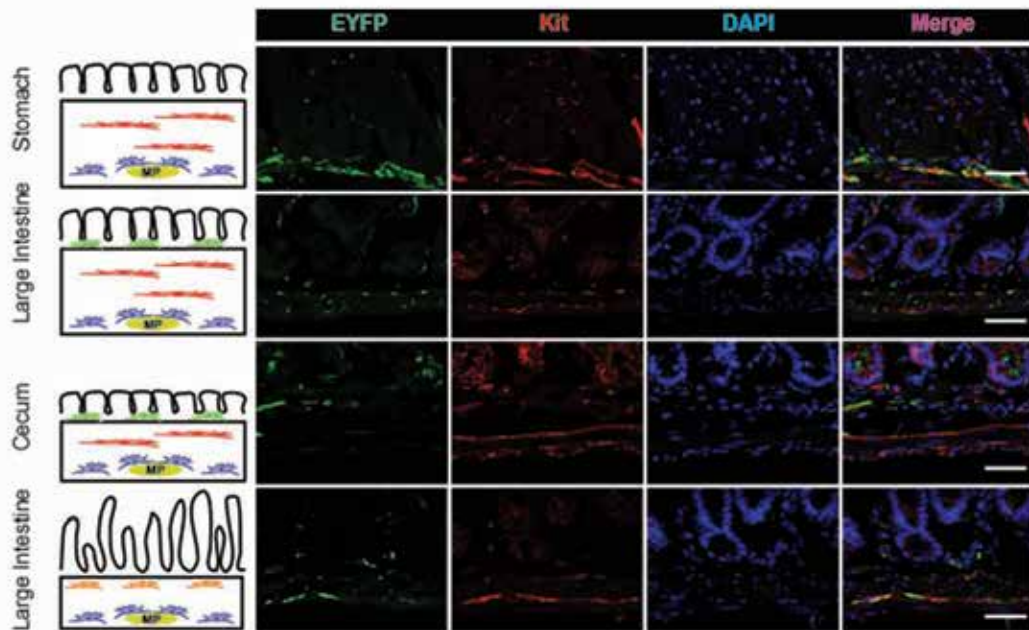


Figure 5.1 *Etv1* is expressed in ICC-IMs and ICC-MYs that are susceptible to GIST tumorigenesis

Cartoons on the left column are schematic showing localization of ICC-MY (blue cells), ICC-IM (red cells), ICC-SMP (green cells) and ICC-DMP (orange cells) in stomach, large intestine, cecum and small intestine. MP, myenteric plexus. All ICC subtypes express Kit (red), but only ICC-IMs and ICC-MYs express *Etv1* as indicated by EYFP (green). Scale bars: 50uM.

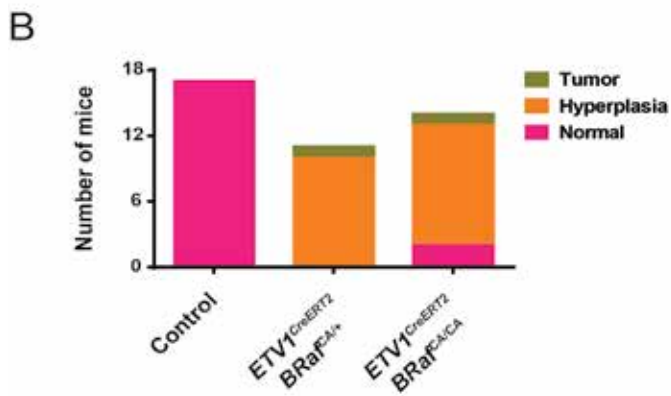
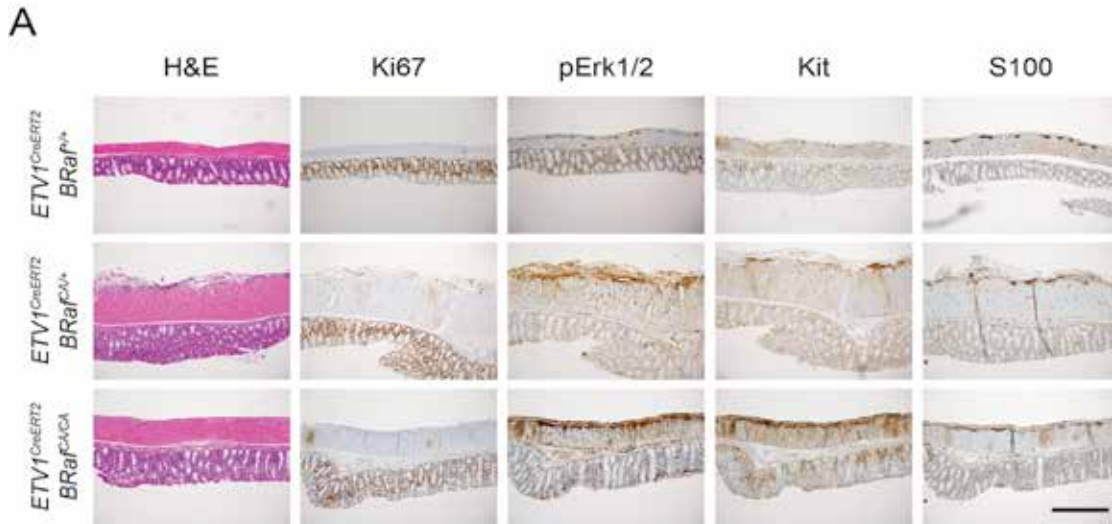


Figure 5.2 $BRaf^{V600E}$ activation induces a minimal hyperplasia phenotype in mouse large intestine

A, Representative H&E histology and IHC of Ki67, phospho-Erk1/2, Kit and S100 of the large intestine from 9-month-old $Etv1^{CreERT2}; BRaf^{+/+}$ mouse (top), $Etv1^{CreERT2}; BRaf^{CA/+}$ mouse (middle), and $Etv1^{CreERT2}; BRaf^{CA/CA}$ mouse (bottom). Scale bar, 400 μ m. **B**, Summary of the histological findings in WT ($Etv1^{CreERT2}$ -), $BRaf^{V600E}$ heterozygous ($Etv1^{CreERT2}; BRaf^{CA/+}$) and $BRaf^{V600E}$ homozygous ($Etv1^{CreERT2}; BRaf^{CA/CA}$) mouse GI tracts examined at 6-12 months after the first tamoxifen injection at 6-8 weeks of age.

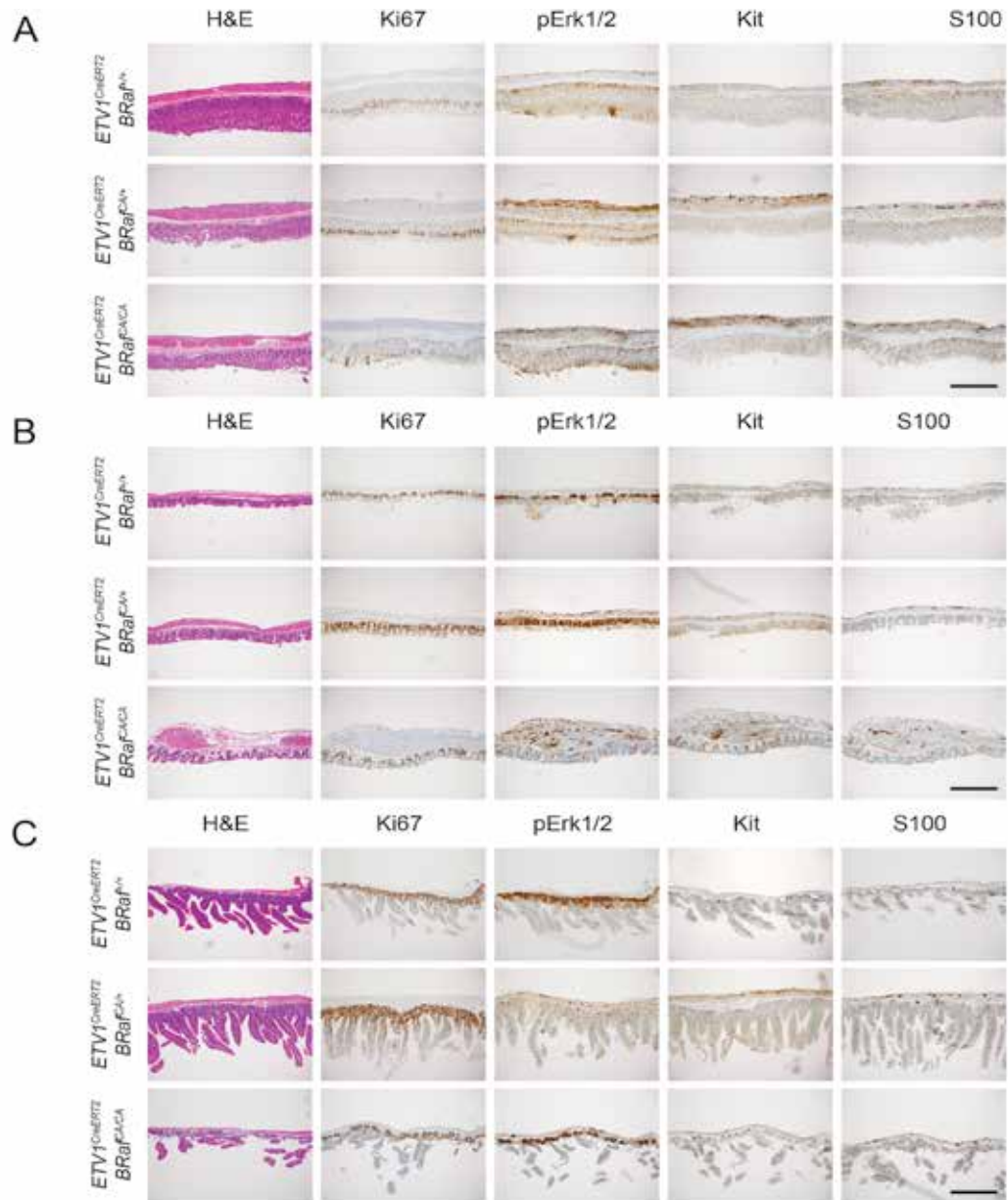


Figure 5.3 *BRaf^{AV600E}* activation induced phenotypes in stomach, cecum and small intestine

Representative H&E histology and IHC of Ki67, phospho-Erk1/2, Kit and S100 of the stomach (A), cecum (B) and small intestine (C) from 9-month-old old *Etv1^{CreERT2}; BRaf^{AV600E}* mouse (top), *Etv1^{CreERT2}; BRaf^{CA/+}* mouse (middle), and *Etv1^{CreERT2}; BRaf^{CA/CA}* mouse (bottom). Scale bars, 400 μ m.

BRaf^{V600E}-induced hyperplasia was frequently located in the stomach and large intestine, rarely located in small intestine and never observed in the cecum. They were stained strongly positive for Kit protein, indicating the ICC origin of the hyperplasia. Nevertheless, the hyperplasia expressed low level of proliferation marker Ki67. Consistent with the activation of *BRaf^{V600E}* mutation, hyperplasia regions showed much high pErk1/2 level compared to non-hyperplasia regions or *Etv1^{creERT2}* control mice. These data showed that *BRaf^{V600E}* mutation has the potential to promote oncogenesis in the *Etv1* expressed ICCs in adult mice. However, *BRaf^{V600E}* mutation alone was not sufficient to cause GIST tumors, suggesting that *BRaf^{V600E}* may need to cooperate with additional oncogenic events to drive GIST tumorigenesis.

To accelerate tumorigenesis driven by *BRaf*^{V600E}, we crossed *Etv1*^{creERT2}; *BRaf*^{CA/CA} mice to *p53*^{flox/flox} mice and investigated GI tract phenotypes. In contrast to the hyperplasia induced in *Etv1*^{creERT2}; *BRaf*^{CA/+} or *Etv1*^{creERT2}; *BRaf*^{CA/CA} mice, *Etv1*^{creERT2}; *BRaf*^{CA/CA}; *p53*^{flox/flox} mice developed highly lethal hyperplasia in stomach and large intestine, and all *Etv1*^{creERT2}; *BRaf*^{CA/CA}; *p53*^{flox/flox} mice died within two weeks after the first tamoxifen injection (**Figure 5.4**). The hyperplasia were stained strongly for pErk1/2, kit and highly proliferative with strong Ki67 staining. In order to evaluate long-term effect of *BRaf*^{V600E} mutation, we generated *Etv1*^{creERT2}; *BRaf*^{CA/+}; *p53*^{flox/flox} mice to reduce the dose of *BRaf*^{V600E} mutant allele. *Etv1*^{creERT2}; *BRaf*^{CA/+}; *p53*^{flox/flox} mice developed multiple GIST tumors in the large intestine and cecum region right next to the conjunction with large intestine (**Figure 5.5A-C**) with 100% penetrance (**Figure 5.5D**), and these mice died from GISTs and dilated GI tracts within 6-8 weeks after the first tamoxifen injection. In addition, strong hyperplasias were observed in stomach and small intestine at lower grade and frequency, and no hyperplasia was observed in the cecum far from large intestine (**Figure 5.6**). These tumors showed spindle cell morphology that highly resembled human GIST histology (**Figure 5.5B**). The tumors and hyperplasias were highly proliferative, with the expression of Kit and activation of Erk1/2. They also stained negatively for S100, showing they were indeed GISTs not gastric melanomas. Collectively, these data suggested that *BRaf*^{V600E} mutation could cooperate with *p53* loss to drive GIST tumorigenesis in *Etv1* expressed cellular compartment.

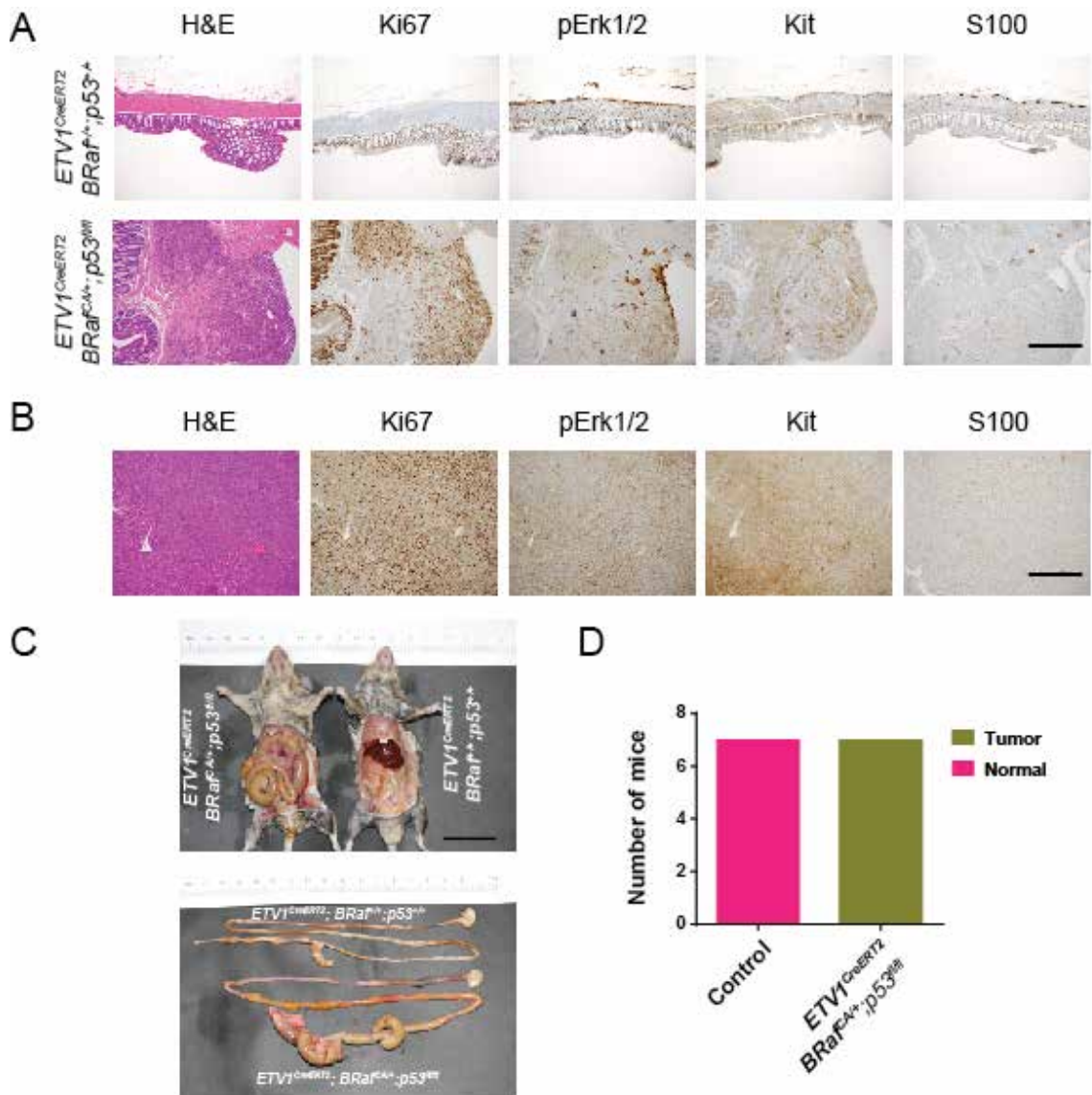


Figure 5.5 *BRAF^{V600E}* robustly cooperates with *p53* loss in GIST tumorigenesis **A**, Representative H&E histology and IHC of Ki67, phospho-Erk1/2, Kit and S100 of the large intestine from 4-month-old wild type control mouse (top) and *Etv1^{CreERT2}; BRAF^{CA/+}; p53^{fl/fl}* mouse (bottom), after 6 weeks of tamoxifen injection. Scale bar, 400 μ m. **B**, Representative H&E histology and IHC of Ki67, phospho-Erk1/2, Kit and S100 of the tumor from the same *Etv1^{CreERT2}; BRAF^{CA/+}; p53^{fl/fl}* mouse in **A**. Scale bar, 400 μ m. **C**, Representative image of mouse abdomen and GI tract appearance in wild type control mouse and *Etv1^{CreERT2}; BRAF^{CA/+}; p53^{fl/fl}* mouse. Scale bar, 3cm. **D**: Summary of the histological findings in control and *Etv1^{CreERT2}; BRAF^{CA/+}; p53^{fl/fl}* mouse GI tracts examined at 6-8 weeks after the first tamoxifen injection at 6-8 weeks of age.

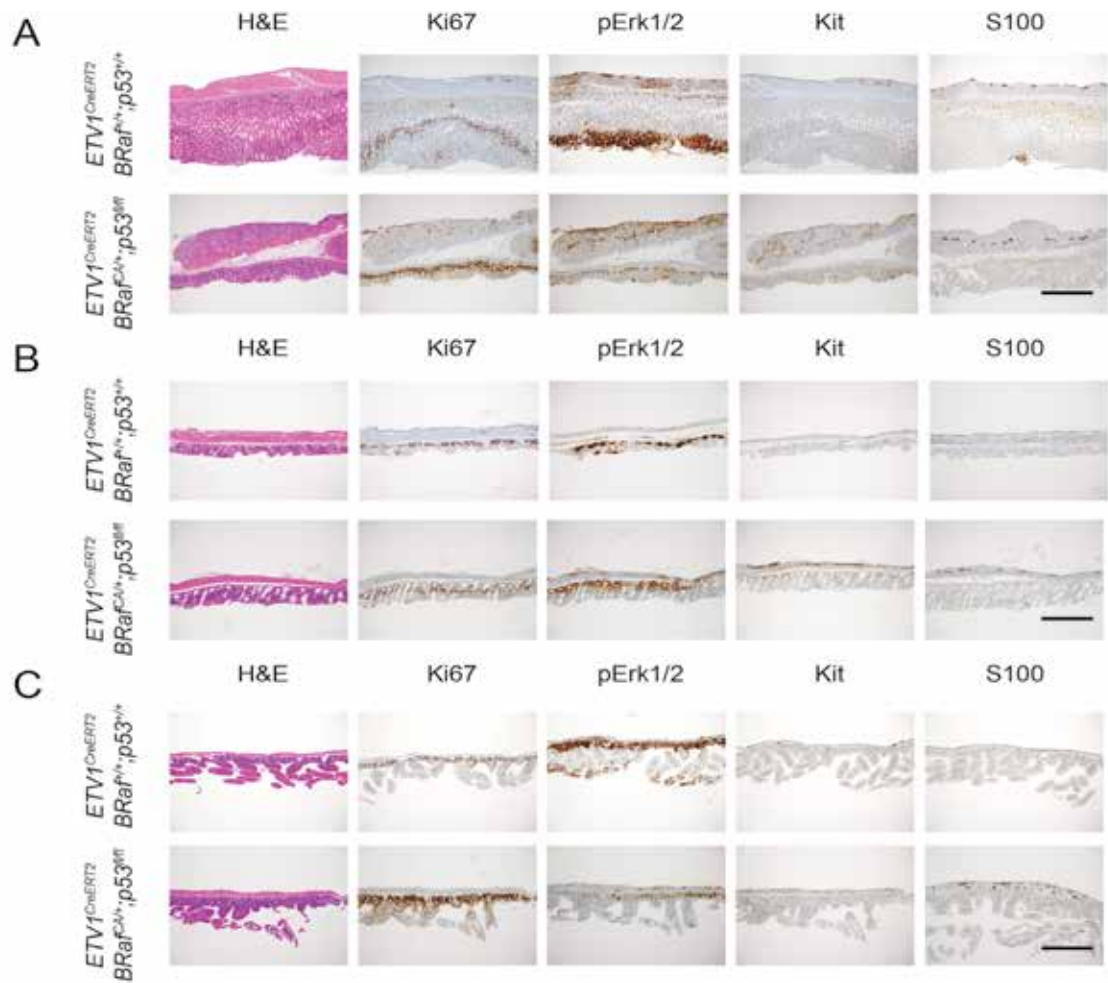


Figure 5.6 Combination of heterozygous *BRaf*^{V600E} and *p53* loss induced phenotypes in stomach, cecum and small intestine

Representative H&E histology and IHC of Ki67, phospho-Erk1/2, Kit and S100 of the stomach (**A**), cecum (**B**) and small intestine (**C**) from 4-month-old wild type control mouse (top) and *Etv1*^{CreERT2}; *BRaf*^{CA/+}; *p53*^{fl/fl} mouse (bottom), after 6 weeks of tamoxifen injection. Scale bars, 400 μ m.

Previous studies showed Dabrafenib, an inhibitor of mutated *BRAF*, could significantly improve the management of metastatic melanoma (Hauschild, Grob et al. 2012). To explore the therapeutic application of the mouse model and determine the effect of dabrafenib on *BRaf* mutated GISTs, *Etv1^{creERT2}; BRaf^{CA/+}; p53^{flox/flox}* mice were injected with tamoxifen to allow GIST tumors develop for 4 weeks, then treated with vehicle or dabrafenib. Tumor burdens in mice were monitored with magnetic resonance imaging (MRI). Mice treated with dabrafenib showed significant tumor shrinkage while the tumors vehicle treated mice continue to grow (**Figure 5.7A**). Dabrafenib treatment induced significant fibrosis by trichrome staining and inhibition of Erk1/2 phosphorylation (**Figure 5.7B, C**). These data suggested that *Etv1^{creERT2}; BRaf^{CA/+}; p53^{flox/flox}* mice could be used a reliable preclinical model to test therapeutic strategies for BRAF-mutated GISTs, and dabrafenib could potentially be an effective treatment for these patients.

Discussion

Using genetically engineered mouse model, we have demonstrated that activation of *BRAF^{V600E}* mutation in *ETV1* expressed lineage resulted in hyperplasia lesions in stomach and large intestine in both heterozygous mutation and homozygous mutation. Further depletion of *p53* together with heterozygous *BRAF^{V600E}* activation mutation led to multiple GISTs formation in the large intestine and cecum, and strong hyperplasia in the stomach. Depletion of *p53* together with homozygous *BRAF^{V600E}* activation mutation led to aggressive hyperplasia in the GI tract and death of mice within 1-2 weeks of tamoxifen activation. There was a clear dose-dependent effect for *BRAF^{V600E}* allele in the *BRAF^{V600E}* alone or in combination with *p53* loss. These observations suggest that *BRAF* activation mutation could be an importance oncogenic driver in *BRAF*-mutated GISTs.

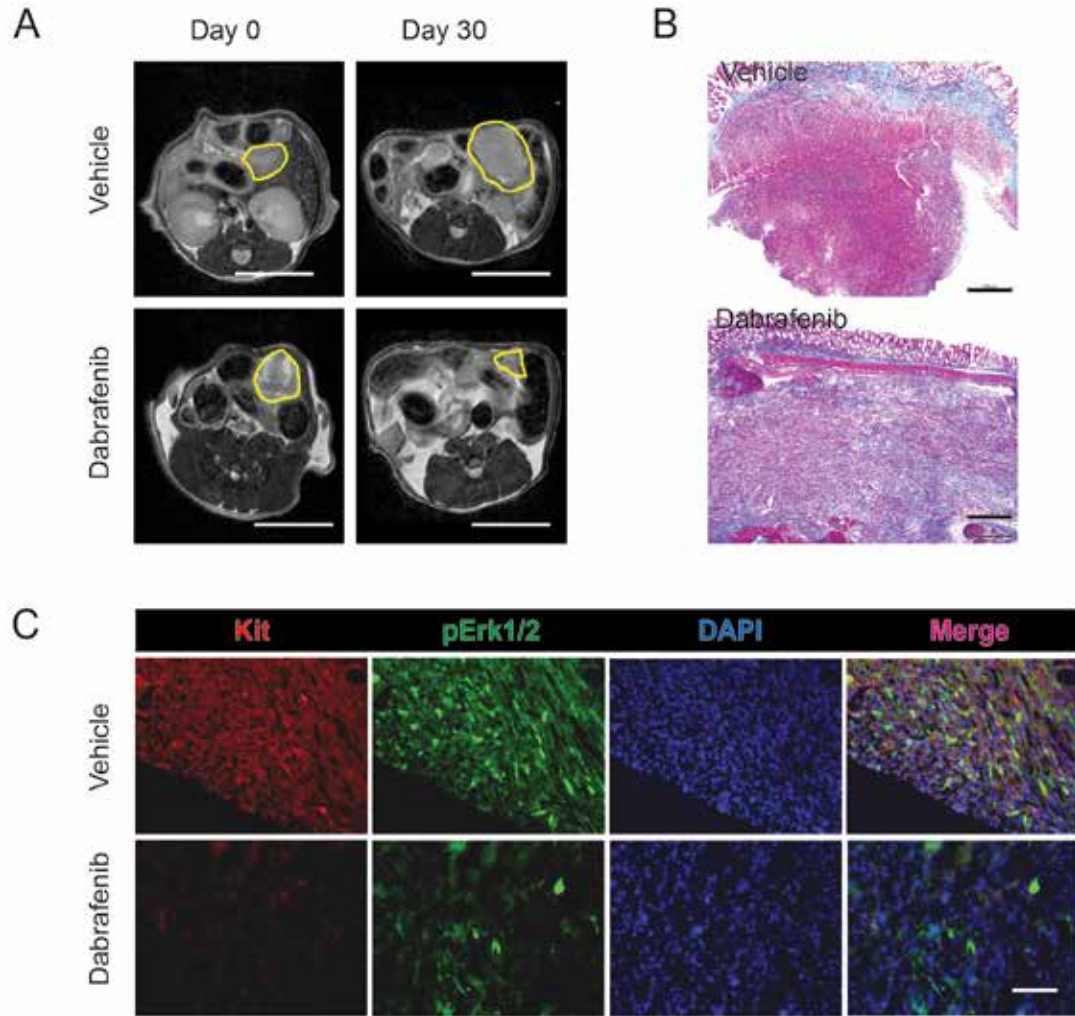


Figure 5.7 Dabrafenib inhibits GIST tumor growth in BRAF mutated GISTs of *Etv1^{CreERT2}; BRaf^{CA/+}; p53^{fl/fl}* mouse

A, Representative MR image for day 0 and day 30 of vehicle treated and Dabrafenib (100mg/kg, twice daily) *Etv1^{CreERT2}; BRaf^{CA/+}; p53^{fl/fl}* mouse. Scale bars: 1cm. **B**, Representative Tricrome images of tumors isolated 2 days after treatment of *Etv1^{CreERT2}; BRaf^{CA/+}; p53^{fl/fl}* mice under the same condition as in **A**. scale bars: 200uM. **C**, Representative IF images of Kit (red), pErk1/2 (green) protein of tumors isolated 2 days after treatment of *Etv1^{CreERT2}; BRaf^{CA/+}; p53^{fl/fl}* mice under the same condition as in **A**. Nuclei (DAPI, blue). Scale bar, 200 μ m.

ICCs have been shown to be the cell-of-origin for GISTs as indicated by KIT expression in the tumors. *ETV1*, an ETS family transcription factor, is shown to be expressed and required for ICCs development.(Chi, Chen et al. 2010) Ablation of *ETV1* leads to defects in ICC-MY and ICC-MY development, resulting in failure of GISTs initiation in *KIT* mutation driven GIST mouse model.(Ran, Sirota et al. 2015) In our *BRAF*-mutation driven GIST mouse model, we further demonstrate that activation of *BRAF* mutation in the *ETV1*-expressed ICC subsets is sufficient to drive GIST-like hyperplasia lesion and GIST tumors when combined with *p53* loss. This observation strongly confirms the previously finding that *ETV1*-expressed ICC subsets are the true cell-of-origin for GIST. Moreover, the success of using *Etv1^{creERT2}* allele to activate *BRAF* mutation and GIST formation suggests that *Etv1^{creERT2}* allele can be a useful tool to model other GIST oncogenic drivers with strict controls.

Clinically, it has been challenging to achieve effective and persistent response in *BRAF*-mutated GIST patients with single agent *BRAF* inhibitors.(Falchook, Trent et al. 2013) Here we showed a similar stabilized disease with *BRAF* inhibitor, dabrafenib, in mouse *BRAF*-driven GISTs. Further studies are important to understand dabrafenib in *BRAF*-mutated GISTs and therapeutic strategies to overcome dabrafenib resistance.

CHAPTER SIX

Combined Inhibition of MAP Kinase and KIT Signaling Synergistically Destabilizes ETV1 and Suppresses GIST Tumor Growth

Introduction

Gastrointestinal stromal tumor (GIST) represents one of the most common subtypes of human sarcomas with approximately 5,000 cases a year in the US. GIST arises from the interstitial cells of Cajal (ICCs) that depend on high level *KIT* expression for lineage specification and survival (Huizinga, Thuneberg et al. 1995, Hirota, Isozaki et al. 1998). Families with germline activating *KIT* mutations develop diffuse hyperplasia of ICCs that progress to GIST (Nishida, Hirota et al. 1998, Li, Fletcher et al. 2005, Agaimy, Wunsch et al. , Miettinen and Lasota 2006). The majority of sporadic GISTs harbor activating mutations in *KIT* and to a lesser extent in *PDGFRA* and *BRAF* (Hirota, Isozaki et al. 1998, Heinrich, Corless et al. 2003, Heinrich, Corless et al. 2003, Agaram, Wong et al. 2008). These mutations are thought to function as oncogenic “drivers” required for growth and survival of GISTs. These observations have provided the scientific rationale for clinically targeting these mutations in GIST.

Imatinib mesylate (Gleevec®), a multi-targeted tyrosine kinase inhibitor (TKI) that targets KIT/PDGFR, is the standard first line therapy in advanced GIST with radiographic response rate of approximately 50%, and disease stabilization in another 25-30% (Demetri 2002, Debiec-Rychter, Dumez et al. 2004, Verweij, Casali et al. 2004, Blanke, Rankin et al. 2008). Despite the early clinical success, the median progression free survival is only 20 to 24 months and the majority of

patients develop resistance to imatinib within 2 years of treatment (Debiec-Rychter, Dumez et al. 2004, Verweij, Casali et al. 2004, Beadling, Jacobson-Dunlop et al. 2008, Blanke, Rankin et al. 2008). Second and third line TKIs that target subsets of imatinib-resistant *KIT* mutations have only limited efficacy and advanced GIST patients eventually die of their disease (de Raedt, Cools et al. 2006, Demetri, van Oosterom et al. 2006, Beadling, Jacobson-Dunlop et al. 2008, Blanke 2008, Demetri, Reichardt et al. 2013). Imatinib resistance remains the greatest challenge in the management of advanced GISTs. Due to the vast heterogeneity of resistance mechanisms both between patients and within individual patient, it is challenging to develop next generation therapies that can address the majority if not all resistance mechanisms (Antonescu, Besmer et al. 2005, Demetri, van Oosterom et al. 2006, Bardsley, Horvath et al. 2010).

Clinically, complete responses with first line imatinib therapy are rare. The residual disease represents a significant repertoire that can adapt, evolve and eventually breakthrough imatinib therapy through a variety of resistance mechanisms. Moreover, the potential existence of a KIT-low and intrinsically imatinib-resistant GIST stem/progenitor population (Bardsley, Horvath et al. 2010) makes it conceivably impossible to eradicate the disease with imatinib alone. We reason that one of the strategies to overcome imatinib-resistance is to develop novel therapeutics that are more effective than imatinib alone and can potentially target the GIST stem/progenitor population and therefore prevent the development of imatinib resistance.

We have previously uncovered that *ETV1*, an *ETS* family transcription factor, is a master regulator of the normal lineage specification and development of the GIST precursor ICCs. *ETV1* is highly expressed in GISTs and is required for the

growth and survival of imatinib-sensitive and imatinib-resistant GIST cell lines. ETV1 is a highly unstable protein and its stability is enhanced by active MAP kinase signaling, and represents an essential effector of mutant *KIT/PDGFR*A-mediated pathogenesis in GIST (Chi, Chen et al. 2010). These observations point to ETV1 as a novel therapeutic target. However, the *in vivo* requirement of *ETV1* in GIST pathogenesis has not been defined. More importantly, an effective therapeutic strategy to target ETV1, a transcription factor, has not been developed. Here, using genetically engineered mouse models, we demonstrate that *Etv1* is required for GIST tumor initiation and proliferation in the physiological *in vivo* context. Taking advantage of the unique regulation of ETV1 protein stability, we further describe an effective therapeutic strategy to target ETV1.

Results

Etv1 is required for tumor initiation and proliferation

To assess whether *Etv1* is required for GIST initiation *in vivo*, we crossed the germline *Kit*^{Δ558V/+} knock-in mouse model that develops ICC hyperplasia throughout the GI tract and GIST-like tumors in the cecum (Antonescu, Sommer et al. 2003, Kwon, Hwang et al. 2009) with the *Etv1*^{-/-} knockout mouse model (Arber, Ladle et al. 2000) that is defective in ICC development (Chi, Chen et al. 2010). Since the *Etv1*^{-/-} mice die at postnatal day 10-14 (P10-P14) (Arber, Ladle et al. 2000), we examined the GI tract of *Etv1*^{-/-};*Kit*^{Δ558V/+} and *Etv1*^{+/+};*Kit*^{Δ558V/+} littermates at day P10. Consistent with prior observations, all three *Etv1*^{+/+};*Kit*^{Δ558V/+} mice developed GIST-like masses in the cecum that stain positively for KIT and ETV1 (**Figure 6.1A, B**) and diffuse ICC hyperplasia in the stomach and large intestines (**Figure 6.1D**). In contrast, one of the three *Etv1*^{-/-};*Kit*^{Δ558V/+} mice developed ICC hyperplasia in the cecum and none developed cecal GIST-like tumors or ICC hyperplasia of the stomach or large intestine (**Figure 6.1A-C, E**). In addition, immunohistochemistry against ICC makers, Kit and Ano1, showed that *Etv1*^{-/-};*Kit*^{Δ558V/+} mice exhibited loss of the intramuscular ICCs (ICC-IM) and myenteric ICCs (ICC-MY) with preservation of the submucosal ICCs (ICC-SMP) (**Figure 6.1 B and Figure 6.2**), phenocopying the ICC loss in *Etv1*^{-/-} mice (Chi, Chen et al. 2010). These observations suggest that *Etv1* is required for GIST tumor initiation *in vivo* through its direct regulation of the lineage specification and development of the GIST precursor ICCs.

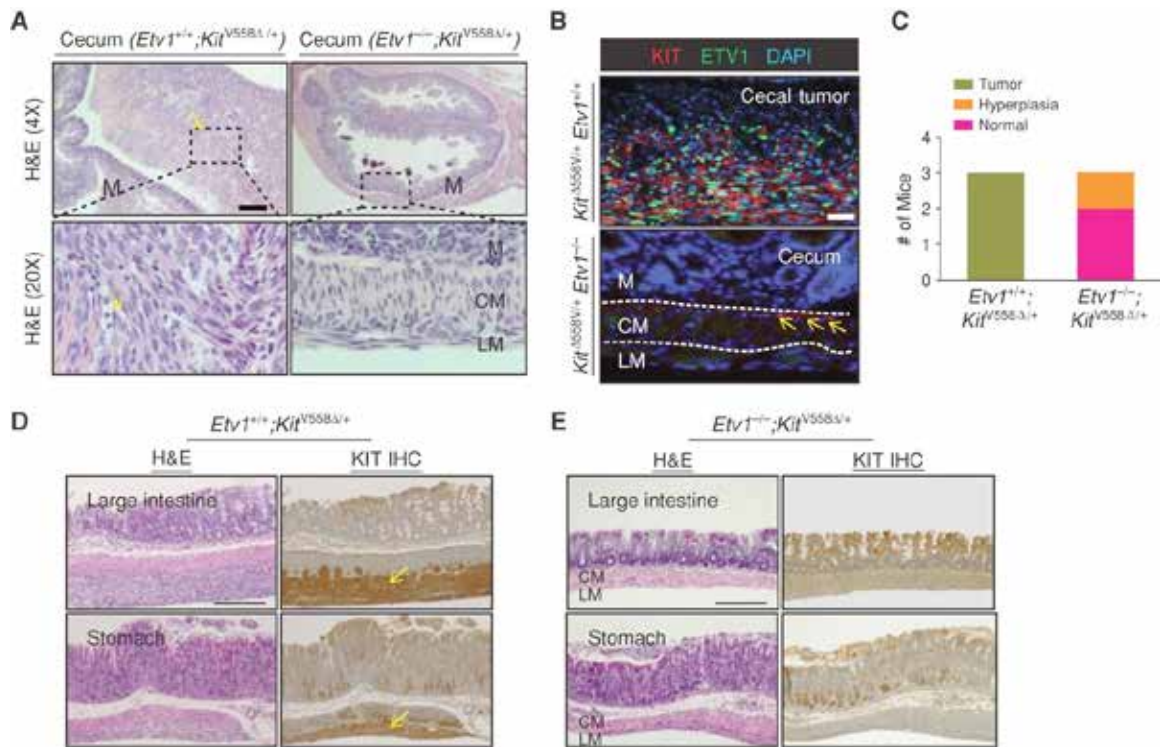


Figure 6.1 ETV1 is required for GIST tumor initiation *in vivo*

A, representative hematoxylin and eosin (H&E) staining of the cecal mass and the cecum of *Etv1*^{+/+};*Kit*^{Δ558V/+} and *Etv1*^{-/-};*Kit*^{Δ558/+} mice, respectively, showing that ETV1 is required for formation of GIST-like cecal tumors (yellow arrows, malignant cells in tumor). M, mucosa; CM, circular muscle; LM, longitudinal muscle. Scale bar, 100 μm. **B**, representative immunofluorescence of KIT (red), ETV1 (green), and DAPI (blue) of the cecal tumor or cecum of *Etv1*^{+/+};*Kit*^{Δ558V/+} and *Etv1*^{-/-};*Kit*^{Δ558/+} mice, respectively. Yellow arrows, preserved ICC-SMP with positive KIT immunostaining. Scale bar, 50 μm. **C**, summary of the histologic findings in *Etv1*^{+/+};*Kit*^{Δ558V/+} and *Etv1*^{-/-};*Kit*^{Δ558/+} cecum examined at 10 days postnatal. **D**, representative H&E and KIT IHC images of the large intestine and stomach in *Etv1*^{+/+};*Kit*^{V558Δ/+} mice, demonstrating hyperplasia of the ICCs (yellow arrows, KIT-positive ICC hyperplasia) in the large intestine and stomach. Scale bar, 50 μm. **E**, representative H&E and KIT IHC images of the large intestine and stomach in *Etv1*^{-/-};*Kit*^{V558Δ/+} mice, demonstrating the lack of a KIT-positive ICC layer between the longitudinal muscle and the circular muscle layers in *Etv1*^{-/-};*Kit*^{V558Δ/+} mice. Scale bar, 50 μm.

Ano1 IHC

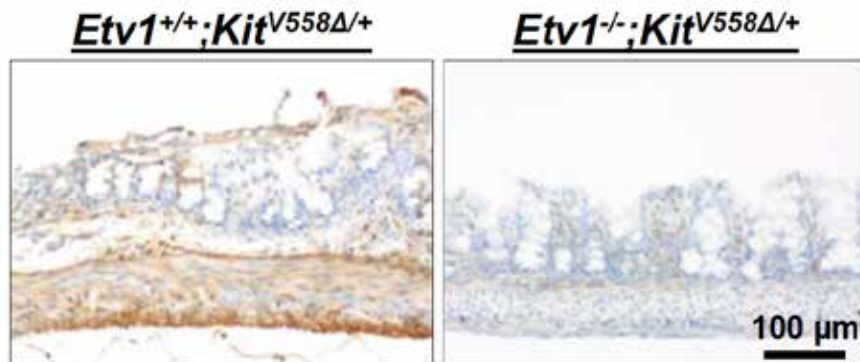


Figure 6.2 *Etv1* is required for intramuscular and myenteric ICC development
Representative images of the Ano1 IHC of the large intestine demonstrating that loss of *Ano1*-expressing intramuscular and myenteric ICCs in the large intestine of *Etv1*^{-/-};*Kit*^{V558Δ/+} compared to *Etv1*^{+/+};*Kit*^{V558Δ/+}. Scale bar: 100 μm.

To evaluate whether *Etv1* is required for GIST tumor proliferation, we crossed the *Etv1^{flox}* conditional knockout mouse model where *Etv1* exon 11 that encodes the DNA binding domain has been placed between LoxP sites (Patel, Kramer et al. 2003) with the *Rosa26^{CreERT2}* mouse that ubiquitously expresses the tamoxifen-activated *CreERT2* to generate a genetically engineered mouse (GEM) model where *Etv1* can be temporally ablated in adult tissues by tamoxifen treatment. Tamoxifen administration in adult *Etv1^{flox/flox};Rosa26^{CreERT2/CreERT2}* mice caused no observable phenotype, suggesting that the degree of *Etv1* ablation achieved is compatible with animal survival (data not shown). We next generated *Etv1^{flox/flox};Kit^{Δ558V/+};Rosa26^{CreERT2/CreERT2}* mice and compared the effect of tamoxifen and vehicle (corn oil) treatment in 2 month-old adult mice. In mice treated with tamoxifen, genomic DNA PCR of cecal tumor samples confirmed significant but incomplete excision of *Etv1* exon 11 (**Figure 6.3A**). Vehicle treated mice exhibited an identical phenotype to the *Kit^{Δ558V/+}* mice, with highly proliferative GIST-like tumors of the cecum and ICC-hyperplasia of the large intestine and the stomach (**Figure 6.4A-C**). In contrast, tamoxifen treated mice exhibited significant reduction of cell proliferation by Ki67 IHC in cecal tumors and ICC hyperplasia (**Figure 6.4A-C**). This level of Ki67 reduction is reminiscent of the imatinib treatment in *Kit^{Δ558V/+}* mice (Rossi, Ehlers et al. 2006). Further, *Etv1* ablation by tamoxifen treatment induced significant fibrosis indicated by Masson's trichrome stain in the cecal tumors similar to imatinib treatment (Kim, Cavnar et al. 2014) (**Figure 6.4D**). These observations demonstrate that *Etv1* is required for GIST tumor proliferation *in vivo*.

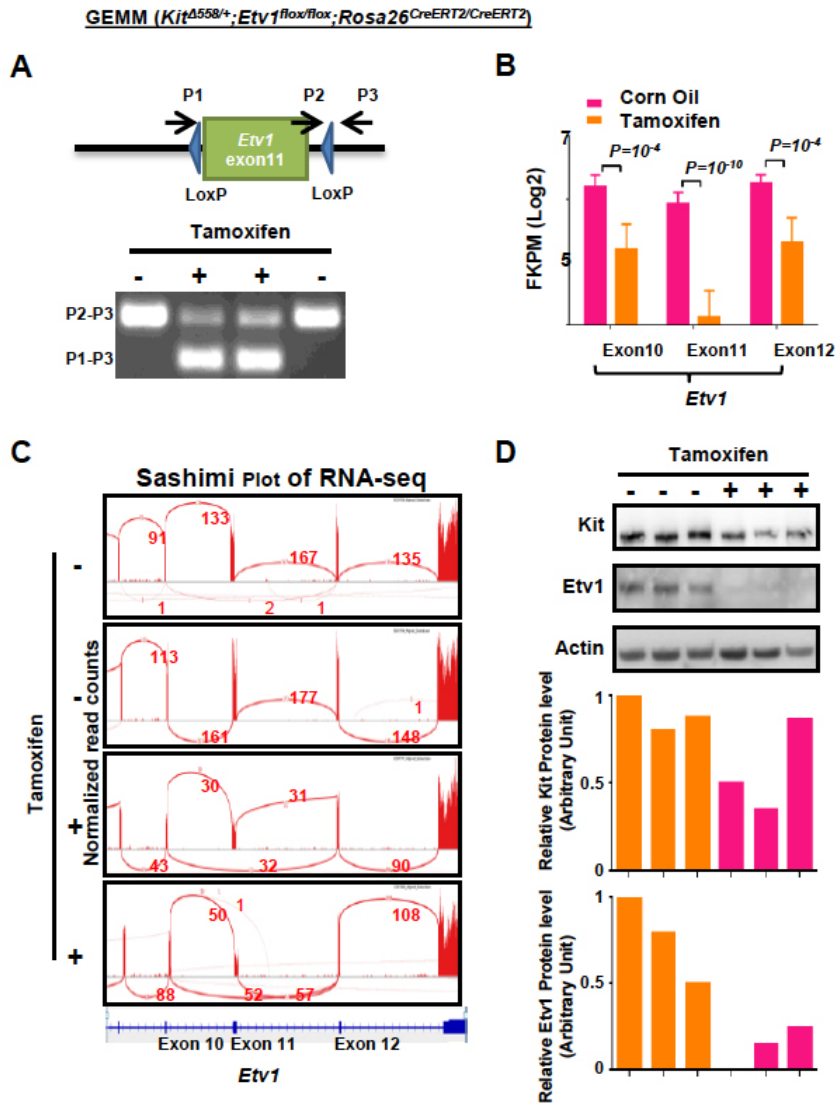


Figure 6.3 *Etv1* ablation with tamoxifen decreases *Etv1* and *Kit* expression in *Kit*^{Δ558/+}; *Etv1*^{fllox/fllox}; *Rosa26*^{CreERT2/CreERT2} mice

A, Schemata of floxed *Etv1* allele in the mouse model and representative genotyping of mice treated with tamoxifen vs. corn oil. **B**, Exonic expression of *Etv1* by RNA-seq in tamoxifen-treated vs. corn oil controls. Exon11 is the floxed exon as in **A**. n=3, Mean ± SEM. **C**, Representative Sashimi Plot of RNA-seq from GIST GEM model (*Kit*^{Δ558/+}; *Etv1*^{fllox/fllox}; *Rosa26*^{CreERT2/CreERT2}) with or without tamoxifen treatment showing approximately 50% ablation of *Etv1* exon 11. **D**, Immunoblot and immunoblot quantification of *Etv1* and *Kit* protein levels with tamoxifen-induced Cre mediated ablation of *Etv1* vs. corn oil control in 3 sets of mice.

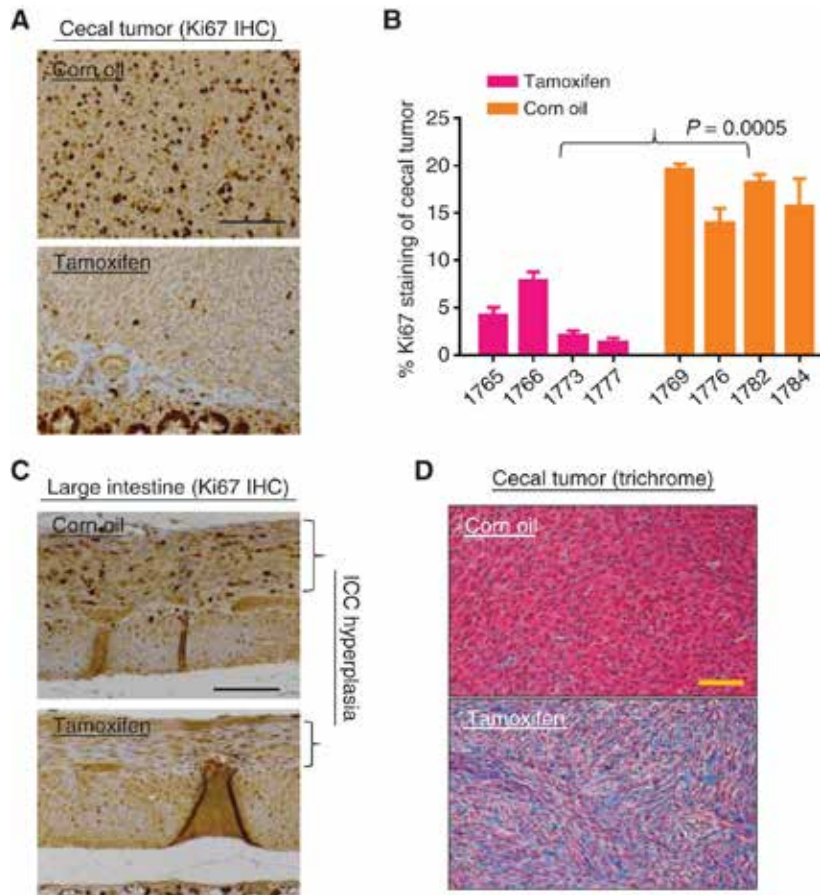


Figure 6.4 *ETV1* is required for GIST tumor proliferation *in vivo*

A, representative images of Ki67 IHC of the cecal tumor of 8- to 9-week-old *Etv1*^{flox/flox};*Kit*^{Δ558V/+};*Rosa26*^{CreERT2/CreERT2} mice treated with either corn oil or tamoxifen, demonstrating a significant reduction of Ki67 in the tamoxifen-treated (*Etv1*-ablated) tissues. Scale bar, 50 μm. B, quantification of Ki67 percentage in cecal tumors of 8- to 9-week-old *Etv1*^{flox/flox};*Kit*^{Δ558V/+};*Rosa26*^{CreERT2/CreERT2} mice treated with either corn oil or tamoxifen. $n = 3$, mean ± SEM; two-tailed unpaired t test ($P = 0.0005$). C, representative images of Ki67 IHC of the large intestine showing a significant reduction of Ki67 in the large intestine of the *Etv1*^{flox/flox};*Kit*^{Δ558V/+};*Rosa26*^{CreERT2/CreERT2} mice treated with tamoxifen compared with corn oil control. Scale bar, 50 μm. D, representative images of trichrome stains of cecal mass of *Etv1*^{flox/flox};*Kit*^{Δ558V/+};*Rosa26*^{CreERT2/CreERT2} mice treated with either corn oil or tamoxifen, demonstrating an increase in fibrosis in the tamoxifen-treated cohort. Scale bar, 50 μm.

ETV1 and KIT form a positive-feedback circuit to regulate target genes

We next examined the *Etv1*-regulated transcriptome by comparing transcriptional profiles between tamoxifen and vehicle treatment of *Etv1^{flox/flox};Kit^{V558Δ/+};Rosa-26^{CreERT2/CreERT2}* cecal tumors. The RNA-seq profile of *Etv1* transcript shows that tamoxifen treated tumors had a ~3.4-fold decrease in the floxed exon 11 count, implying a 3.4-fold decrease in full-length, functional *Etv1* transcript (**Figure 6.3B, C**). This decrease is due to 1) 1.7-fold decrease in *Etv1* overall transcript level and 2) ~50% of the remaining transcripts showing aberrant splicing from exon 10 to 12 skipping the floxed exon 11. The reduction of the overall transcript level with *Etv1* genetic ablation suggests that *Etv1* positively regulates its own transcription. Immunoblot and immunofluorescence analyses confirmed a decrease in *Etv1* protein levels in tamoxifen treated tumors compared to controls (**Figure 6.3D**).

Despite the incomplete ablation of *Etv1*, tamoxifen treatment induced robust transcriptional changes as seen by hierarchical clustering (**Figure 6.5A**). The RNA transcripts of known *Etv1* transcriptional targets including *Dusp6*, *Gpr20* and *Edn3* (Chi, Chen et al. 2010) were significantly reduced (**Figure 6.5B**). Interestingly, the *Kit* RNA transcript level was reduced by 1.7-fold with *Etv1* ablation (**Figure 6.5B**). Immunoblot, immunofluorescence and IHC analyses showed a consistent decrease in *Kit* protein levels in tamoxifen-treated cecal tumors (**Figure 6.3D and Figure 6.5C,D**). The ICC hyperplasia of the large intestine and stomach also showed a reduction in *Kit* protein levels with tamoxifen treatment (**Figure 6.5D and Figure 6.6**).

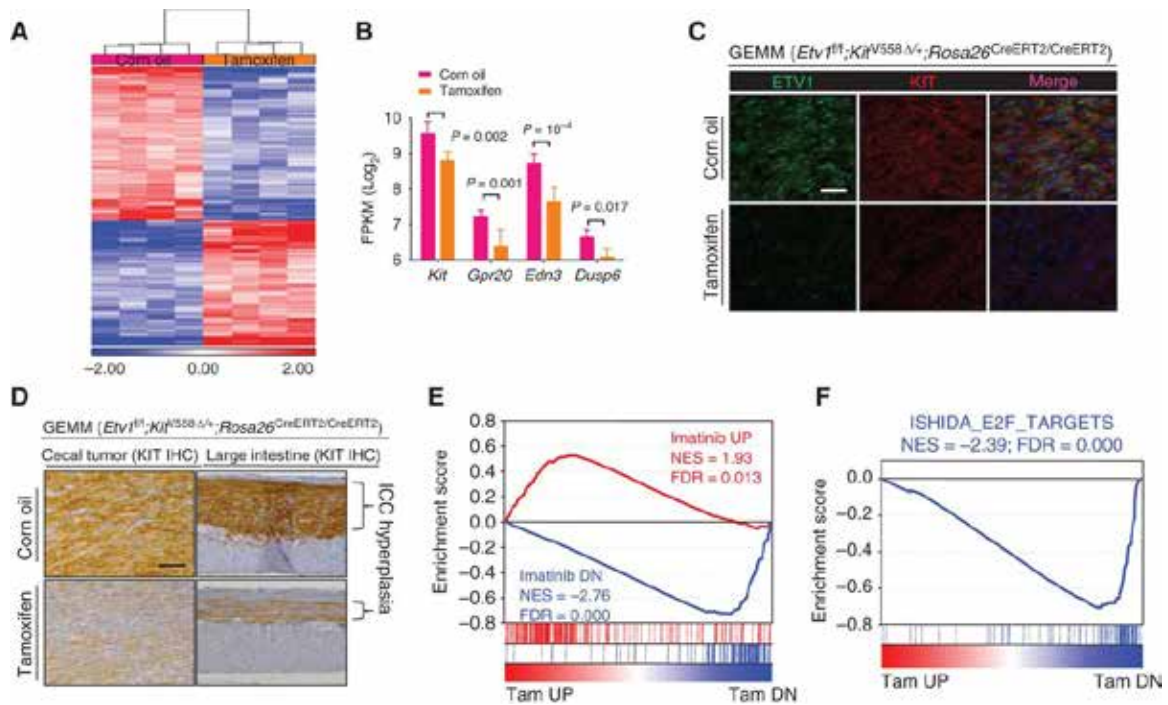


Figure 6.5 *ETV1* positively regulates *Kit* expression in murine GISTs

A, heatmap of significantly differentially expressed genes between corn oil control- and tamoxifen-treated murine GIST tumors identified by RNA-seq. Clustering was based on the most differentially expressed 228 genes with FDR <0.05 and fold change >2.0. Samples are color coded based on treatment status: pink, corn oil-treated; orange, tamoxifen-treated. Scale bar, mean normalized fold change by \log_2 . **B**, RNA-seq gene expression quantification (FPKM, fragments per kilobase mapped) of *Kit* and a representative group of *ETV1* transcriptional targets in tamoxifen-treated versus corn oil-treated murine GISTs. **C**, representative IF images of *ETV1* (green) and *KIT* (red) protein in cecal tumors from *Etv1*^{fl/fl};*Kit*^{V558Δ/+};*Rosa26*^{CreERT2/CreERT2} mice treated with tamoxifen or corn oil, demonstrating *ETV1* ablation and decreased *KIT* protein level. Nuclei (DAPI, blue). Scale bar, 50 μ m. **D**, representative *KIT* IHC images of the cecal tumors and ICC hyperplasia in the large intestines of mice treated as in **C**. Scale bars, 50 μ m. **E**, GSEA plots of the ranked list of the differentially expressed genes between tamoxifen (Tam)-treated versus corn oil-treated murine GIST tumor samples, using two gene sets, Imatinib UP (imatinib upregulated) and Imatinib DN (imatinib downregulated). **F**, GSEA plots of the ranked list of the differentially expressed genes between tamoxifen-treated versus corn oil-treated murine GIST tumor samples, using the ISHIDA_E2F_TARGETS gene set. GEMM, genetically engineered mouse model; NES, normalized enrichment score.

GEMM (*Etv1*^{f/f};*Kit*^{V558Δ/+};*Rosa26*^{CreERT2/+})

Stomach (Kit IHC)

Corn Oil

Tamoxifen

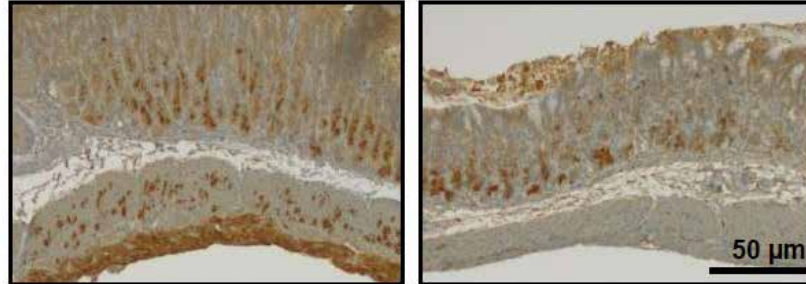


Figure 6.6 *Etv1* positively regulates Kit expression in murine stomach
Representative images of the Kit IHC of the stomach demonstrating Kit protein reduction in the stomach of the *Etv1*^{flox/flox};*Kit*^{V558Δ/+};*Rosa26*^{CreERT2/CreERT2} mice treated with tamoxifen compared to corn oil control. Scale bar: 50 μm.

To determine the biological processes perturbed by *Etv1* ablation, we performed Gene Set Enrichment Analysis (GSEA) comparing tamoxifen and corn oil treated tumors (Subramanian, Tamayo et al. 2005). Remarkably, the set of genes most down-regulated by imatinib in *Kit*^{V558Δ/+} mice (*Imatinib DN*) (Kwon, Hwang et al.) is the most enriched gene set among those downregulated by tamoxifen treatment (**Figure 6.5E**). Likewise, the set of genes most up-regulated by imatinib is highly enriched among those upregulated by tamoxifen treatment, suggesting that *Etv1* and *Kit* regulate a common set of core transcriptional program. This is consistent with the model that *Etv1* is a major downstream effector of *Kit*, and also that *Etv1* regulates *Kit* expression, which in turn, regulates *Kit*-dependent genes. In addition, multiple cell-cycle related gene sets, including one of E2F target genes are enriched in those downregulated by tamoxifen treatment (**Figure 6.5F**). These data are consistent with the decrease in Ki67 staining after tamoxifen treatment and suggest that *Etv1* is required for tumor proliferation and growth *in vivo*.

To determine whether *ETV1* regulates *KIT* transcription in human GIST, we knocked down *ETV1* with shRNA in three GIST cell lines: GIST48, GIST882 and GIST-T1. In each line, there was a modest decrease in *KIT* transcript levels after *ETV1* knockdown (**Figure 6.7A**). CRISPR/Cas9-mediated knockout of *ETV1* in GIST48 cells also resulted in decrease in both *KIT* transcript and protein levels (**Figure 6.8A,B**). We next retrovirally overexpressed *ETV1* in GIST882 and GIST-T1 cells and found a modest upregulation in *KIT* transcript level (**Figure 6.7B**). We performed GSEA of *ETV1* knockdown in each of the three cell lines and for each cell line, the genes most downregulated by imatinib was the most enriched gene set among downregulated genes by *ETV1* knockdown while genes most upregulated by imatinib was the most enriched gene set among unregulated genes by *ETV1* knockdown (**Figure 6.7C**), consistent with our observation in mouse tissues (**Figure 6.5**).

To determine whether *KIT* is a direct transcriptional target of *ETV1*, we analyzed ChIP-seq of *ETV1* in human GIST cells. We found multiple binding sites of *ETV1* at the *KIT* enhancer regions characterized by high H3K4me1 and low H3K4me3 marks in human GIST cells (**Figure 6.7D**). The direct and specific binding of *ETV1* to the enhancer regions of the *KIT* locus was confirmed by ChIP-qPCR with siRNA-mediated suppression of *ETV1* in all three GIST cell lines (**Figure 6.7E-G**). These observations suggest that in addition to the regulation of *ETV1* protein stability by MAP kinase signaling downstream of mutant *KIT* signaling, *ETV1* directly and positively regulates *KIT* expression and therefore, it cooperates with mutant *KIT* by forming a positive feedback circuit to promote GIST tumorigenesis.

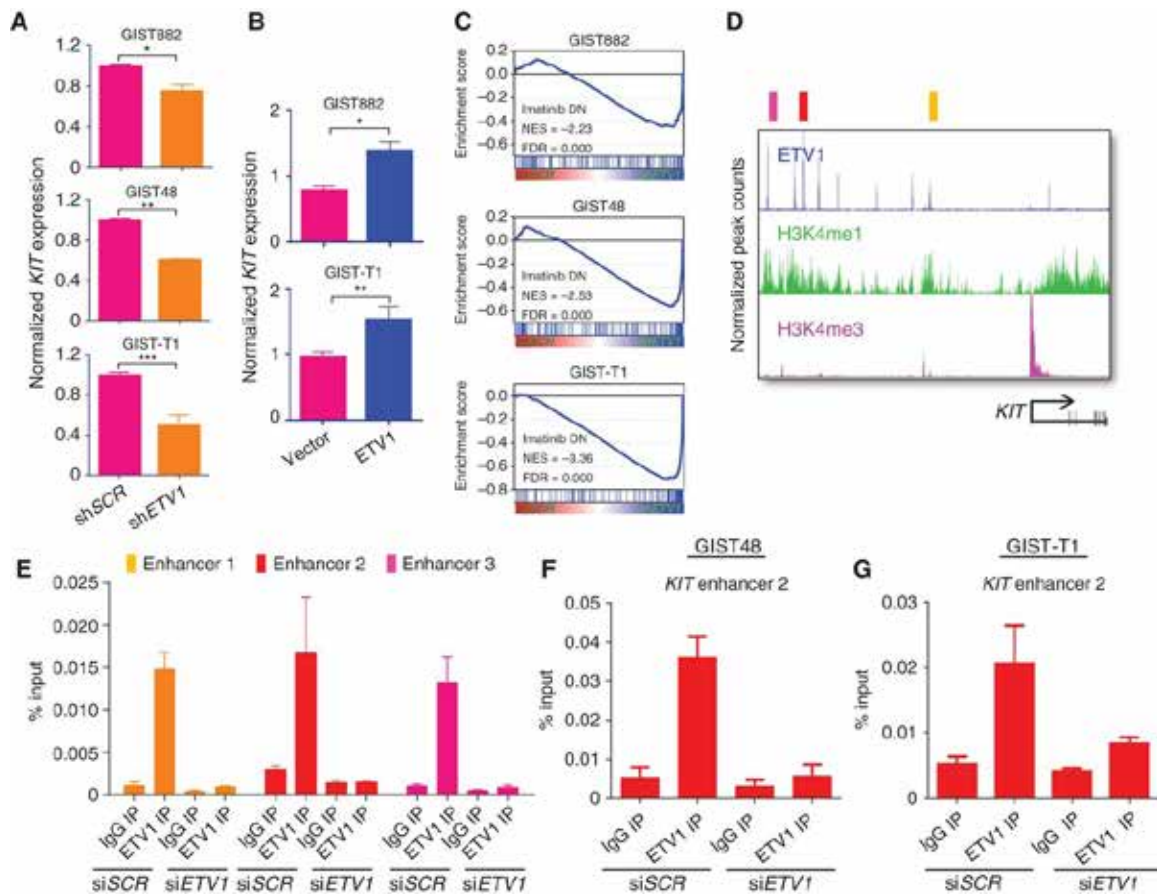


Figure 6.7 *ETV1* positively regulates *KIT* expression through direct binding to *KIT* enhancers in human GIST cells and forms a positive feedback circuit in GIST oncogenesis

A, mRNA expression of *KIT* in human GIST882, GIST48, and GIST-T1 cells with *ETV1*-specific shRNA. $n = 3$, mean \pm SEM. Two-tailed unpaired t test: *, $P < 0.05$; **, $P < 0.01$; ***, $P < 0.001$. **B**, mRNA expression of *KIT* in GIST882 and GIST-T1 cells 48 hours after retroviral transduction of *ETV1* expression vector or empty vector control. $n = 3$, mean \pm SEM. Two-tailed unpaired t test: *, $P < 0.05$; **, $P < 0.01$. **C**, GSEA plots of the ranked list of the sh*ETV1*-downregulated genes in human GIST cells, using the Imatinib DN (imatinib downregulated) gene set. **D**, representative of ChIP-seq reads of *ETV1*, H3K4me1, and H3K4me3 at the *KIT* transcription start site (H3K4me3) and enhancer regions (H3K4me1 and *ETV1*) in human GIST48 cells. Pink, red, and yellow colors represent regions selected for ChIP-qPCR studies. **E**, ChIP-qPCR of *ETV1* at the *KIT* enhancer loci as indicated by color code as in **G** with siRNA-mediated suppression of *ETV1* (si*ETV1*) versus scrambled control siRNA (siSCR) in GIST882 cells. $n = 3$, mean \pm SD. **F**, ChIP-qPCR of *ETV1* at the *KIT* enhancer 2 (red mark in **D**) in GIST48 cells. $n = 3$, mean \pm SD. **G**, ChIP-qPCR of *ETV1* at the *KIT* enhancer 2 (red mark in **D**) in GIST-T1 cells. $n = 3$, mean \pm SD.

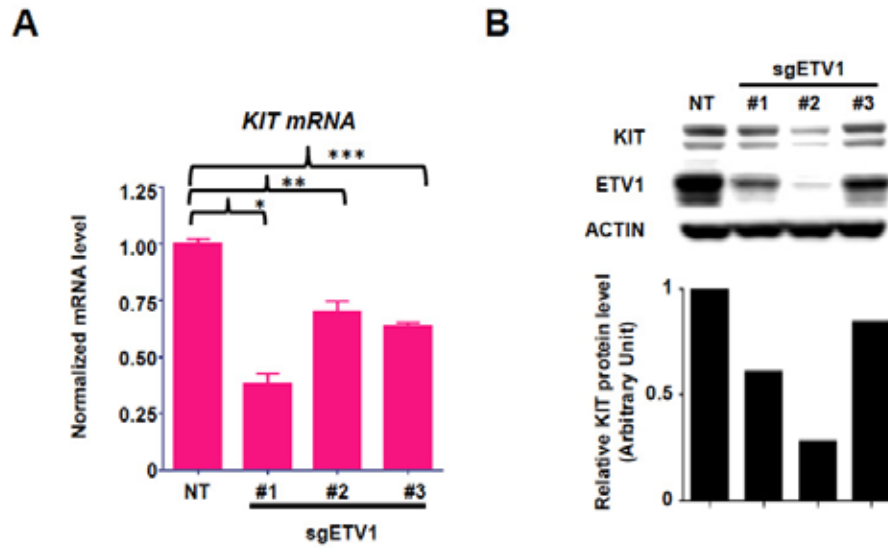


Figure 6.8 *ETV1* regulates *KIT* expression in GIST48 cells

A, Normalized mRNA level of *KIT* in GIST48 cells with CRISPR-mediated *ETV1* knockout. NT: non-targeting control for *ETV1* sgRNA. n=3, Mean \pm SEM. * $p < 0.0001$; ** $p < 0.0001$; *** $p < 0.0001$. **B**, Immunoblot and immunoblot quantification of *ETV1* and *KIT* protein levels in GIST48 cells with CRISPR-mediated *ETV1* knockout.

Combined inhibition of the KIT and MAP kinase signaling represents an effective strategy to target ETV1 and suppress GIST tumor growth

The fact that the ETV1 protein stability requires active MAP kinase signaling downstream of active KIT signaling (Chi, Chen et al. 2010) has provided us with the rationale to target ETV1 protein stability by inhibiting the MAP kinase and the KIT signaling pathways. When we treated the imatinib-sensitive GIST882 and GIST-T1 cells with either imatinib (a KIT inhibitor) or MEK162 (a MEK inhibitor), we observed a rapid inhibition of the MAP kinase activity (assayed by pERK) accompanied by rapid loss of the ETV1 protein (**Figure 6.9A**). This reduction of the total ETV1 protein level is associated with a reduction of ETV1 binding at the *ETV1*-regulated gene loci, e.g., *DUSP6* and *KIT* (**Figure 6.9B**) and a reduction of the *DUSP6* and *KIT* transcripts by 8 hours of treatment (**Figure 6.10A-D**). Notably, the ability of MEK162 to durably inhibit MAP kinase pathway and the ETV1 protein stability is cell line specific—GIST882 cells displayed sustained inhibition while GIST-T1 cells showed reactivation of the MAP kinase pathway and re-accumulation of ETV1 protein starting at 2 hours after treatment (**Figure 6.9A**). We then evaluated the combined lineage inhibition using MEK162 and imatinib. *In vitro*, we observed additive effects on growth suppression across a range of doses of MEK162 and imatinib. A synergistic effect on growth suppression was best appreciated at lower doses of each drug, best seen when 0.5 μ M MEK162 was combined with low dose imatinib (62.5 nM in GIST882 and 40 nM in GIST-T1; **Figure 6.9C, D**).

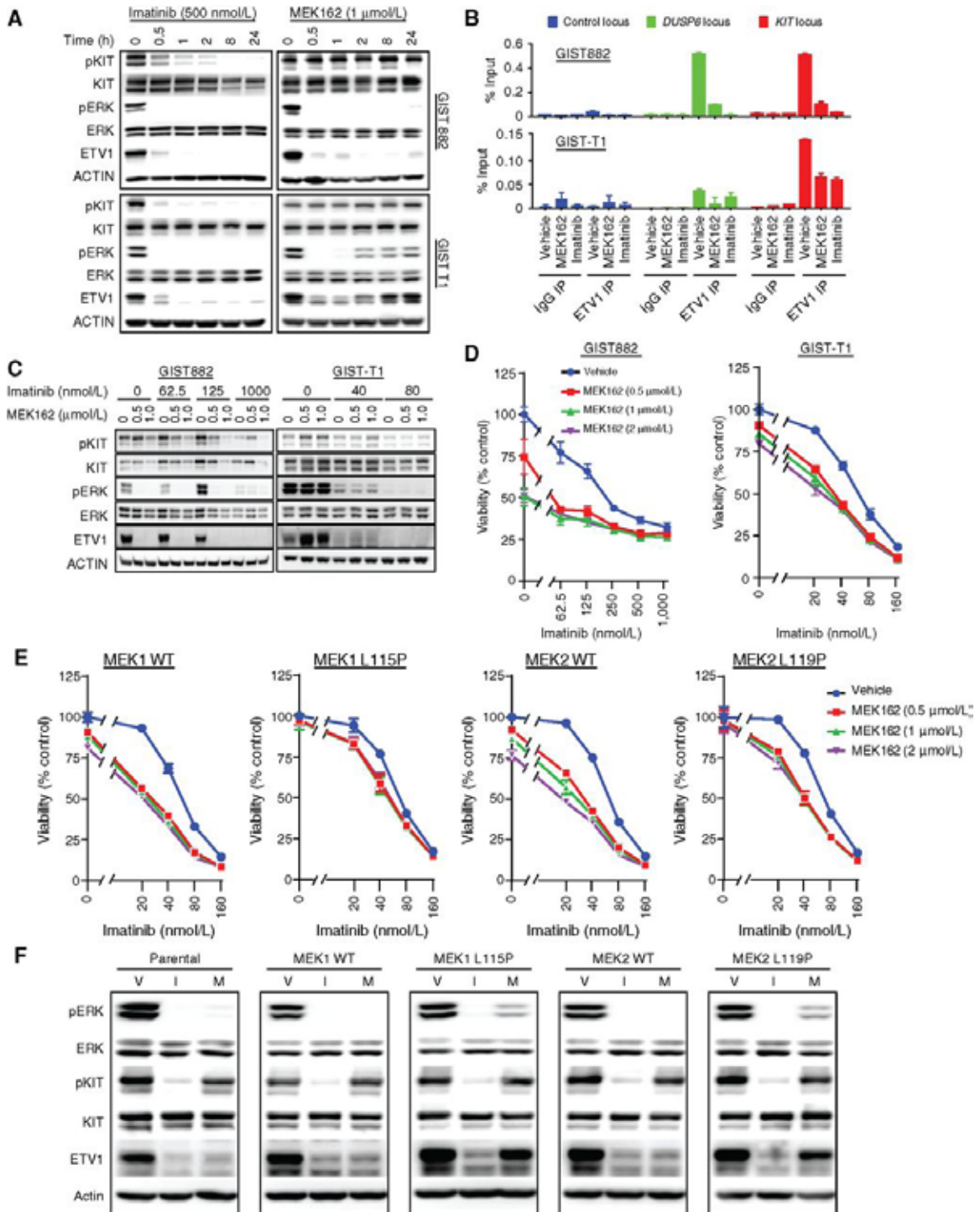


Figure 6.9 Combined inhibition of MAP kinase and KIT signaling destabilizes ETV1 protein and results in enhanced growth suppression of human GIST cells

A, immunoblot of ETV1, pKIT, and pERK levels in GIST882 and GIST-T1 cells treated with imatinib (500 nmol/L) or MEK162 (1 μ mol/L) for the indicated time points. **B**, ETV1 localization at the target gene loci (i.e., KIT and DUSP6) by ChIP-qPCR in GIST cells treated with imatinib (1 μ mol/L) or MEK162 (500 nmol/L) for 8 hours in GIST882 cells, or imatinib (80 nmol/L) or MEK162 (500 nmol/L) for 2 hours in GIST-T1 cells. **C**, immunoblot of ETV1 and KIT, MAP kinase, and AKT signaling pathways in GIST882 and GIST-T1 cells treated with various doses of imatinib and MEK162 as indicated for 8 hours. **D**, cell viability by Alamar Blue of GIST882 and GIST-T1 cells treated with various doses of imatinib and MEK162 as indicated for 7 days. $n = 3$, mean \pm SEM. **E**, cell viability by Alamar Blue of GIST-T1 cell expressing different MEK constructs treated with various doses of imatinib and MEK162 as indicated for 7 days. $n = 3$, mean \pm SEM. **F**, immunoblot of ETV1, KIT, and MAP kinase signaling in GIST-T1 parental cells, GIST-T1 cells expressing MEK1^{WT}, MEK1^{L115P}, MEK2^{WT}, and MEK2^{L119P}. Cells were treated for 1 hour as indicated. V, DMSO; I, imatinib (500 nmol/L); M, MEK162 (1,000 nmol/L).

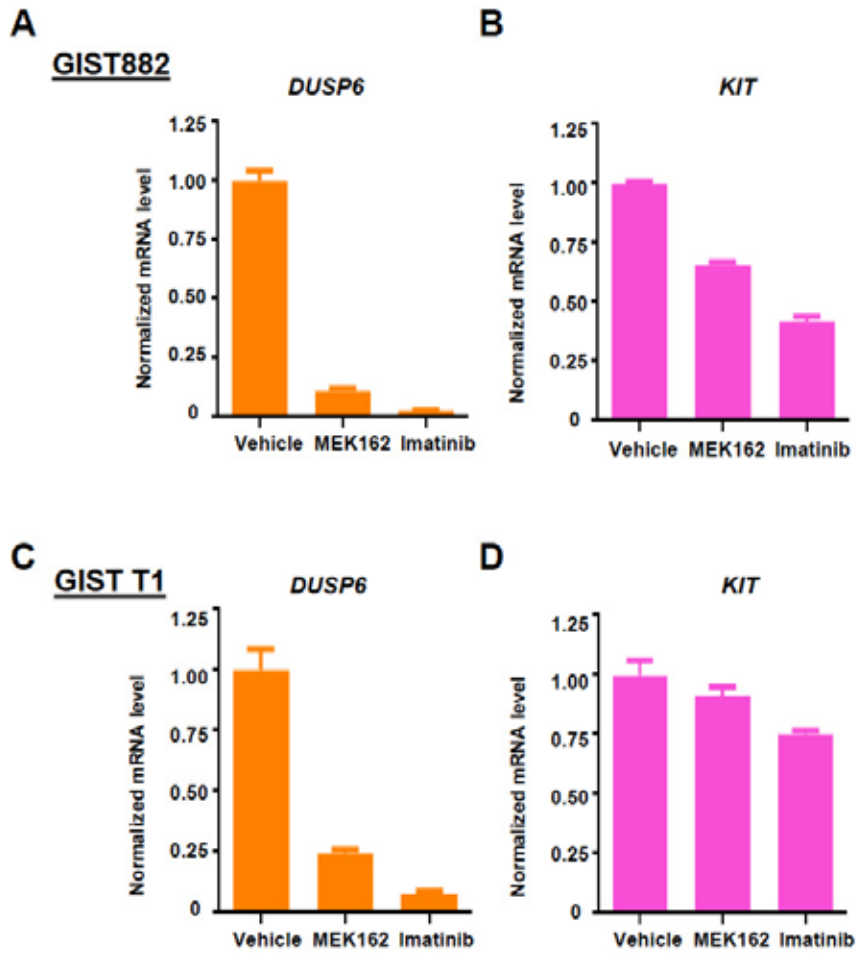


Figure 6.10 MAP kinase pathway inhibition decreases *ETV1* target gene expression

Normalized mRNA expression of *DUSP6* (**A, C**) and *KIT* (**B, D**) in GIST cells. **A, B**, GIST882 cells treated with DMSO, MEK162 (500 nM), Imatinib (1000 nM) or the combination for 8 hours. **C, D**, GIST T1 cells treated with DMSO, MEK162 (500 nM), Imatinib (40 nM) or the combination for 8 hours. n=3, Mean \pm SEM

To access whether the synergistic effect is due to on-target effect of MEK162, we expressed wild-type MEK1/2 (WT) or MEK1/2 mutants (*MEK1^{L115P}*, *MEK2^{L119P}*) that are resistant to allosteric MEK inhibitors such as MEK162 due to reduced drug binding (Delaney, Printen et al. 2002). GIST-T1 cells expressing either *MEK1^{L115P}* or *MEK2^{L119P}* were more resistant to MEK162 alone. Moreover, the combination of MEK162 to imatinib conferred less synergistic growth inhibition in the presence of *MEK1^{L115P}* or *MEK2^{L119P}* in GIST-T1 cells (**Figure 6.9E**). This corresponded to a decreased ability of MEK162 to inhibit ERK phosphorylation and ETV1 protein stability (**Figure 6.9F**). These data indicate that the synergistic effect of MEK162 and imatinib combination treatment is the result of on-target effect of MEK162.

Next, we tested the effect of combined MEK162 and imatinib *in vivo*. In the GIST882 xenograft model, single agent imatinib or MEK162 stabilized tumor growth at the maximum tolerated doses (**Figure 6.11A**). Remarkably, the combination of imatinib and MEK162 treatment resulted in a dramatic reduction (>50%) of tumor size within 7 days and complete responses with prolonged treatment even at significantly reduced doses of MEK162 (10 mg/kg) or imatinib (50 mg/kg) (**Figure 6.11A, B**). Combination therapy provided more potent and durable inhibition of MAP kinase signaling (**Figure 6.11C, Figure 6.12A**). Importantly, the ETV1 protein level was more potently and durably inhibited, which was associated with reduction of *ETV1* transcriptional targets (e.g., *DUSP6* and *KIT*) than either imatinib or MEK162 alone (**Figure 6.11C, Figure 6.12B**). When GIST882-xenografted mice were treated from the same day of cell implantation, only the combination of imatinib and MEK162 successfully prevented xenograft tumor formation, suggesting that dual lineage inhibition could also inhibit GIST tumor formation *in vivo* (**Figure 6.12C**).

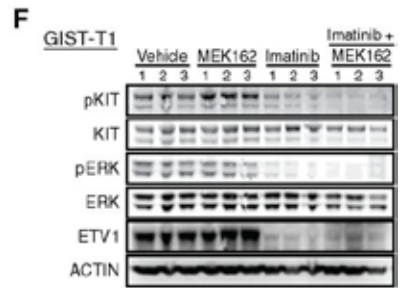
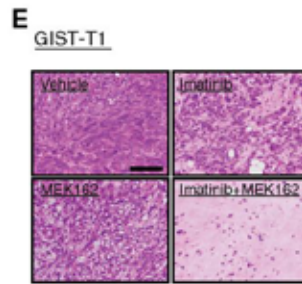
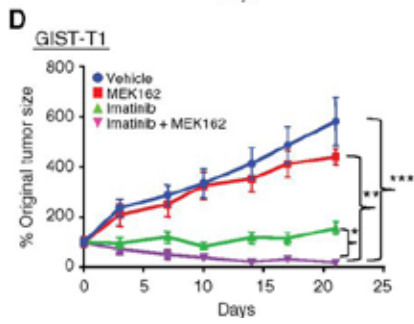
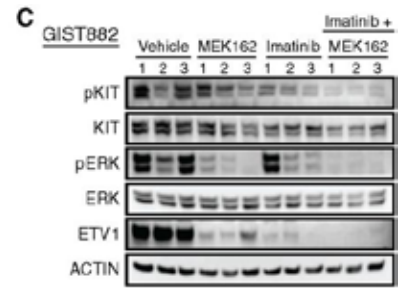
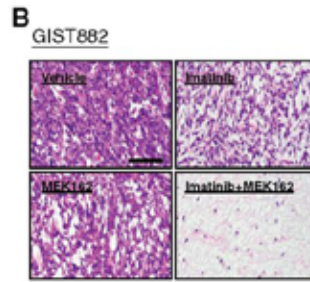
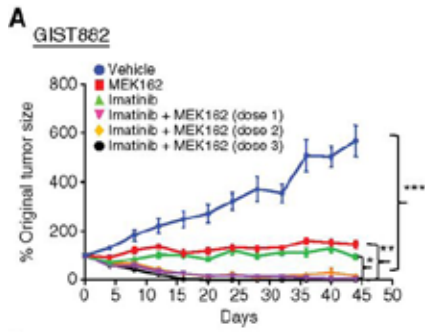


Figure 6.11 Combined inhibition of the MAP kinase and KIT signaling synergistically suppresses tumor growth in *in vivo* GIST xenograft mouse models

A, treatment response of GIST882 xenografts in SCID mice. The treatments are: (i) Vehicle (blue): water; (ii) imatinib (green): 100 mg/kg twice a day; (iii) MEK162 (red): 30 mg/kg twice a day; (iv) imatinib + MEK162 (dose 1; magenta): imatinib (100 mg/kg twice/day) + MEK162 (10 mg/kg twice/day); (v) imatinib + MEK162 (dose 2; yellow): imatinib (50 mg/kg twice/day) + MEK162 (30 mg/kg twice a day); (vi) imatinib + MEK162 (dose 3; black): imatinib (100 mg/kg twice a day) + MEK162 (30 mg/kg twice a day; dose 3; black). $n = 6-8$, mean \pm SEM. Two-tailed unpaired t test: *, $P < 0.0001$; **, $P < 0.0001$; ***, $P < 0.0001$. **B**, representative H&E images of GIST882 xenografts after 14 days of drug treatment by oral gavage as indicated. Vehicle: water; imatinib: 100 mg/kg twice a day; MEK162: 30 mg/kg twice a day; imatinib (100 mg/kg twice a day) + MEK162 (30 mg/kg twice a day). Scale bar, 50 μ m. **C**, immunoblots of three representative GIST882 xenograft tumors explanted after 2 days of drug treatment by oral gavage as indicated. Vehicle: water; imatinib: 100 mg/kg twice a day; MEK162: 30 mg/kg twice a day; imatinib (100 mg/kg twice a day) + MEK162 (30 mg/kg twice a day). **D**, treatment response of GIST-T1 xenografts in SCID mice as indicated by oral gavage. The treatments are: (i) Vehicle: water; (ii) imatinib: 80 mg/kg twice a day; (iii) MEK162: 30 mg/kg twice a day; (iv) imatinib (80 mg/kg twice a day) + MEK162 (30 mg/kg twice a day). $n = 10$, mean \pm SEM. Two-tailed unpaired t test: *, $P < 0.0001$; **, $P < 0.0001$; ***, $P < 0.0001$. **E**, representative H&E images of GIST-T1 xenografts after 21 days of drug treatment by oral gavage as indicated. Vehicle (blue): water; imatinib (green): 80 mg/kg twice a day; MEK162 (red): 30 mg/kg twice a day; imatinib + MEK162 (magenta): imatinib (80 mg/kg twice a day) + MEK162 (30 mg/kg twice a day). Scale bar, 50 μ m. **F**, immunoblots of three representative GIST-T1 xenograft tumors explanted after 2 days of drug treatment by oral gavage as indicated. Vehicle: water; imatinib: 80 mg/kg twice a day; MEK162: 30 mg/kg twice a day; imatinib (80 mg/kg twice a day) + MEK162 (30 mg/kg twice a day).

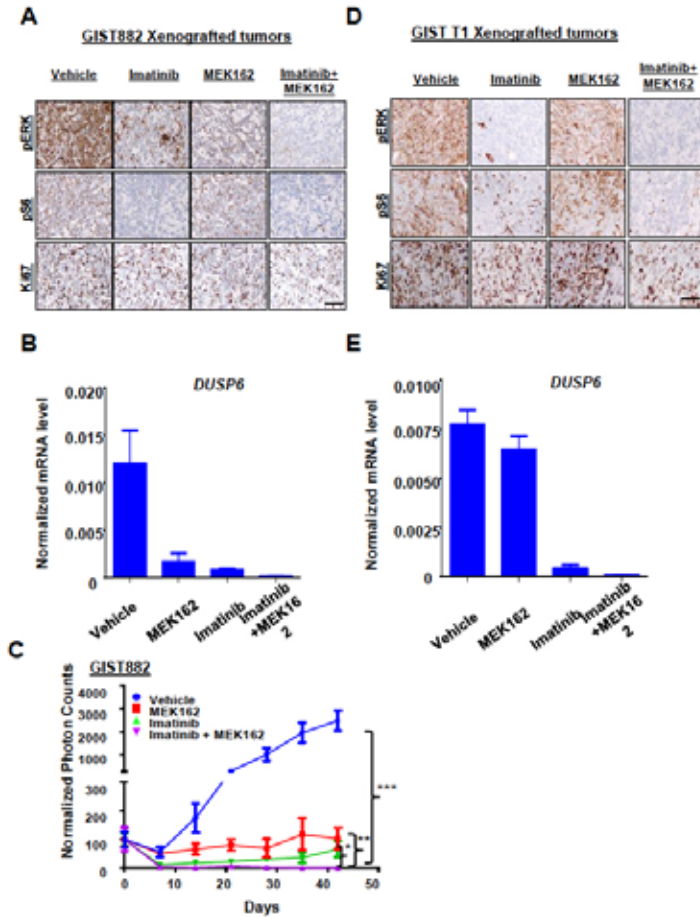


Figure 6.12 Dual lineage inhibition inhibits tumor initiation *in vivo*

A, Immunohistochemistry (IHC) of representative xenografted GIST882 xenografts treated under conditions as indicated for 2 days by oral gavages. Vehicle: water; MEK162: 30mg/Kg, BID; Imatinib: 100 mg/Kg, BID; Imatinib+MEK162: Imatinib (100 mg/Kg, BID) in combination with MEK162 (30mg/Kg, BID); **B**, Normalized mRNA expression of *DUSP6* in explanted GIST882 xenografts after treatment under the same conditions as in **A**. n=3, Mean \pm SEM. **C**, Bioluminescence of luciferase labeled GIST882 grafted tumours in SCID mice with various treatment as indicated by oral gavages from the day of implantation. The treatment cohorts are as the following: 1) Vehicle: water; 2) Imatinib: 80 mg/kg BID; 3) MEK162: 30 mg/kg BID; 4) Imatinib (80 mg/kg BID) + MEK162 (30 mg/kg BID). n=4, Mean \pm SEM. Two-tailed unpaired t test: * $p < 0.05$; ** $p < 0.05$; *** $p < 0.001$. **D**, Immunohistochemistry (IHC) of representative xenografted GIST-T1 xenografts treated under conditions as indicated for 2 days by oral gavages. Vehicle: water; MEK162: 30mg/Kg, BID; Imatinib: 80 mg/Kg, BID; Imatinib+MEK162: Imatinib (80 mg/Kg, BID) in combination with MEK162 (30mg/Kg, BID); Scale bar: 100 μ m. N=3 for each treatment conditions. **E**, Normalized mRNA expression of *DUSP6* in explanted GIST-T1 xenografts after treatment under the same conditions as in **D**. n=3, Mean \pm SEM.

In the GIST-T1 xenograft model, single agent imatinib led to tumor stabilization. However, single agent MEK162 did not significantly inhibit tumor growth (**Figure 6.11D**), consistent with the inability of MEK162 to durably inhibit the MAP kinase pathway in GIST-T1 cells (**Figure 6.9A, C** and **Figure 6.11F**). Yet, as in GIST882 xenografts, the combination of imatinib and MEK162 resulted in near complete response in GIST-T1 xenografts within 3 weeks of treatment (**Figure 6.11D, E**). The treatment effects correlated with KIT and MAP kinase signaling pathway inhibition, ETV1 protein destabilization, and downregulation of ETV1 target genes (i.e., *DUSP6* and *KIT*) (**Figure 6.11F** and **Figure 6.12D, E**). These observations demonstrated a clear synergistic growth inhibitory effect of imatinib and MEK162 in GIST tumor growth *in vivo*. It is notable that the synergy of combination is more apparent in *in vivo* human GIST xenograft studies than in *in vitro* cell line assays.

We next examined the combination targeting strategy in the genetically engineered *Kit*^{V558Δ/+} GIST mouse model that is partially sensitive to imatinib treatment (Rossi, Ehlers et al. 2006). Treatment with single agent MEK162 or imatinib for 5 days resulted in a reduction of tumor proliferation by Ki67 and increased tumor fibrosis by trichrome staining (**Figure 6.13A-D**). The combination treatment of imatinib and MEK162 lead to increased tumor fibrosis and significantly greater reduction of Ki-67 than either single agent (**Figure 6.13A, B**). Moreover, the combination treatment had significantly reduced tumor weight compared to either single agent alone or to vehicle (**Figure 6.13C**). These treatment effects of the combination therapy are accompanied by increased inhibition of the Kit and MAP kinase signaling pathways, decreased Etv1 protein and its downstream target *Dusp6* (**Figure 6.13D**). The treatment data in both xenografted human GIST models and genetically engineered GIST mouse models indicate that the combination therapy of imatinib and MEK162 is a more effective treatment for imatinib-sensitive GIST than either single agent alone *in vivo*.

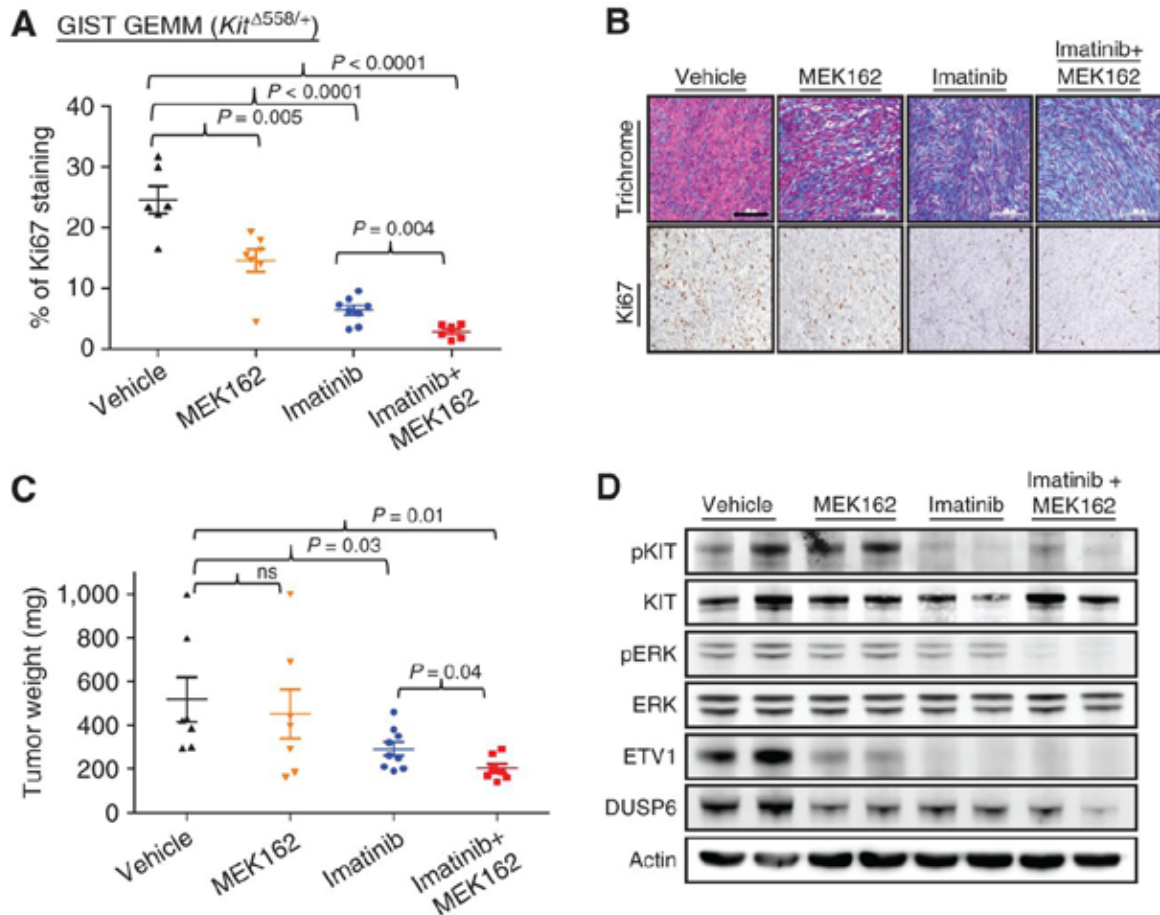


Figure 6.13 Combined inhibition of MAP kinase and KIT signaling synergistically suppresses tumor growth in genetically engineered GIST mouse model

A, Ki67 percentage of murine cecal GISTs isolated after 5 days of drug treatment by oral gavage of the GIST GEMM (*Kit*^{V558Δ/+}). Vehicle (black): water; imatinib (blue): 50 mg/kg twice a day; MEK162 (yellow): 30 mg/kg twice a day; imatinib + MEK162 (red): imatinib (50 mg/kg twice a day) + MEK162 (30 mg/kg twice a day). $n = 7-9$, mean \pm SEM. Two-tailed unpaired t test, P value indicated in figure. **B**, representative Trichrome and Ki67 IHC images of murine cecal GISTs isolated after 5 days of drug treatment by oral gavage of the GIST GEMM (*Kit*^{V558Δ/+}) under the same conditions as in A. Scale bar, 50 μ m. **C**, tumor weight of murine cecal GISTs isolated after 5 days of drug treatment by oral gavage of the GIST GEMM (*Kit*^{V558Δ/+}) under the same conditions as in A. $n = 7-9$, mean \pm SEM. Two-tailed unpaired t test, P value indicated in figure. **D**, immunoblots of representative cecal tumors from GIST GEMM (*Kit*^{Δ558/+}) treated under the same drug treatment conditions as indicated in A for 1.5 days. Two cecal tumors from two different mice for each treatment conditions. DUSP6 is one of the transcriptional targets of ETV1. GEMM, genetically engineered mouse model.

Discussion

Using genetically engineered mouse models, we have demonstrated the *in vivo* requirement of the lineage specific master regulator, ETV1, in GIST initiation and proliferation. We have further demonstrated that ETV1 positively regulates *KIT* expression level by direct binding to the *KIT* enhancer regions and it forms a positive feedback circuit to cooperate with mutant *KIT* in GIST oncogenesis. These observations posit ETV1 as a relevant therapeutic target for the treatment of GISTs. In addition, since *ETV1* is required for the survival of GIST precursor ICCs and is required for GIST tumor initiation *in vivo*, it may also represent a therapeutic target for the Kit-low GIST progenitor/stem cell population. Importantly, targeting ETV1 will help break the positive feedback circuit and indirectly target *KIT* expression independent of the *KIT* mutational status.

While it is challenging to therapeutically target non-ligand dependent transcription factors, the unique MAP kinase signaling dependent regulation of ETV1 protein stability has allowed us to target ETV1 protein stability in GIST. The acquisition of *KIT* activating mutations during GIST tumorigenesis activates downstream MAP kinase signaling and augmented stability of ETV1 protein (Chi, Chen et al. 2010). Our data in two imatinib-sensitive GIST cell lines suggest that mutant *KIT* is the principal driver of MAP kinase activation as imatinib treatment significantly inhibited MAP kinase activation, ETV1 protein stability and *ETV1*-mediated transcription. *In vitro*, MEK162 synergized with lower doses of imatinib but higher doses of imatinib alone can maximally suppress MAP kinase activity and cell proliferation (**Figure 6.8**). However, in both xenograft systems and genetically engineered mouse models *in vivo*, maximum tolerated doses of imatinib cannot adequately and durably suppress MAP kinase activity and ETV1 protein levels. This may be due to either the inability to attain sufficient drug levels to fully inhibit

KIT (Kim, Cavnar et al. 2014) or the presence of paracrine signals that activate MAP kinase pathway bypassing KIT (Rossi, Ehlers et al. 2006). The survival signals that bypass KIT may be heterogeneous dependent on the tumor contexts. Here, addition of even low doses of MEK162, leads to durable destabilization of ETV1 protein and dramatically augments tumor response, resulting in complete responses.

The response to single agent imatinib in our model systems mirrors that of patients undergoing first-lines imatinib treatment. While the majority of patients attain clinical benefits with imatinib treatment, the RESIST response rate is only ~50% and radiographic or pathologic complete responses rarely occur. Our data suggest that the combination therapy represents a significantly more effective strategy than imatinib alone in GIST clinical management and may prevent the development of imatinib-resistance in advanced GIST if used upfront.

CHAPTER SEVEN

Discussion and Future Directions

The current study represents a comprehensive investigation at the oncogenic roles of *ETV1* across two cancer types. We demonstrate that *ETV1* is highly expressed in MPNST and required for MPNST survival likely through regulating key sets of genes. We further identify genetic alterations of three critical pathways in MPNSTs (*NF1*, *CDKN2A* and *PRC2*) when using comprehensive genomic approaches to understand MPNST pathogenesis. *ETV1* was shown to be the lineage specific survival transcription factor for another type of sarcoma, GISTs. Using genetic engineered mouse modeling, we show that *ETV1* is expressed in the cell of origin for GIST, ICC-MY and ICC-IM. Activation of oncogenic *BRAFV600E* and *p53* mutations in the GIST precursor ICCs with *ETV1*-driven cre recombinase lead to GISTs tumorigenesis that highly resembled human GISTs, suggesting the potential application of *ETV1*-driven cre allele to model characteristic mutations in human GISTs or other *ETV1*-driven cancers. Furthermore, we describe a novel strategy of targeting *ETV1* protein stability by the combination of MEK and KIT inhibitors that synergistically suppress tumor growth. This strategy has the potential to change first-line therapy in GIST clinical management and provide insights for management of other *ETV1*-driven cancers.

Role of ETV1 in MPNST pathogenesis

Our results demonstrate that *ETV1* is highly expressed in MPNST and required for MPNST survival. While we show the deregulation of *ETV1* in majority of MPNST cell lines and MPNST patient tumors, the mechanism through which

ETV1 is expressed or upregulated in MPNST is unclear. *ETV1* has been shown to be upregulated in cancers through translocations in Ewing sarcomas and prostate cancer, amplification in melanoma, or inherited in the cancer precursor cell and stabilized by up-regulated MAPK signaling in GIST.(Jeon, Davis et al. 1995, Mehra, Tomlins et al. 2007, Chi, Chen et al. 2010, Jane-Valbuena, Widlund et al. 2010) Comprehensive genomic analysis, including whole-exome sequencing, RNA-seq, SNP-array, fail to identify any significant genomic alterations of *ETV1* in MPNSTs. This observation suggests that *ETV1* is not activated through genomic alterations in MPNSTs. Instead, it may be inherited from cell of origin for MPNST or through other novel mechanisms. Although it is generally accepted MPNSTs arise from Schwann cell lineage, it is still under constant debate that what types and stages of Schwann cell lineage are the cell of origin for MPNSTs. It will be important to investigate the expression of *ETV1* in Schwann cell lineage of different developmental stages. The EYFP lineage tracing system can be exploited using *Etv1^{creERT}; Rosa26-EYFP^{LSL}* mice to detect *Etv1* expression in the Schwann cell lineage at different developmental stages. Different Schwann cell type markers can be used to identify different populations of Schwann cells.

However, it is still possible that *ETV1* may be activated through novel mechanisms other than genetic alterations and lineage inheritance. It is shown previously that there are subsets of enhancers that can activate gene expression upon signaling stimulation during differentiation or environmental cues.(Lam, Li et al. 2014) One possible mechanism of *ETV1* activation may be through activation of enhancers through aberrant signaling in addition to protein stability such as MAPK kinase signaling driven by *NF1* loss in MPNST. It would be interesting to explore the importance of *ETV1* enhancers and regulation of these enhancers by MAPK signaling in MPNSTs. ChIP-sequencing for enhancer epigenetic mark-

ers, H3K27ac and H3K4me1, can be informative to identify enhancers regions of *ETV1* gene. We can further interference these enhancers, if there is any, with CRPSR interference methods in MPNSTs to evaluate the importance of these enhancer for *ETV1* expression. Modeling of *ETV1* expression activation and *NF1* loss in a MPNST relevant lineage (schwann cell) can potentially help us understand the regulation of *ETV1* expression by MAP kinase signaling.

Given that *ETV1* is shown to be the lineage specific transcription factor for GIST, it will also be interesting to explore the potential role of ETV1 in cell of origin for MPNSTs. As discussed in the previous paragraph, *ETV1* expression in Schwann cell lineage may provide novel insights for MPNST precursors. If *ETV1* is expressed in Schwann cell lineage, we can ablate the three critical pathways that are lost in majority of MPNSTs specifically in the *Etv1* expressed cells with *Etv1^{CreERT}* allele in genetically engineered mouse model. If *Etv1*-expressed compartment is the cell of origin for MPNST, we may expect MPNST tumorigenesis within the appropriate timeframe. Additionally, Schwann cell lineage development in *Etv1* knockout mice will be investigated to evaluate the importance of *Etv1* for MPNST precursor development.

Despite the import role of *ETV1* we defined in MPNSTs, further studies need to be perform for therapeutic targeting of *ETV1* in MPNSTs. We demonstrate that knockdown of *ETV1* lead to cell death and attenuation of tumorigenesis, suggesting *ETV1* can be a potential drug target for MPNST treatment. As described in chapter five, MAP kinase signaling tightly regulates ETV1 protein stability. Inhibition of MAP kinase signaling leads to rapid degradation of ETV1 protein, allowing indirect target of ETV1 protein stability with MAP kinase inhibitors. Reasoning this, MAP kinase pathway inhibitors such as MEK inhibitors can be used to target

ETV1 for effective response. However, single agent MEK inhibitor show minimal response in clinic, most likely due to feedback reactivation of MAP kinase pathways.(Jessen, Miller et al. 2013) Effective inhibition of MAP kinase signaling is essential for persistent *ETV1* inhibition. It is important to explore novel therapeutic strategies either as single agent or combination therapies for effective *ETV1* targeting. Novel ETV1 inhibitor may be effective in MPNST, but it requires further investigation for the specificity and toxicity of ETV1 inhibitor.

Our comprehensive genomic analysis in chapter four also uncovers loss of three critical pathways in MPNSTs, *NF1*, *CKDN2A* and *PRC2*. It is the first time to show PRC2 is loss in more than 80% of MPNSTs through alterations in PRC2 components EED and SUZ12, resulting in complete loss of H3K27me3. The high frequency of PRC2 in MPNSTs is especially valuable in clinic since H3K27me3 immunohistochemistry could be used as biomarkers for the more acute diagnosis of MPNST. Nevertheless, the molecular mechanism through which PRC2 loss contributes to MPNST pathogenesis needs to be elucidated. PRC2 is thought to be oncogenic in various cancers through *EZH2* overexpression or activation mutations of *EZH2*.(Varambally 2002, Morin, Johnson et al. 2010) Surprisingly, recent works and our finding suggest that PRC2 is a tumor suppressor through loss of function mutations.(Ernst, Chase et al. 2010, Nikoloski, Langemeijer et al. 2010, Ntziachristos, Tsirigos et al. 2012, Zhang, Ding et al. 2012, Lee, Teckie et al. 2014) Role of PRC2 in MPNST pathogenesis can be studied with MPNST cell lines and *in vivo* mouse modeling with *PRC2* loss, *NF1* loss and *CKDN2A* loss. It is also important to investigate the cooperativity between the three pathways due to their high co-occurrence.

Role of ETV1 in GIST

Using genetically engineered mouse modeling, we demonstrate ETV1 is expressed in GIST precursor ICCs, activation of oncogenic mutations in these compartment lead to GIST tumorigenesis. Our mouse model represents the first murine model for *BRAFV600E*-mutant GISTs that highly resembles human GISTs. Similar to previously GIST mouse models, GISTs in the *Etv1^{CreERT2} BRaf^{CA/+}; p53^{fl/fl}* mouse model arise in the large intestine and cecum. However, clinically, human GISTs are most often seen in the stomach, followed by samllled intestine and then large intestine. Our mouse model showed spindle cell histology and molecular features just as *BRAF*-mutated GIST patients such as highly proliferative Ki67 staining, KIT protein staining and Erk1/2 activation. Therefore, *Etv1^{CreERT2}; BRaf^{CA/+}; p53^{fl/fl}* mouse model is a reliable *BRAF*-mutated GIST model to understand the pathogenesis of *BRAF*-mutated GIST and evaluate therapeutic strategies for this subtype of GISTs. Additionally, *Etv1^{CreERT2}* can also be used to develop other GIST models driven by different genetic perturbations, such as *SDHA/B* loss and *NF1* loss.

Our results further show *BRAF* inhibitor dabrafenib can effectively inhibit GIST tumor growth in the mouse model, which is consistent with the clinical observation of patient response. However, similar to patient response, the mice eventually develop disease progression. It is important to investigate the mechanism of dabrafenib resistance in *BRAF*-mutated GISTs. Studies indicate resistance for dabrafenib can be developed through reactivation of MAP kinase signaling. Mouse model and cell lines for *BRAF*-mutated GISTs can be development for study of potential reactivation of upstream signaling reactivations. Combination with inhibitors targeting upstream players may be beneficial for overcoming dabrafenib resistance.

One novel strategy to target ETV1 is developed in this study through combination of MEK inhibitor and KIT inhibitor in KIT-mutated GISTs. ETV1 is stabilized by up-regulated MAP kinase signaling driven by ligand-independent KIT mutations. Stabilized ETV1 enhances KIT expression through direct binding to KIT enhancers, forming a positive feedback during GIST tumorigenesis (**Figure 7.1**). Although it is challenging to directly target ETV1 with small molecule inhibitors, we demonstrate that ETV1 protein stability can be effectively targeted with combination of MEK inhibitor MEK162 and KIT inhibitor imatinib. This combination therapy results in complement response in xenograft mouse model, while single agent can only lead to stabilized disease. Our study presents a novel strategy to target ETV1 through inhibiting upstream signaling, which can be important for explore therapeutic treatments for other cancers, such as MPNST. As a next step, a clinical trial (phase Ib/II) testing the concept of ETV1 inhibition via combined imatinib/MEK162 treatment has been designed (NCT01991379). Follow up of patient responses, especially potential resistance to this combination therapy, in the clinical trial is critical for better management of GISTs.

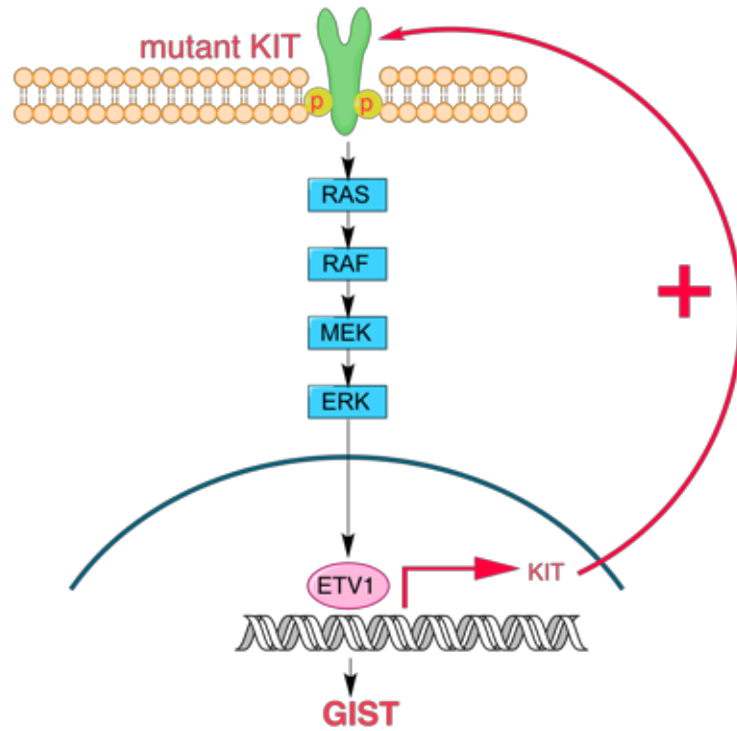


Figure 7.1 Schematic model of ETV1-mutant KIT feed forward circuit in GIST oncogenesis

ETV1 protein is stabilized by MAP kinase signaling downstream of mutant KIT signaling in the GIST precursor ICCs during GIST oncogenesis. ETV1 directly and positively regulates *KIT* expression and, therefore, it cooperates with mutant KIT by forming a positive feedback circuit to promote GIST tumorigenesis.

BIBLIOGRAPHY

Agaimy, A., L. M. Terracciano, S. Dirnhofer, L. Tornillo, A. Foerster, A. Hartmann and M. P. Bihl (2009). "V600E BRAF mutations are alternative early molecular events in a subset of KIT/PDGFR α wild-type gastrointestinal stromal tumours." Journal of Clinical Pathology **62**(7): 613-616.

Agaimy, A., P. H. Wunsch, L. H. Sobin, J. Lasota and M. Miettinen (2006). "Occurrence of other malignancies in patients with gastrointestinal stromal tumors." Semin Diagn Pathol **23**(2): 120-129.

Agaram, N. P., M. P. Laquaglia, B. Ustun, T. Guo, G. C. Wong, N. D. Socci, R. G. Maki, R. P. DeMatteo, P. Besmer and C. R. Antonescu (2008). "Molecular characterization of pediatric gastrointestinal stromal tumors." Clinical Cancer Research **14**(10): 3204-3215.

Agaram, N. P., G. C. Wong, T. Guo, R. G. Maki, S. Singer, R. P. DeMatteo, P. Besmer and C. R. Antonescu (2008). "Novel V600E BRAF mutations in imatinib-naive and imatinib-resistant gastrointestinal stromal tumors." Genes Chromosomes & Cancer **47**(10): 853-859.

Agaram, N. P., G. C. Wong, T. Guo, R. G. Maki, S. Singer, R. P. Dematteo, P. Besmer and C. R. Antonescu (2008). "Novel V600E BRAF mutations in imatinib-naive and imatinib-resistant gastrointestinal stromal tumors." Genes Chromosomes Cancer **47**(10): 853-859.

Anders, S. and W. Huber (2010). "Differential expression analysis for sequence count data." Genome Biology **11**(10).

Anders, S., P. T. Pyl and W. Huber (2015). "HTSeq-a Python framework to work with high-throughput sequencing data." Bioinformatics **31**(2): 166-169.

Andersson, J., P. Bummig, J. M. Meis-Kindblom, H. Sihto, N. Nupponen, H. Joensuu, A. Oden, B. Gustavsson, L. G. Kindblom and B. Nilsson (2006). "Gastrointestinal stromal tumors with KIT Exon 11 deletions are associated with poor prognosis." Gastroenterology **130**(6): 1573-1581.

Andersson, J., H. Sihto, J. M. Meis-Kindblom, H. Joensuu, N. Nupponen and L. G. Kindblom (2005). "NF1-associated gastrointestinal stromal tumors have unique clinical, phenotypic and genotypic characteristics." American Journal of Surgical Pathology **29**(9): 1170-1176.

Andor, N., J. V. Harness, S. Muller, H. W. Mewes and C. Petritsch (2014). "EXPANDS: expanding ploidy and allele frequency on nested subpopulations." Bioinformatics **30**(1): 50-60.

Anghileri, M., R. Miceli, M. Fiore, L. Mariani, A. Ferrari, C. Mussi, L. Lozza, P.

Collini, P. Olmi, P. G. Casali, S. Pilotti and A. Gronchi (2006). "Malignant peripheral nerve sheath tumors - Prognostic factors and survival in a series of patients treated at a single institution." Cancer **107**(5): 1065-1074.

Antonescu, C. R., P. Besmer, T. Guo, K. Arkun, G. Hom, B. Koryotowski, M. A. Leversha, P. D. Jeffrey, D. Desantis, S. Singer, M. F. Brennan, R. G. Maki and R. P. DeMatteo (2005). "Acquired resistance to imatinib in gastrointestinal stromal tumor occurs through secondary gene mutation." Clin Cancer Res **11**(11): 4182-4190.

Antonescu, C. R., B. W. Scheithauer and J. M. Woodruff (2013). Tumors of the Peripheral Nervous System.

Antonescu, C. R., Scheithauer, B. W., Woodruff, J. M. (2013). Tumors of the Peripheral Nervous System. Silver Spring, Maryland, The American Registry of Pathology.

Antonescu, C. R., G. Sommer, L. Sarran, S. J. Tschernyavsky, E. Riedel, J. M. Woodruff, M. Robson, R. Maki, M. F. Brennan, M. Ladanyi, R. P. DeMatteo and P. Besmer (2003). "Association of KIT exon 9 mutations with nongastric primary site and aggressive behavior: KIT mutation analysis and clinical correlates of 120 gastrointestinal stromal tumors." Clin Cancer Res **9**(9): 3329-3337.

Aravind, L., A. F. Neuwald and C. P. Ponting (1999). "Sec14p-like domains in NF1 and Dbl-like proteins indicate lipid regulation of Ras and Rho signaling." Current Biology **9**(6): R195-R197.

Arber, S., D. R. Ladle, J. H. Lin, E. Frank and T. M. Jessell (2000). "ETS gene Er81 controls the formation of functional connections between group Ia sensory afferents and motor neurons." Cell **101**(5): 485-498.

Arber, S., D. R. Ladle, J. H. Lin, E. Frank and T. M. Jessell (2000). "ETS gene Er81 controls the formation of functional connections between group Ia sensory afferents and motor neurons." Cell **101**(5): 485-498.

Badache, A. and G. H. De Vries (1998). "Neurofibrosarcoma-derived Schwann cells overexpress platelet-derived growth factor (PDGF) receptors and are induced to proliferate by PDGF BB." J Cell Physiol **177**(2): 334-342.

Badache, A., N. Muja and G. H. De Vries (1998). "Expression of Kit in neurofibromin-deficient human Schwann cells: role in Schwann cell hyperplasia associated with type 1 neurofibromatosis." Oncogene **17**(6): 795-800.

Ballester, R., D. Marchuk, M. Boguski, A. Saulino, R. Letcher, M. Wigler and F. Collins (1990). "The Nf1 Locus Encodes a Protein Functionally Related to Mammalian Gap and Yeast Ira Proteins." Cell **63**(4): 851-859.

Bardsley, M. R., V. J. Horvath, D. T. Asuzu, A. Lorincz, D. Redelman, Y. Hayashi, L. N. Popko, D. L. Young, G. A. Lomberk, R. A. Urrutia, G. Farrugia,

B. P. Rubin and T. Ordog (2010). "Kitlow stem cells cause resistance to Kit/platelet-derived growth factor alpha inhibitors in murine gastrointestinal stromal tumors." Gastroenterology **139**(3): 942-952.

Beadling, C., E. Jacobson-Dunlop, F. S. Hodi, C. Le, A. Warrick, J. Patterson, A. Town, A. Harlow, F. Cruz, 3rd, S. Azar, B. P. Rubin, S. Muller, R. West, M. C. Heinrich and C. L. Corless (2008). "KIT gene mutations and copy number in melanoma subtypes." Clin Cancer Res **14**(21): 6821-6828.

Bengtsson, H., P. Neuvial and T. P. Speed (2010). "TumorBoost: Normalization of allele-specific tumor copy numbers from a single pair of tumor-normal genotyping microarrays." Bmc Bioinformatics **11**.

Bindal, N., S. A. Forbes, D. Beare, P. Gunasekaran, K. Leung, C. Y. Kok, M. M. Jia, S. Bamford, C. Cole, S. Ward, J. Teague, M. R. Stratton, P. Campbell and P. A. Futreal (2011). "COSMIC: the Catalogue of Somatic Mutations in Cancer." Genome Biology **12**: 5-5.

Blanke, C. D. (2008). "Perforation and Stage-II Colon Cancer: Is it Always High Risk?" Gastrointest Cancer Res **2**(2): 103-104.

Blanke, C. D., C. Rankin, G. D. Demetri, C. W. Ryan, M. von Mehren, R. S. Benjamin, A. K. Raymond, V. H. Bramwell, L. H. Baker, R. G. Maki, M. Tanaka, J. R. Hecht, M. C. Heinrich, C. D. Fletcher, J. J. Crowley and E. C. Borden (2008). "Phase III randomized, intergroup trial assessing imatinib mesylate at two dose levels in patients with unresectable or metastatic gastrointestinal stromal tumors expressing the kit receptor tyrosine kinase: S0033." J Clin Oncol **26**(4): 626-632.

Blanke, C. D., C. Rankin, G. D. Demetri, C. W. Ryan, M. von Mehren, R. S. Benjamin, A. K. Raymond, V. H. C. Bramwell, L. H. Baker, R. G. Maki, M. Tanaka, J. R. Hecht, M. C. Heinrich, C. D. M. Fletcher, J. J. Crowley and E. C. Borden (2008). "Phase III randomized, intergroup trial assessing imatinib mesylate at two dose levels in patients with unresectable or metastatic gastrointestinal stromal tumors expressing the kit receptor tyrosine kinase: S0033." Journal of Clinical Oncology **26**(4): 626-632.

Bollag, G., F. McCormick and R. Clark (1993). "Characterization of Full-Length Neurofibromin - Tubulin Inhibits Ras Gap Activity." Embo Journal **12**(5): 1923-1927.

Brannan, C. I., A. S. Perkins, K. S. Vogel, N. Ratner, M. L. Nordlund, S. W. Reid, A. M. Buchberg, N. A. Jenkins, L. F. Parada and N. G. Copeland (1994). "Targeted disruption of the neurofibromatosis type-1 gene leads to developmental abnormalities in heart and various neural crest-derived tissues." Genes Dev **8**(9): 1019-1029.

Brennan, M. F., C. Antonescu and R. Maki (2013). Management of Soft Tissue

Sarcoma. new york, Springer New York Heidelberg Dordrecht London.

Brennan, M. F., C. R. Antonescu and R. G. Maki (2013). Management of Soft Tissue Sarcoma: 149-160.

Brose, M. S., P. Volpe, M. Feldman, M. Kumar, I. Rishi, R. Gerrero, E. Einhorn, M. Herlyn, J. Minna, A. Nicholson, J. A. Roth, S. M. Albelda, H. Davies, C. Cox, G. Brignell, P. Stephens, P. A. Futreal, R. Wooster, M. R. Stratton and B. L. Weber (2002). "BRAF and RAS mutations in human lung cancer and melanoma." Cancer Research **62**(23): 6997-7000.

Cairns, P., T. J. Polascik, Y. Eby, K. Tokino, J. Califano, A. Merlo, L. Mao, J. Herath, R. Jenkins, W. Westra, J. L. Rutter, A. Buckler, E. Gabrielson, M. Tockman, K. R. Cho, L. Hedrick, G. S. Bova, W. Isaacs, W. Koch, D. Schwab, D. Sidransky and et al. (1995). "Frequency of homozygous deletion at p16/CDKN2 in primary human tumours." Nat Genet **11**(2): 210-212.

Cantwell-Dorris, E. R., J. J. O'Leary and O. M. Sheils (2011). "BRAF(V600E): Implications for Carcinogenesis and Molecular Therapy." Molecular Cancer Therapeutics **10**(3): 385-394.

Carroll, S. L. and N. Ratner (2008). "How Does the Schwann Cell Lineage Form Tumors in NF1?" Glia **56**(14): 1590-1605.

Cashen, D. V., R. C. Parisien, K. Raskin, F. J. Hornicek, M. C. Gebhardt and H. J. Mankin (2004). "Survival data for patients with malignant schwannoma." Clinical Orthopaedics and Related Research(426): 69-73.

Cerami, E., J. Gao, U. Dogrusoz, B. E. Gross, S. O. Sumer and B. A. Aksoy (2012). "The cBio Cancer Genomics Portal: An Open Platform for Exploring Multidimensional Cancer Genomics Data (vol 2, pg 401, 2012)." Cancer Discovery **2**(10): 960-960.

Chen, Z., C. Liu, A. J. Patel, C. P. Liao, Y. Wang and L. Q. Le (2014). "Cells of origin in the embryonic nerve roots for NF1-associated plexiform neurofibroma." Cancer Cell **26**(5): 695-706.

Chi, P. (2010). "ETV1 is a lineage survival factor that cooperates with KIT in gastrointestinal stromal tumours." Nature **467**: 849-853.

Chi, P., Y. Chen, L. Zhang, X. Guo, J. Wongvipat, T. Shamu, J. A. Fletcher, S. Dewell, R. G. Maki, D. Zheng, C. R. Antonescu, C. D. Allis and C. L. Sawyers (2010). "ETV1 is a lineage survival factor that cooperates with KIT in gastrointestinal stromal tumours." Nature **467**(7317): 849-853.

Chi, P., Y. Chen, L. Zhang, X. Y. Guo, J. Wongvipat, T. Shamu, J. A. Fletcher, S. Dewell, R. G. Maki, D. Y. Zheng, C. R. Antonescu, C. D. Allis and C. L. Sawyers (2010). "ETV1 is a lineage survival factor that cooperates with KIT in gastrointestinal stromal tumours." Nature **467**(7317): 849-U117.

- Cho, S. D., Y. Kitadai, S. Yoshida, S. Tanaka, M. Yoshihara, K. Yoshida and K. Chayama (2006). "Deletion of the KIT gene is associated with liver metastasis and poor prognosis in patients with gastrointestinal stromal tumor in the stomach." International Journal of Oncology **28**(6): 1361-1367.
- Cibulskis, K., M. S. Lawrence, S. L. Carter, A. Sivachenko, D. Jaffe, C. Sougnez, S. Gabriel, M. Meyerson, E. S. Lander and G. Getz (2013). "Sensitive detection of somatic point mutations in impure and heterogeneous cancer samples." Nature Biotechnology **31**(3): 213-219.
- Cichowski, K., T. S. Shih, E. Schmitt, S. Santiago, K. Reilly, M. E. McLaughlin, R. T. Bronson and T. Jacks (1999). "Mouse models of tumor development in neurofibromatosis type 1." Science **286**(5447): 2172-2176.
- Corless, C. (2014). "Gastrointestinal stromal tumors: what do we know now?" Modern Pathology **27**(S1): S1-S6.
- Corless, C. L., C. M. Barnett and M. C. Heinrich (2011). "Gastrointestinal stromal tumours: origin and molecular oncology." Nature Reviews Cancer **11**(12): 865-878.
- Corless, C. L., J. A. Fletcher and M. C. Heinrich (2004). "Biology of gastrointestinal stromal tumors." Journal of Clinical Oncology **22**(18): 3813-3825.
- Corless, C. L., A. Schroeder, D. Griffith, A. Town, L. McGreevey, P. Harrell, S. Shiraga, T. Bainbridge, J. Morich and M. C. Heinrich (2005). "PDGFRA mutations in gastrointestinal stromal tumors: Frequency, spectrum and in vitro sensitivity to imatinib." Journal of Clinical Oncology **23**(23): 5357-5364.
- Costa, R. M., T. Yang, D. P. Huynh, S. M. Pulst, D. H. Viskochil, A. J. Silva and C. I. Brannan (2001). "Learning deficits, but normal development and tumor predisposition, in mice lacking exon 23a of Nf1." Nature Genetics **27**(4): 399-405.
- Coutte, L., D. Monte, K. Imai, L. Pouilly, F. Dewitte, M. Vidaud, J. Adamski, J. L. Baert and Y. de Launoit (1999). "Characterization of the human and mouse ETV1/ER81 transcription factor genes: role of the two alternatively spliced isoforms in the human." Oncogene **18**(46): 6278-6286.
- D'Angelo, I., S. Welte, F. Bonneau and K. Scheffzek (2006). "A novel bipartite phospholipid-binding module in the neurofibromatosis type 1 protein." Embo Reports **7**(2): 174-179.
- Dang, I., J. K. Nelson and G. H. DeVries (2005). "c-Kit receptor expression in normal human Schwann cells and Schwann cell lines derived from neurofibromatosis type 1 tumors." J Neurosci Res **82**(4): 465-471.
- Daniels, M., I. Lurkin, R. Pauli, E. Erbstosser, U. Hildebrandt, K. Hellwig, U. Zschille, P. Luders, G. Kruger, J. Knolle, B. Stengel, F. Prall, K. Hertel, H. Lo-

beck, B. Popp, F. Theissig, P. Wunsch, E. Zwarthoff, A. Agaimy and R. Schneider-Stock (2011). "Spectrum of KIT/PDGFR α /BRAF mutations and Phosphatidylinositol-3-Kinase pathway gene alterations in gastrointestinal stromal tumors (GIST)." Cancer Letters **312**(1): 43-54.

Dankort, D., E. Filenova, M. Collado, M. Serrano, K. Jones and M. McMahon (2007). "A new mouse model to explore the initiation, progression, and therapy of BRAF(V600E)-induced lung tumors." Genes & Development **21**(4): 379-384.

Dasgupta, B., L. L. Dugan and D. H. Gutmann (2003). "The neurofibromatosis 1 gene product neurofibromin regulates pituitary adenylate cyclase-activating polypeptide-mediated signaling in astrocytes." J Neurosci **23**(26): 8949-8954.

Davies, H., G. R. Bignell, C. Cox, P. Stephens, S. Edkins, S. Clegg, J. Teague, H. Woffendin, M. J. Garnett, W. Bottomley, N. Davis, N. Dicks, R. Ewing, Y. Floyd, K. Gray, S. Hall, R. Hawes, J. Hughes, V. Kosmidou, A. Menzies, C. Mould, A. Parker, C. Stevens, S. Watt, S. Hooper, R. Wilson, H. Jayatilake, B. A. Gusterson, C. Cooper, J. Shipley, D. Hargrave, K. Pritchard-Jones, N. Maitland, G. Chenevix-Trench, G. J. Riggins, D. D. Bigner, G. Palmieri, A. Cossu, A. Flanagan, A. Nicholson, J. W. C. Ho, S. Y. Leung, S. T. Yuen, B. L. Weber, H. F. Siegler, T. L. Darrow, H. Paterson, R. Marais, C. J. Marshall, R. Wooster, M. R. Stratton and P. A. Futreal (2002). "Mutations of the BRAF gene in human cancer." Nature **417**(6892): 949-954.

De Giorgi, U. and J. Verweij (2005). "Imatinib and gastrointestinal stromal tumors: Where do we go from here?" Molecular Cancer Therapeutics **4**(3): 495-501.

De Raedt, T., E. Beert, E. Pasmant, A. Luscan, H. Brems, N. Ortonne, K. Helin, J. L. Hornick, V. Mautner, H. Kehrer-Sawatzki, W. Clapp, J. Bradner, M. Vidaud, M. Upadhyaya, E. Legius and K. Cichowski (2014). "PRC2 loss amplifies Ras-driven transcription and confers sensitivity to BRD4-based therapies." Nature **514**(7521): 247-+.

de Raedt, T., J. Cools, M. Debiec-Rychter, H. Brems, N. Mentens, R. Sciot, J. Himpens, I. de Wever, P. Schoffski, P. Marynen and E. Legius (2006). "Intestinal neurofibromatosis is a subtype of familial GIST and results from a dominant activating mutation in PDGFR α ." Gastroenterology **131**(6): 1907-1912.

Debiec-Rychter, M., H. Dumez, I. Judson, B. Wasag, J. Verweij, M. Brown, S. Dimitrijevic, R. Sciot, M. Stul, H. Vranck, M. Scurr, A. Hagemeyer, M. van Glabbeke and A. T. van Oosterom (2004). "Use of c-KIT/PDGFR α mutational analysis to predict the clinical response to imatinib in patients with advanced gastrointestinal stromal tumours entered on phase I and II studies of the EORTC Soft Tissue and Bone Sarcoma Group." Eur J Cancer **40**(5): 689-695.

Debiec-Rychter, M., B. Wasag, M. Stul, I. De Wever, A. Van Oosterom, A. Hagemeyer and R. Sciot (2004). "Gastrointestinal stromal tumours (GISTs) neg-

ative for KIT (CD117 antigen) immunoreactivity." Journal of Pathology **202**(4): 430-438.

Delaney, A. M., J. A. Printen, H. Chen, E. B. Fauman and D. T. Dudley (2002). "Identification of a novel mitogen-activated protein kinase kinase activation domain recognized by the inhibitor PD 184352." Mol Cell Biol **22**(21): 7593-7602.

DeMatteo, R. P., J. J. Lewis, D. Leung, S. S. Mudan, J. M. Woodruff and M. F. Brennan (2000). "Two hundred gastrointestinal stromal tumors - Recurrence patterns and prognostic factors for survival." Annals of Surgery **231**(1): 51-58.

Demetri, G. D. (2002). "Identification and treatment of chemoresistant inoperable or metastatic GIST: experience with the selective tyrosine kinase inhibitor imatinib mesylate (STI571)." Eur J Cancer **38 Suppl 5**: S52-59.

Demetri, G. D., P. Reichardt, Y. K. Kang, J. Y. Blay, P. Rutkowski, H. Gelderblom, P. Hohenberger, M. Leahy, M. von Mehren, H. Joensuu, G. Badalamenti, M. Blackstein, A. Le Cesne, P. Schoffski, R. G. Maki, S. Bauer, B. B. Nguyen, J. Xu, T. Nishida, J. Chung, C. Kappeler, I. Kuss, D. Laurent, P. G. Casali and G. s. investigators (2013). "Efficacy and safety of regorafenib for advanced gastrointestinal stromal tumours after failure of imatinib and sunitinib (GRID): an international, multicentre, randomised, placebo-controlled, phase 3 trial." Lancet **381**(9863): 295-302.

Demetri, G. D., A. T. van Oosterom, C. R. Garrett, M. E. Blackstein, M. H. Shah, J. Verweij, G. McArthur, I. R. Judson, M. C. Heinrich, J. A. Morgan, J. Desai, C. D. Fletcher, S. George, C. L. Bello, X. Huang, C. M. Baum and P. G. Casali (2006). "Efficacy and safety of sunitinib in patients with advanced gastrointestinal stromal tumour after failure of imatinib: a randomised controlled trial." Lancet **368**(9544): 1329-1338.

Demetri, G. D., M. von Mehren, C. D. Blanke, A. D. Van den Abbeele, B. Eisenberg, P. J. Roberts, M. C. Heinrich, D. A. Tuveson, S. Singer, M. Janicek, J. A. Fletcher, S. G. Silverman, S. L. Silberman, R. Capdeville, B. Kiese, B. Peng, S. Dimitrijevic, B. J. Druker, C. Corless, C. D. M. Fletcher and H. Joensuu (2002). "Efficacy and safety of imatinib mesylate in advanced gastrointestinal stromal tumors." New England Journal of Medicine **347**(7): 472-480.

DePinho, R. A. (1998). "Transcriptional repression. The cancer-chromatin connection." Nature **391**(6667): 533, 535-536.

Dobin, A., C. A. Davis, F. Schlesinger, J. Drenkow, C. Zaleski, S. Jha, P. Batut, M. Chaisson and T. R. Gingeras (2013). "STAR: ultrafast universal RNA-seq aligner." Bioinformatics **29**(1): 15-21.

Dougherty, M. J., C. Compton, M. Talbert and W. C. Wood (1991). "Sarcomas of the Gastrointestinal-Tract - Separation into Favorable and Unfavorable Prognostic Groups by Mitotic Count." Annals of Surgery **214**(5): 569-574.

- Ducatman, B. S., B. W. Scheithauer, D. G. Piepgras, H. M. Reiman and D. M. Ilstrup (1986). "Malignant peripheral nerve sheath tumors. A clinicopathologic study of 120 cases." Cancer **57**(10): 2006-2021.
- Eisenberg, B. L. and J. M. Pipas (2012). "Gastrointestinal Stromal Tumor-Background, Pathology, Treatment." Hematology-Oncology Clinics of North America **26**(6): 1239-+.
- Ellison, D. A., J. Corredor-Buchmann, D. M. Parham and R. J. Jackson (2005). "Malignant triton tumor presenting as a rectal mass in an 11-month-old." Pediatric and Developmental Pathology **8**(2): 235-239.
- Ernst, S. I., A. E. Hubbs, R. M. Przygodzki, T. S. Emory, L. H. Sobin and T. J. O'Leary (1998). "KIT mutation portends poor prognosis in gastrointestinal stromal/smooth muscle tumors." Laboratory Investigation **78**(12): 1633-1636.
- Ernst, T., A. J. Chase, J. Score, C. E. Hidalgo-Curtis, C. Bryant, A. V. Jones, K. Waghorn, K. Zoi, F. M. Ross, A. Reiter, A. Hochhaus, H. G. Drexler, A. Duncombe, F. Cervantes, D. Oscier, J. Boulton, F. H. Grand and N. C. Cross (2010). "Inactivating mutations of the histone methyltransferase gene EZH2 in myeloid disorders." Nat Genet **42**(8): 722-726.
- Evans, D. G. R., M. E. Baser, J. McGaughan, S. Sharif, E. Howard and A. Moran (2002). "Malignant peripheral nerve sheath tumours in neurofibromatosis 1." Journal of Medical Genetics **39**(5): 311-314.
- Ezhkova, E., W. H. Lien, N. Stokes, H. A. Pasolli, J. M. Silva and E. Fuchs (2011). "EZH1 and EZH2 cogovern histone H3K27 trimethylation and are essential for hair follicle homeostasis and wound repair." Genes Dev **25**(5): 485-498.
- Falchook, G. S., J. C. Trent, M. C. Heinrich, C. Beadling, J. Patterson, C. C. Bastida, S. C. Blackman and R. Kurzrock (2013). "BRAF Mutant Gastrointestinal Stromal Tumor: First report of regression with BRAF inhibitor dabrafenib (GSK2118436) and whole exomic sequencing for analysis of acquired resistance." Oncotarget **4**(2): 310-315.
- Flames, N. and O. Hobert (2009). "Gene regulatory logic of dopamine neuron differentiation." Nature **458**(7240): 885-U887.
- Fleiss, J. L. (1971). "Measuring Nominal Scale Agreement among Many Raters." Psychological Bulletin **76**(5): 378-382.
- Fleiss, J. L. (1971). Measuring nominal scale agreement among many raters. Psychological Bulletin. **76**(5): 378-382.
- Fletcher, C. D. M., J. J. Berman, C. Corless, F. Gorstein, J. Lasota, B. J. Longley, M. Miettinen, T. J. O'Leary, H. Remotti, B. P. Rubin, B. Shmookler, L. H. Sobin and S. W. Weiss (2002). "Diagnosis of gastrointestinal stromal tumors: A

consensus approach." Human Pathology **33**(5): 459-465.

Gari, M., A. Goodeve, G. Wilson, P. Winship, S. Langabeer, D. Linch, E. Vandenberghe, I. Peake and J. Reilly (1999). "c-kit proto-oncogene exon 8 in-frame deletion plus insertion mutations in acute myeloid leukaemia." British Journal of Haematology **105**(4): 894-900.

Geist, R. T. and D. H. Gutmann (1996). "Expression of a developmentally-regulated neuron-specific isoform of the neurofibromatosis 1 (NF1) gene." Neuroscience Letters **211**(2): 85-88.

Goettsch, W. G., S. D. Bos, N. Breekveldt-Postma, M. Casparie, R. M. C. Herings and P. C. W. Hogendoorn (2005). "Incidence of gastrointestinal stromal tumours is underestimated: Results of a nation-wide study." European Journal of Cancer **41**(18): 2868-2872.

Gold, J. S. and R. P. DeMatteo (2006). "Combined surgical and molecular therapy - The gastrointestinal stromal tumor model." Annals of Surgery **244**(2): 176-184.

Grobmyer, S. R., J. D. Reith, A. Shahlaee, C. H. Bush and S. N. Hochwald (2008). "Malignant Peripheral Nerve Sheath Tumor: molecular pathogenesis and current management considerations." J Surg Oncol **97**(4): 340-349.

Grobmyer, S. R., J. D. Reith, A. Shahlaee, C. H. Bush and S. N. Hochwald (2008). "Malignant peripheral nerve sheath tumor: Molecular pathogenesis and current management considerations." Journal of Surgical Oncology **97**(4): 340-349.

Guha, A., N. Lau, I. Huvar, D. Gutmann, J. Provias, T. Pawson and G. Boss (1996). "Ras-GTP levels are elevated in human NF1 peripheral nerve tumors." Oncogene **12**(3): 507-513.

Guo, A. T., A. J. Liu, L. X. Wei and X. Song (2012). "Malignant Peripheral Nerve Sheath Tumors: Differentiation Patterns and Immunohistochemical Features - A Mini-Review and Our New Findings." Journal of Cancer **3**: 303-309.

Gupta, P., M. Tewari and H. S. Shukla (2008). "Gastrointestinal stromal tumor." Surg Oncol **17**(2): 129-138.

Gutmann, D. H. (2001). "The neurofibromatoses: when less is more." Human Molecular Genetics **10**(7): 747-755.

Gutmann, D. H., J. L. Cole and F. S. Collins (1995). "Expression of the neurofibromatosis type 1 (NF1) gene during mouse embryonic development." Gene Expression in the Central Nervous System **105**: 327-335.

Gutmann, D. H., R. T. Geist, K. Rose and D. E. Wright (1995). "Expression of two new protein isoforms of the neurofibromatosis type 1 gene product, neurofi-

bromin, in muscle tissues." Dev Dyn **202**(3): 302-311.

Gutmann, D. H., R. T. Geist, D. E. Wright and W. D. Snider (1995). "Expression of the Neurofibromatosis-1 (Nf1) Isoforms in Developing and Adult-Rat Tissues." Cell Growth & Differentiation **6**(3): 315-323.

Gutmann, D. H., Y. J. Zhang and A. Hirbe (1999). "Developmental regulation of a neuron-specific neurofibromatosis 1 isoform." Annals of Neurology **46**(5): 777-782.

Hanks, S. K., A. M. Quinn and T. Hunter (1988). "The Protein-Kinase Family - Conserved Features and Deduced Phylogeny of the Catalytic Domains." Science **241**(4861): 42-52.

Haque, S. and P. J. Dean (1992). "Stromal Neoplasms of the Rectum and Anal-Canal." Human Pathology **23**(7): 762-767.

Hauschild, A., J. J. Grob, L. V. Demidov, T. Jouary, R. Gutzmer, M. Millward, P. Rutkowski, C. U. Blank, W. H. Miller, E. Kaempgen, S. Martin-Algarra, B. Karaszewska, C. Mauch, V. Chiarion-Sileni, A. M. Martin, S. Swann, P. Haney, B. Mirakhur, M. E. Guckert, V. Goodman and P. B. Chapman (2012). "Dabrafenib in BRAF-mutated metastatic melanoma: a multicentre, open-label, phase 3 randomised controlled trial." Lancet **380**(9839): 358-365.

Hayashi, Y., T. Okazaki, A. Yamataka, T. Yanai, Y. Yamashiro, M. Tsurumaru, Y. Kajiyama and T. Miyano (2005). "Gastrointestinal stromal tumor in a child and review of the literature." Pediatric Surgery International **21**(11): 914-917.

He, L. J., B. S. Wang and C. C. Chen (1988). "Smooth-Muscle Tumors of the Digestive-Tract - Report of 160 Cases." British Journal of Surgery **75**(2): 184-186.

Heinrich, M. C., C. L. Corless, G. D. Demetri, C. D. Blanke, M. von Mehren, H. Joensuu, L. S. McGreevey, C. J. Chen, A. D. Van den Abbeele, B. J. Druker, B. Kiese, B. Eisenberg, P. J. Roberts, S. Singer, C. D. Fletcher, S. Silberman, S. Dimitrijevic and J. A. Fletcher (2003). "Kinase mutations and imatinib response in patients with metastatic gastrointestinal stromal tumor." J Clin Oncol **21**(23): 4342-4349.

Heinrich, M. C., C. L. Corless, G. D. Demetri, C. D. Blanke, M. von Mehren, H. Joensuu, L. S. McGreevey, C. J. Chen, A. D. Van den Abbeele, B. J. Druker, B. Kiese, B. Eisenberg, P. J. Roberts, S. Singer, C. D. M. Fletcher, S. Silberman, S. Dimitrijevic and J. A. Fletcher (2003). "Kinase mutations and imatinib response in patients with metastatic gastrointestinal stromal tumor." Journal of Clinical Oncology **21**(23): 4342-4349.

Heinrich, M. C., C. L. Corless, A. Duensing, L. McGreevey, C. J. Chen, N. Joseph, S. Singer, D. J. Griffith, A. Haley, A. Town, G. D. Demetri, C. D. Fletcher and J. A. Fletcher (2003). "PDGFRA activating mutations in gastrointestinal

stromal tumors." Science **299**(5607): 708-710.

Henderson, S. R., D. Guiliano, N. Presneau, S. McLean, R. Frow, S. Vujovic, J. Anderson, N. Sebire, J. Whelan, N. Athanasou, A. M. Flanagan and C. Boshoff (2005). "A molecular map of mesenchymal tumors." Genome Biology **6**(9).

Hinman, M. N., A. Sharma, G. B. Luo and H. Lou (2014). "Neurofibromatosis Type 1 Alternative Splicing Is a Key Regulator of Ras Signaling in Neurons (vol 34, 2188, 2014)." Molecular and Cellular Biology **34**(15): 2944-2944.

Hirota, S., K. Isozaki, Y. Moriyama, K. Hashimoto, T. Nishida, S. Ishiguro, K. Kawano, M. Hanada, A. Kurata, M. Takeda, G. Muhammad Tunio, Y. Matsuzawa, Y. Kanakura, Y. Shinomura and Y. Kitamura (1998). "Gain-of-function mutations of c-kit in human gastrointestinal stromal tumors." Science **279**(5350): 577-580.

Hirota, S., K. Isozaki, Y. Moriyama, K. Hashimoto, T. Nishida, S. Ishiguro, K. Kawano, M. Hanada, A. Kurata, M. Takeda, G. M. Tunio, Y. Matsuzawa, Y. Kanakura, Y. Shinomura and Y. Kitamura (1998). "Gain-of-function mutations of c-kit in human gastrointestinal stromal tumors." Science **279**(5350): 577-580.

Hirota, S., T. Nishida, K. Isozaki, M. Taniguchi, K. Nishikawa, A. Ohashi, A. Takabayashi, T. Obayashi, T. Okuno, K. Kinoshita, H. Chen, Y. Shinomura and Y. Kitamura (2002). "Familial gastrointestinal stromal tumors associated with dysphagia and novel type germline mutation of KIT gene." Gastroenterology **122**(5): 1493-1499.

Hirota, S., A. Ohashi, T. Nishida, K. Isozaki, K. Kinoshita, Y. Shinomura and Y. Kitamura (2003). "Gain-of-function mutations of platelet-derived growth factor receptor alpha gene in gastrointestinal stromal tumors." Gastroenterology **125**(3): 660-667.

Holm, K., D. Grabau, K. Lovgren, S. Aradottir, S. Gruvberger-Saal, J. Howlin, L. H. Saal, S. P. Ethier, P. O. Bendahl, O. Stal, P. Malmstrom, M. Ferno, L. Ryden, C. Hegardt, A. Borg and M. Ringner (2012). "Global H3K27 trimethylation and EZH2 abundance in breast tumor subtypes." Molecular Oncology **6**(5): 494-506.

Hornick, J. L. and C. D. M. Fletcher (2002). "Immunohistochemical staining for KIT (CD117) in soft tissue sarcomas is very limited in distribution." American Journal of Clinical Pathology **117**(2): 188-193.

Hostein, I., N. Faur, C. Primois, F. Boury, J. Denard, J. F. Emile, P. P. Bringuier, J. Y. Scoazec and J. M. Coindre (2010). "BRAF Mutation Status in Gastrointestinal Stromal Tumors." American Journal of Clinical Pathology **133**(1): 141-148.

Hostein, I., M. Longy, B. Gastaldello, G. Geneste and J. M. Coindre (2006). "Detection of a new mutation in KIT exon 9 in a gastrointestinal stromal tumor." Int J Cancer **118**(8): 2089-2091.

- Huang, D. W., B. T. Sherman and R. A. Lempicki (2009). "Systematic and integrative analysis of large gene lists using DAVID bioinformatics resources." Nature Protocols **4**(1): 44-57.
- Huizinga, J. D., L. Thuneberg, M. Kluppel, J. Malysz, H. B. Mikkelsen and A. Bernstein (1995). "W/kit gene required for interstitial cells of Cajal and for intestinal pacemaker activity." Nature **373**(6512): 347-349.
- Huizinga, J. D., L. Thuneberg, M. Kluppel, J. Malysz, H. B. Mikkelsen and A. Bernstein (1995). "W/Kit Gene Required for Interstitial-Cells of Cajal and for Intestinal Pacemaker Activity." Nature **373**(6512): 347-349.
- Ismat, F. A., J. Xu, M. M. Lu and J. A. Epstein (2006). "The neurofibromin GAP-related domain rescues endothelial but not neural crest development in Nf1 mice." J Clin Invest **116**(9): 2378-2384.
- Izawa, I., N. Tamaki and H. Saya (1996). "Phosphorylation of neurofibromatosis type 1 gene product (neurofibromin) by cAMP-dependent protein kinase." Febs Letters **382**(1-2): 53-59.
- Jacks, T., T. S. Shih, E. M. Schmitt, R. T. Bronson, A. Bernards and R. A. Weinberg (1994). "Tumour predisposition in mice heterozygous for a targeted mutation in Nf1." Nat Genet **7**(3): 353-361.
- Jane-Valbuena, J., H. R. Widlund, S. Perner, L. A. Johnson, A. C. Dibner, W. M. Lin, A. C. Baker, R. M. Nazarian, K. G. Vijayendran, W. R. Sellers, W. C. Hahn, L. M. Duncan, M. A. Rubin, D. E. Fisher and L. A. Garraway (2010). "An Oncogenic Role for ETV1 in Melanoma." Cancer Research **70**(5): 2075-2084.
- Janeway, K. A., S. Y. Kim, M. Lodish, V. Nose, P. Rustin, J. Gaal, P. L. M. Dahiya, B. Liegl, E. R. Ball, M. Raygada, A. H. Lai, L. Kelly, J. L. Hornick, M. O'Sullivan, R. R. de Krijger, W. N. M. Dinjens, G. D. Demetri, C. R. Antonescu, J. A. Fletcher, L. Helman, C. A. Stratakis and N. P. W. T. G. Clinic (2011). "Defects in succinate dehydrogenase in gastrointestinal stromal tumors lacking KIT and PDGFRA mutations." Proceedings of the National Academy of Sciences of the United States of America **108**(1): 314-318.
- Jeon, I. S., J. N. Davis, B. S. Braun, J. E. Sublett, M. F. Roussel, C. T. Denny and D. N. Shapiro (1995). "A variant Ewing's sarcoma translocation (7;22) fuses the EWS gene to the ETS gene ETV1." Oncogene **10**(6): 1229-1234.
- Jessen, K. R. and R. Mirsky (2005). "The origin and development of glial cells in peripheral nerves." Nat Rev Neurosci **6**(9): 671-682.
- Jessen, W. J., S. J. Miller, E. Jousma, J. Wu, T. A. Rizvi, M. E. Brundage, D. Eaves, B. Widemann, M. O. Kim, E. Dombi, J. Sabo, A. Hardiman Dudley, M. Niwa-Kawakita, G. P. Page, M. Giovannini, B. J. Aronow, T. P. Cripe and N. Ratner (2013). "MEK inhibition exhibits efficacy in human and mouse neurofibromatosis tumors." J Clin Invest **123**(1): 340-347.

Joensuu, H., P. Hohenberger and C. L. Corless (2013). "Gastrointestinal stromal tumour." Lancet **382**(9896): 973-983.

Joseph, N. M., J. T. Mosher, J. Buchstaller, P. Snider, P. E. McKeever, M. Lim, S. J. Conway, L. F. Parada, Y. Zhu and S. J. Morrison (2008). "The loss of Nf1 transiently promotes self-renewal but not tumorigenesis by neural crest stem cells." Cancer Cell **13**(2): 129-140.

Kamb, A., N. A. Gruis, J. Weaverfeldhaus, Q. Y. Liu, K. Harshman, S. V. Tavtigian, E. Stockert, R. S. Day, B. E. Johnson and M. H. Skolnick (1994). "A Cell-Cycle Regulator Potentially Involved in Genesis of Many Tumor Types." Science **264**(5157): 436-440.

Kang, H. J., S. W. Nam, H. K. Kim, H. Rhee, N. G. Kim, H. Y. Kim, W. J. Hyung, S. H. Noh, J. H. Kim, C. O. Yun, E. T. Liu and H. G. Kim (2005). "Correlation of KIT and platelet-derived growth factor receptor alpha mutations with gene activation and expression profiles in gastrointestinal stromal tumors." Oncogene **24**(6): 1066-1074.

Killian, J. K., S. Y. Kim, M. Miettinen, C. Smith, M. Merino, M. Tsokos, M. Quezado, W. I. Smith, M. S. Jahromi, P. Xekouki, E. Szarek, R. L. Walker, J. Lasota, M. Raffeld, B. Klotzle, Z. F. Wang, L. Jones, Y. L. Zhu, Y. H. Wang, J. J. Waterfall, M. J. O'Sullivan, M. Bibikova, K. Pacak, C. Stratakis, K. A. Jane-way, J. D. Schiffman, J. B. Fan, L. Helman and P. S. Meltzer (2013). "Succinate Dehydrogenase Mutation Underlies Global Epigenomic Divergence in Gastrointestinal Stromal Tumor." Cancer Discovery **3**(6): 648-657.

Kim, J., A. J. Woo, J. Chu, J. W. Snow, Y. Fujiwara, C. G. Kim, A. B. Cantor and S. H. Orkin (2010). "A Myc network accounts for similarities between embryonic stem and cancer cell transcription programs." Cell **143**(2): 313-324.

Kim, J., A. J. Woo, J. L. Chu, J. W. Snow, Y. Fujiwara, C. G. Kim, A. B. Cantor and S. H. Orkin (2010). "A Myc Network Accounts for Similarities between Embryonic Stem and Cancer Cell Transcription Programs." Cell **143**(2): 313-324.

Kim, T. S., M. J. Cavnar, N. A. Cohen, E. C. Sorenson, J. B. Greer, A. M. Seifert, M. H. Crawley, B. L. Green, R. Popow, N. Pillarsetty, D. R. Veach, A. T. Ku, F. Rossi, P. Besmer, C. R. Antonescu, S. Zeng and R. P. Dematteo (2014). "Increased KIT inhibition enhances therapeutic efficacy in gastrointestinal stromal tumor." Clin Cancer Res **20**(9): 2350-2362.

Kindblom, L. G., H. E. Remotti, F. Aldenborg and J. M. Meis-Kindblom (1998). "Gastrointestinal pacemaker cell tumor (GIPACT) - Gastrointestinal stromal tumors show phenotypic characteristics of the interstitial cells of Cajal." American Journal of Pathology **152**(5): 1259-1269.

Kissel, H., I. Timokhina, M. P. Hardy, G. Rothschild, Y. Tajima, V. Soares, M. Angeles, S. R. Whitlow, K. Manova and P. Besmer (2000). "Point mutation in Kit

receptor tyrosine kinase reveals essential roles for Kit signaling in spermatogenesis and oogenesis without affecting other Kit responses." Embo Journal **19**(6): 1312-1326.

Kluwe, L., R. E. Friedrich, M. Peiper, J. Friedman and V. F. Mautner (2003). "Constitutional NF1 mutations in neurofibromatosis 1 patients with malignant peripheral nerve sheath tumors." Hum Mutat **22**(5): 420.

Koboldt, D. C., Q. Y. Zhang, D. E. Larson, D. Shen, M. D. McLellan, L. Lin, C. A. Miller, E. R. Mardis, L. Ding and R. K. Wilson (2012). "VarScan 2: Somatic mutation and copy number alteration discovery in cancer by exome sequencing." Genome Research **22**(3): 568-576.

Kolberg, M., M. Holand, T. H. Agesen, H. R. Brekke, K. Liestol, K. S. Hall, F. Mertens, P. Picci, S. Smeland and R. A. Lothe (2013). "Survival meta-analyses for > 1800 malignant peripheral nerve sheath tumor patients with and without neurofibromatosis type 1." Neuro-Oncology **15**(2): 135-147.

Kourea, H. P., I. Orlow, B. W. Scheithauer, C. Cordon-Cardo and J. M. Woodruff (1999). "Deletions of the INK4A gene occur in malignant peripheral nerve sheath tumors but not in neurofibromas." Am J Pathol **155**(6): 1855-1860.

Kwon, J. G., S. J. Hwang, G. W. Hennig, Y. Bayguinov, C. McCann, H. Chen, F. Rossi, P. Besmer, K. M. Sanders and S. M. Ward (2009). "Changes in the structure and function of ICC networks in ICC hyperplasia and gastrointestinal stromal tumors." Gastroenterology **136**(2): 630-639.

LaFemina, J. (2013). "Oncologic outcomes of sporadic, neurofibromatosis-associated, and radiation-induced malignant peripheral nerve sheath tumors." Ann. Surg. Oncol. **20**: 66-72.

Lam, M. T., W. Li, M. G. Rosenfeld and C. K. Glass (2014). "Enhancer RNAs and regulated transcriptional programs." Trends Biochem Sci **39**(4): 170-182.

Lasota, J., C. L. Corless, M. C. Heinrich, M. Debiec-Rychter, R. Sciot, E. Wardelmann, S. Merkelbach-Bruse, H. U. Schildhaus, S. E. Steigen, J. Stachura, A. Wozniak, C. Antonescu, O. Daum, J. Martin, J. G. Del Muro and M. Miettinen (2008). "Clinicopathologic profile of gastrointestinal stromal tumors (GISTs) with primary KIT exon 13 or exon 17 mutations: a multicenter study on 54 cases." Mod Pathol **21**(4): 476-484.

Lasota, J., A. Dansonka-Mieszkowska, L. H. Sobin and M. Miettinen (2004). "A great majority of GISTs with PDGFRA mutations represent gastric tumors of low or no malignant potential." Laboratory Investigation **84**(7): 874-883.

Lasota, J., M. Jasinski, M. Sarlomo-Rikala and M. Miettinen (1999). "Mutations in exon 11 of c-kit occur preferentially in malignant versus benign gastrointestinal stromal tumors and do not occur in leiomyomas or leiomyosarcomas." American Journal of Pathology **154**(1): 53-60.

- Lasota, J., J. Kopczynski, M. Sarlomo-Rikala, R. Schneider-Stock, T. Stachura, R. Kordek, M. Michal and C. Boltze (2003). "KIT 1530ins6 mutation defines a subset of predominantly malignant gastrointestinal stromal tumors of intestinal origin." Human Pathology **34**(12): 1306-1312.
- Lawrence, W., M. F. Brennan, J. E. Niederhuber and S. A. Rosenberg (1998). "Retroperitoneal soft-tissue sarcoma - Analysis of 500 patients treated and followed at a single institution - Discussion." Annals of Surgery **228**(3): 363-365.
- Le, L. Q., C. C. Liu, T. Shipman, Z. G. Chen, U. Suter and L. F. Parada (2011). "Susceptible Stages in Schwann Cells for NF1-Associated Plexiform Neurofibroma Development." Cancer Research **71**(13): 4686-4695.
- Le, L. Q. and L. F. Parada (2007). "Tumor microenvironment and neurofibromatosis type I: connecting the GAPs." Oncogene **26**(32): 4609-4616.
- Le, L. Q., T. Shipman, D. K. Burns and L. F. Parada (2009). "Cell of origin and microenvironment contribution for NF1-associated dermal neurofibromas." Cell Stem Cell **4**(5): 453-463.
- Lee, W., S. Teckie, T. Wiesner, L. L. Ran, C. N. P. Granada, M. Y. Lin, S. N. Zhu, Z. Cao, Y. P. Liang, A. Sboner, W. D. Tap, J. A. Fletcher, K. H. Huberman, L. X. Qin, A. Viale, S. Singer, D. Y. Zheng, M. F. Berger, Y. Chen, C. R. Antonescu and P. Chi (2014). "PRC2 is recurrently inactivated through EED or SUZ12 loss in malignant peripheral nerve sheath tumors." Nature Genetics **46**(11): 1227-1232.
- Levy, A. D., H. E. Remotti, W. M. Thompson, L. H. Sobin and M. Miettinen (2003). "From the archives of the AFIP - Gastrointestinal stromal tumors: Radiologic features with pathologic correlation." Radiographics **23**(2): 283-304.
- Li, F. P., J. A. Fletcher, M. C. Heinrich, J. E. Garber, S. E. Sallan, C. Curiel-Lewandrowski, A. Duensing, M. van de Rijn, L. E. Schnipper and G. D. Demetri (2005). "Familial gastrointestinal stromal tumor syndrome: phenotypic and molecular features in a kindred." J Clin Oncol **23**(12): 2735-2743.
- Li, G., R. Margueron, M. C. Ku, P. Chambon, B. E. Bernstein and D. Reinberg (2010). "Jarid2 and PRC2, partners in regulating gene expression." Genes & Development **24**(4): 368-380.
- Li, H. and R. Durbin (2010). "Fast and accurate long-read alignment with Burrows-Wheeler transform." Bioinformatics **26**(5): 589-595.
- Li, W. D., Y. J. Cui, S. A. Kushner, R. A. M. Brown, J. D. Jentsch, P. W. Frankland, T. D. Cannon and A. J. Silva (2005). "The HMG-CoA reductase inhibitor lovastatin reverses the learning and attention deficits in a mouse model of neurofibromatosis type 1." Current Biology **15**(21): 1961-1967.
- Lim, K. H., M. J. Huang, L. T. Chen, T. E. Wang, C. L. Liu, C. S. Chang, M. C.

- Liu, R. K. Hsieh and C. Y. Tzen (2008). "Molecular analysis of secondary kinase mutations in imatinib-resistant gastrointestinal stromal tumors." Medical Oncology **25**(2): 207-213.
- Liu, X. H., C. G. Bai, Q. Xie, F. Feng, Z. Y. Xu and D. L. Ma (2005). "Prognostic value of KIT mutation in gastrointestinal stromal tumors." World Journal of Gastroenterology **11**(25): 3948-3952.
- Longley, B. J., L. Tyrrell, S. Z. Lu, Y. S. Ma, K. Langley, T. G. Ding, T. Duffy, P. Jacobs, L. H. Tang and I. Modlin (1996). "Somatic c-KIT activating mutation in urticaria pigmentosa and aggressive mastocytosis: Establishment of clonality in a human mast cell neoplasm." Nature Genetics **12**(3): 312-314.
- Lopes, L. F., R. B. West, L. M. Bacchi, M. van de Rijn and C. E. Bacchi (2010). "DOG1 for the Diagnosis of Gastrointestinal Stromal Tumor (GIST): Comparison Between 2 Different Antibodies." Applied Immunohistochemistry & Molecular Morphology **18**(4): 333-337.
- Lux, M. L., B. P. Rubin, T. L. Biase, C. J. Chen, T. Maclure, G. Demetri, S. Xiao, S. Singer, C. D. M. Fletcher and J. A. Fletcher (2000). "KIT extracellular and kinase domain mutations in gastrointestinal stromal tumors." American Journal of Pathology **156**(3): 791-795.
- Maeda, H., A. Yamagata, S. Nishikawa, K. Yoshinaga, S. Kobayashi, K. Nishi and S. Nishikawa (1992). "Requirement of C-Kit for Development of Intestinal Pacemaker System." Development **116**(2): 369-375.
- Mahadevan, D., L. Cooke, C. Riley, R. Swart, B. Simons, K. Della Croce, L. Wisner, M. Iorio, K. Shakalya, H. Garewal, R. Nagle and D. Bearss (2007). "A novel tyrosine kinase switch is a mechanism of imatinib resistance in gastrointestinal stromal tumors." Oncogene **26**(27): 3909-3919.
- Mantripragada, K. K., T. Diaz de Stahl, C. Patridge, U. Menzel, R. Andersson, N. Chuzhanova, L. Kluwe, A. Guha, V. Mautner, J. P. Dumanski and M. Upadhyaya (2009). "Genome-wide high-resolution analysis of DNA copy number alterations in NF1-associated malignant peripheral nerve sheath tumors using 32K BAC array." Genes Chromosomes Cancer **48**(10): 897-907.
- Mantripragada, K. K., G. Spurlock, L. Kluwe, N. Chuzhanova, R. E. Ferner, I. M. Frayling, J. P. Dumanski, A. Guha, V. Mautner and M. Upadhyaya (2008). "High-resolution DNA copy number profiling of malignant peripheral nerve sheath tumors using targeted microarray-based comparative genomic hybridization." Clin Cancer Res **14**(4): 1015-1024.
- Margueron, R., G. Li, K. Sarma, A. Blais, J. Zavadil, C. L. Woodcock, B. D. Dynlacht and D. Reinberg (2008). "Ezh1 and Ezh2 maintain repressive chromatin through different mechanisms." Molecular cell **32**(4): 503-518.
- Margueron, R. and D. Reinberg (2011). "The Polycomb complex PRC2 and its

mark in life." Nature **469**(7330): 343-349.

Martin, G. A., D. Viskochil, G. Bollag, P. C. McCabe, W. J. Crosier, H. Haubruck, L. Conroy, R. Clark, P. Oconnell, R. M. Cawthon, M. A. Innis and F. McCormick (1990). "The Gap-Related Domain of the Neurofibromatosis Type-1 Gene-Product Interacts with Ras P21." Cell **63**(4): 843-849.

Martin, J., A. Poveda, A. Llombart-Bosch, R. Ramos, J. A. Lopez-Guerrero, J. G. del Muro, J. Maurel, S. Calabuig, A. Gutierrez, J. L. G. de Sande, J. Martinez, A. De Juan, N. Lainez, F. Losa, V. Alija, P. Escudero, A. Casado, P. Garcia, R. Blanco and J. M. Buesa (2005). "Deletions affecting codons 557-558 of the c-KIT gene indicate a poor prognosis in patients with completely resected gastrointestinal stromal tumors: A study by the Spanish Group for Sarcoma Research (GEIS)." Journal of Clinical Oncology **23**(25): 6190-6198.

Martinho, O., A. Gouveia, P. Silva, A. Pimenta, R. M. Reis and J. M. Lopes (2009). "Loss of RKIP expression is associated with poor survival in GISTs." Virchows Archiv **455**(3): 277-284.

Mason, E. F. and J. L. Hornick (2013). "Succinate dehydrogenase deficiency is associated with decreased 5-hydroxymethylcytosine production in gastrointestinal stromal tumors: implications for mechanisms of tumorigenesis." Modern Pathology **26**(11): 1492-1497.

McGaughran, J. M., D. I. Harris, D. Donnai, D. Teare, R. MacLeod, R. Westerbeek, H. Kingston, M. Super, R. Harris and D. G. Evans (1999). "A clinical study of type 1 neurofibromatosis in north west England." J Med Genet **36**(3): 197-203.

McKenna, A., M. Hanna, E. Banks, A. Sivachenko, K. Cibulskis, A. Kernytzky, K. Garimella, D. Altshuler, S. Gabriel, M. Daly and M. A. DePristo (2010). "The Genome Analysis Toolkit: A MapReduce framework for analyzing next-generation DNA sequencing data." Genome Research **20**(9): 1297-1303.

Medeiros, F., C. L. Corless, A. Duensing, J. L. Hornick, A. M. Oliveira, M. C. Heinrich, J. A. Fletcher and C. D. M. Fletcher (2004). "KIT-negative gastrointestinal stromal tumors - Proof of concept and therapeutic implications." American Journal of Surgical Pathology **28**(7): 889-894.

Mehra, R., S. A. Tomlins, R. Shen, O. Nadeem, L. Wang, J. T. Wei, K. J. Pienta, D. Ghosh, M. A. Rubin, A. M. Chinnaiyan and R. B. Shah (2007). "Comprehensive assessment of TMPRSS2 and ETS family gene aberrations in clinically localized prostate cancer." Mod Pathol **20**(5): 538-544.

Meissner, A., T. S. Mikkelsen, H. Gu, M. Wernig, J. Hanna, A. Sivachenko, X. Zhang, B. E. Bernstein, C. Nusbaum, D. B. Jaffe, A. Gnirke, R. Jaenisch and E. S. Lander (2008). "Genome-scale DNA methylation maps of pluripotent and differentiated cells." Nature **454**(7205): 766-770.

Menon, A. G., K. M. Anderson, V. M. Riccardi, R. Y. Chung, J. M. Whaley, D. W. Yandell, G. E. Farmer, R. N. Freiman, J. K. Lee, F. P. Li and et al. (1990). "Chromosome 17p deletions and p53 gene mutations associated with the formation of malignant neurofibrosarcomas in von Recklinghausen neurofibromatosis." Proc Natl Acad Sci U S A **87**(14): 5435-5439.

Mertens, F., C. R. Antonescu, P. Hohenberger, M. Ladanyi, P. Modena, M. D'Incalci, P. G. Casali, M. Aglietta and T. Alvegard (2009). "Translocation-Related Sarcomas." Seminars in Oncology **36**(4): 312-323.

Miettinen, M. and J. Lasota (2001). "Gastrointestinal stromal tumors - definition, clinical, histological, immunohistochemical, and molecular genetic features and differential diagnosis." Virchows Archiv-an International Journal of Pathology **438**(1): 1-12.

Miettinen, M. and J. Lasota (2006). "Gastrointestinal stromal tumors: review on morphology, molecular pathology, prognosis, and differential diagnosis." Arch Pathol Lab Med **130**(10): 1466-1478.

Miettinen, M., M. Majidi and J. Lasota (2002). "Pathology and diagnostic criteria of gastrointestinal stromal tumors (GISTs): a review." European Journal of Cancer **38**: S39-S51.

Miettinen, M., M. Sarlomo-Rikala, L. H. Sobin and J. Lasota (2000). "Esophageal stromal tumors - A clinicopathologic, immunohistochemical, and molecular genetic study of 17 cases and comparison with esophageal leiomyomas and leiomyosarcomas." American Journal of Surgical Pathology **24**(2): 211-222.

Miettinen, M., M. Sarlomo-Rikala, L. H. Sobin and J. Lasota (2000). "Gastrointestinal stromal tumors and leiomyosarcomas in the colon - A clinicopathologic, immunohistochemical, and molecular genetic study of 44 cases." American Journal of Surgical Pathology **24**(10): 1339-1352.

Miettinen, M., L. H. Sobin and M. Sarlomo-Rikala (2000). "Immunohistochemical spectrum of GISTs at different sites and their differential diagnosis with a reference to CD117 (KIT)." Modern Pathology **13**(10): 1134-1142.

Miettinen, M., M. Virolainen and Maaritsarlorikala (1995). "Gastrointestinal Stromal Tumors - Value of Cd34 Antigen in Their Identification and Separation from True Leiomyomas and Schwannomas." American Journal of Surgical Pathology **19**(2): 207-216.

Mikkelsen, T. S., M. Ku, D. B. Jaffe, B. Issac, E. Lieberman, G. Giannoukos, P. Alvarez, W. Brockman, T. K. Kim, R. P. Koche, W. Lee, E. Mendenhall, A. O'Donovan, A. Presser, C. Russ, X. Xie, A. Meissner, M. Wernig, R. Jaenisch, C. Nusbaum, E. S. Lander and B. E. Bernstein (2007). "Genome-wide maps of chromatin state in pluripotent and lineage-committed cells." Nature **448**(7153): 553-560.

Miller, S. J., F. Rangwala, J. Williams, P. Ackerman, S. Kong, A. G. Jegga, S. Kaiser, B. J. Aronow, S. Frahm, L. Kluwe, V. Mautner, M. Upadhyaya, D. Muir, M. Wallace, J. Hagen, D. E. Quelle, M. A. Watson, A. Perry, D. H. Gutmann and N. Ratner (2006). "Large-scale molecular comparison Schwann cells to malignant peripheral nerve sheath tumor cell lines and tissues." Cancer Research **66**(5): 2584-2591.

Miranda, C., M. Nucifora, F. Molinari, E. Conca, M. C. Anania, A. Bordoni, P. Saletti, L. Mazzucchelli, S. Pilotti, M. A. Pierotti, E. Tamborini, A. Greco and M. Frattini (2012). "KRAS and BRAF Mutations Predict Primary Resistance to Imatinib in Gastrointestinal Stromal Tumors." Clinical Cancer Research **18**(6): 1769-1776.

Morin, R. D., N. A. Johnson, T. M. Severson, A. J. Mungall, J. An, R. Goya, J. E. Paul, M. Boyle, B. W. Woolcock, F. Kuchenbauer, D. Yap, R. K. Humphries, O. L. Griffith, S. Shah, H. Zhu, M. Kimbara, P. Shashkin, J. F. Charlot, M. Tcherpakov, R. Corbett, A. Tam, R. Varhol, D. Smailus, M. Moksa, Y. Zhao, A. Delaney, H. Qian, I. Birol, J. Schein, R. Moore, R. Holt, D. E. Horsman, J. M. Connors, S. Jones, S. Aparicio, M. Hirst, R. D. Gascoyne and M. A. Marra (2010). "Somatic mutations altering EZH2 (Tyr641) in follicular and diffuse large B-cell lymphomas of germinal-center origin." Nat Genet **42**(2): 181-185.

Mucciarini, C., G. Rossi, F. Bertolini, R. Valli, C. Cirilli, I. Rashid, L. Marcheselli, G. Luppi and M. Federico (2007). "Incidence and clinicopathologic features of gastrointestinal stromal tumors. A population-based study." Bmc Cancer **7**.

Nagata, H., A. S. Worobec, C. K. Oh, B. A. Chowdhury, S. Tannenbaum, Y. Suzuki and D. D. Metcalfe (1995). "Identification of a Point Mutation in the Catalytic Domain of the Protooncogene C-Kit in Peripheral-Blood Mononuclear-Cells of Patients Who Have Mastocytosis with an Associated Hematologic Disorder." Proceedings of the National Academy of Sciences of the United States of America **92**(23): 10560-10564.

Nakai, N., T. Ishikawa, A. Nishitani, N. N. Liu, M. Shincho, H. Hao, K. Isozaki, T. Kanda, T. Nishida, J. Fujimoto and S. Hirota (2008). "A mouse model of a human multiple GIST family with KIT-Asp820Tyr mutation generated by a knock-in strategy." Journal of Pathology **214**(3): 302-311.

Nakai, N., T. Okada, K. Oh, M. Shincho, T. Ito, I. Matsuda, J. Fujimoto and S. Hirota (2008). "A mouse model of human multiple GIST family with Kit-Asp-820tyr mutation generated by knock-in strategy." Gastroenterology **134**(4): A296-A296.

Namba, H., M. Nakashima, T. Hayashi, N. Hayashida, S. Maeda, T. I. Rogounovitch, A. Ohtsuru, V. A. Saenko, T. Kanematsu and S. Yamashita (2003). "Clinical implication of hot spot BRAF mutation, V599E, in papillary thyroid cancers." Journal of Clinical Endocrinology & Metabolism **88**(9): 4393-4397.

Nekrasov, M., T. Klymenko, S. Fraterman, B. Papp, K. Oktaba, T. Kocher, A. Cohen, H. G. Stunnenberg, M. Wilm and J. Muller (2007). "Pcl-PRC2 is needed to generate high levels of H3-K27 trimethylation at Polycomb target genes." Embo Journal **26**(18): 4078-4088.

Nielsen, G. P., A. O. Stemmer-Rachamimov, Y. Ino, M. B. Moller, A. E. Rosenberg and D. N. Louis (1999). "Malignant transformation of neurofibromas in neurofibromatosis 1 is associated with CDKN2A/p16 inactivation." Am J Pathol **155**(6): 1879-1884.

Nikoloski, G., S. M. Langemeijer, R. P. Kuiper, R. Knops, M. Massop, E. R. Tonnissen, A. van der Heijden, T. N. Scheele, P. Vandenberghe, T. de Witte, B. A. van der Reijden and J. H. Jansen (2010). "Somatic mutations of the histone methyltransferase gene EZH2 in myelodysplastic syndromes." Nat Genet **42**(8): 665-667.

Nilsson, B., P. Bummig, J. M. Meis-Kindblom, A. Oden, A. Dortok, B. Gustavsson, K. Sablinska and L. G. Kindblom (2005). "Gastrointestinal stromal tumors: The incidence, prevalence, clinical course, and prognostication in the pre-matinib mesylate era - A population-based study in western Sweden." Cancer **103**(4): 821-829.

Nishida, T., S. Hirota, M. Taniguchi, K. Hashimoto, K. Isozaki, H. Nakamura, Y. Kanakura, T. Tanaka, A. Takabayashi, H. Matsuda and Y. Kitamura (1998). "Familial gastrointestinal stromal tumours with germline mutation of the KIT gene." Nat Genet **19**(4): 323-324.

Nishida, T., S. Hirota, M. Taniguchi, K. Hashimoto, K. Isozaki, H. Nakamura, Y. Kanakura, T. Tanaka, A. Takabayashi, H. Matsuda and Y. Kitamura (1998). "Familial gastrointestinal stromal tumours with germline mutation of the KIT gene." Nature Genetics **19**(4): 323-324.

Nobori, T., K. Miura, D. J. Wu, A. Lois, K. Takabayashi and D. A. Carson (1994). "Deletions of the Cyclin-Dependent Kinase-4 Inhibitor Gene in Multiple Human Cancers." Nature **368**(6473): 753-756.

Ntziachristos, P., A. Tsigos, P. Van Vlierberghe, J. Nedjic, T. Trimarchi, M. S. Flaherty, D. Ferres-Marco, V. da Ros, Z. Tang, J. Siegle, P. Asp, M. Hadler, I. Rigo, K. De Keersmaecker, J. Patel, T. Huynh, F. Utro, S. Poglio, J. B. Samon, E. Paietta, J. Racevskis, J. M. Rowe, R. Rabadan, R. L. Levine, S. Brown, F. Pflumio, M. Dominguez, A. Ferrando and I. Aifantis (2012). "Genetic inactivation of the polycomb repressive complex 2 in T cell acute lymphoblastic leukemia." Nat Med **18**(2): 298-301.

O'Riain, C., C. L. Corless, M. C. Heinrich, D. Keegan, M. Vioreanu, D. Maguire and K. Sheahan (2005). "Gastrointestinal stromal tumors: insights from a new familial GIST kindred with unusual genetic and pathologic features." Am J Surg Pathol **29**(12): 1680-1683.

- Ortiz-Hidalgo, C., B. D. Bojorge and J. Albores-Saavedra (2000). "Stromal tumor of the gallbladder with phenotype of interstitial cells of Cajal - A previously unrecognized neoplasm." American Journal of Surgical Pathology **24**(10): 1420-1423.
- Patel, T. D., I. Kramer, J. Kucera, V. Niederkofler, T. M. Jessell, S. Arber and W. D. Snider (2003). "Peripheral NT3 signaling is required for ETS protein expression and central patterning of proprioceptive sensory afferents." Neuron **38**(3): 403-416.
- Perez, E. A., A. S. Livingstone, D. Franceschi, C. Rocha-Lima, D. J. Lee, N. Hodgson, M. Jorda and L. G. Koniaris (2006). "Current incidence and outcomes of gastrointestinal mesenchymal tumors including gastrointestinal stromal tumors." J Am Coll Surg **202**(4): 623-629.
- Perrone, F., S. Tabano, F. Colombo, G. Dagrada, S. Birindelli, A. Gronchi, M. Colecchia, M. A. Pierotti and S. Pilotti (2003). "p15INK4b, p14ARF, and p16INK4a inactivation in sporadic and neurofibromatosis type 1-related malignant peripheral nerve sheath tumors." Clin Cancer Res **9**(11): 4132-4138.
- Pidhorecky, I., R. T. Cheney, W. G. Kraybill and J. F. Gibbs (2000). "Gastrointestinal stromal tumors: Current diagnosis, biologic behavior, and management." Annals of Surgical Oncology **7**(9): 705-712.
- Prakash, S., L. Sarran, N. Socci, R. P. DeMatteo, J. Eisenstat, A. M. Greco, R. G. Maki, L. H. Wexler, M. P. LaQuaglia, P. Besmer and C. R. Antonescu (2005). "Gastrointestinal stromal tumors in children and young adults - A clinicopathologic, molecular, and genomic study of 15 cases and review of the literature." Journal of Pediatric Hematology Oncology **27**(4): 179-187.
- Quelle, D. E., F. Zindy, R. A. Ashmun and C. J. Sherr (1995). "Alternative reading frames of the INK4a tumor suppressor gene encode two unrelated proteins capable of inducing cell cycle arrest." Cell **83**(6): 993-1000.
- Radner, H., I. Blumcke, G. Reifenberger and O. D. Wiestler (2002). "The new WHO classification of tumors of the nervous system 2000. Pathology and genetics." Pathologie **23**(4): 260-283.
- Rahim, S., T. Minas, S. H. Hong, S. Justvig, H. Celik, Y. S. Kont, J. Han, A. T. Kallarakal, Y. L. Kong, M. A. Rudek, M. L. Brown, B. Kallakury, J. A. Toretsky and A. Uren (2014). "A Small Molecule Inhibitor of ETV1, YK-4-279, Prevents Prostate Cancer Growth and Metastasis in a Mouse Xenograft Model." Plos One **9**(12).
- Rajagopalan, H., A. Bardelli, C. Lengauer, K. W. Kinzler, B. Vogelstein and V. E. Velculescu (2002). "Tumorigenesis - RAF/RAS oncogenes and mismatch-repair status." Nature **418**(6901): 934-934.
- Ran, L. L., I. Sirota, Z. Cao, D. Murphy, Y. D. Chen, S. Shukla, Y. Y. Xie, M. C.

Kaufmann, D. Gao, S. N. Zhu, F. Rossi, J. Wongvipat, T. Taguchi, W. D. Tap, I. K. Mellinshoff, P. Besmer, C. R. Antonescu, Y. Chen and P. Chi (2015). "Combined Inhibition of MAP Kinase and KIT Signaling Synergistically Destabilizes ETV1 and Suppresses GIST Tumor Growth." Cancer Discovery **5**(3): 304-315.

Reith, J. D., J. R. Goldblum, R. H. Lyles and S. W. Weiss (2000). "Extragastrointestinal (Soft tissue) stromal tumors: An analysis of 48 cases with emphasis on histologic predictors of outcome." Modern Pathology **13**(5): 577-585.

Rodriguez, F. J. (2012). "Peripheral nerve sheath tumors: the elegant chapter in surgical neuropathology." Acta Neuropathol. **123**: 293-294.

Roskoski, R. (2005). "Signaling by Kit protein-tyrosine kinase - The stem cell factor receptor." Biochemical and Biophysical Research Communications **337**(1): 1-13.

Rossi, F., I. Ehlers, V. Agosti, N. D. Socci, A. Viale, G. Sommer, Y. Yozgat, K. Manova, C. R. Antonescu and P. Besmer (2006). "Oncogenic Kit signaling and therapeutic intervention in a mouse model of gastrointestinal stromal tumor." Proc Natl Acad Sci U S A **103**(34): 12843-12848.

Rubin, B. P., C. R. Antonescu, J. P. Scott-Browne, M. L. Comstock, Y. S. Gu, M. R. Tanas, C. B. Ware and J. Woodell (2005). "A knock-in mouse model of gastrointestinal stromal tumor harboring Kit K641E." Cancer Research **65**(15): 6631-6639.

Sabah, M., R. Cummins, M. Leader and E. Kay (2006). "Altered expression of cell cycle regulatory proteins in gastrointestinal stromal tumors: markers with potential prognostic implications." Human Pathology **37**(6): 648-655.

Sakurai, S., T. Hasegawa, Y. Sakuma, Y. Takazawa, A. Motegi, T. Nakajima, K. Saito, M. Fukayama and T. Shimoda (2004). "Myxoid epithelioid gastrointestinal stromal tumor (GIST) with mast cell infiltrations: A subtype of GIST with mutations of platelet-derived growth factor receptor alpha gene." Human Pathology **35**(10): 1223-1230.

Sakurama, K., K. Noma, M. Takaoka, Y. Tomono, N. Watanabe, S. Hatakeyama, O. Ohmori, S. Hirota, T. Motoki, Y. Shirakawa, T. Yamatsuji, M. Haisa, J. Matsuoka, N. Tanaka and Y. Naomoto (2009). "Inhibition of focal adhesion kinase as a potential therapeutic strategy for imatinib-resistant gastrointestinal stromal tumor." Molecular Cancer Therapeutics **8**(1): 127-134.

Saunders, C. T., W. S. W. Wong, S. Swamy, J. Becq, L. J. Murray and R. K. Cheetham (2012). "Strelka: accurate somatic small-variant calling from sequenced tumor-normal sample pairs." Bioinformatics **28**(14): 1811-1817.

Sedy, J., S. Tseng, J. M. Walro, M. Grim and J. Kucera (2006). "ETS transcription factor ER81 is required for the Pacinian corpuscle development." Developmental Dynamics **235**(4): 1081-1089.

- Seger, R. and E. G. Krebs (1995). "Protein Kinases .7. The Mapk Signaling Cascade." Faseb Journal **9**(9): 726-735.
- Serrano, J., S. U. Goebel, P. L. Peghini, I. A. Lubensky, F. Gibril and R. T. Jensen (2000). "Alterations in the p16INK4a/CDKN2A tumor suppressor gene in gastrinomas." J Clin Endocrinol Metab **85**(11): 4146-4156.
- Shen, X., Y. Liu, Y. J. Hsu, Y. Fujiwara, J. Kim, X. Mao, G. C. Yuan and S. H. Orkin (2008). "EZH1 mediates methylation on histone H3 lysine 27 and complements EZH2 in maintaining stem cell identity and executing pluripotency." Molecular cell **32**(4): 491-502.
- Sherr, C. J. and J. M. Roberts (1999). "CDK inhibitors: positive and negative regulators of G1-phase progression." Genes Dev **13**(12): 1501-1512.
- Simon, J. A. and C. A. Lange (2008). "Roles of the EZH2 histone methyltransferase in cancer epigenetics." Mutat Res **647**(1-2): 21-29.
- Singer, S. (2001). "The effect of surgery and grade on outcome of gastrointestinal stromal tumors - Discussion." Archives of Surgery **136**(4): 389-389.
- Singer, S., B. P. Rubin, M. L. Lux, C. J. Chen, G. D. Demetri, C. D. M. Fletcher and J. A. Fletcher (2002). "Prognostic value of KIT mutation type, mitotic activity, and histologic subtype in gastrointestinal stromal tumors." Journal of Clinical Oncology **20**(18): 3898-3905.
- Sommer, G., V. Agosti, I. Ehlers, F. Rossi, S. Corbacioglu, J. Farkas, M. Moore, K. Manova, C. R. Antonescu and P. Besmer (2003). "Gastrointestinal stromal tumors in a mouse model by targeted mutation of the Kit receptor tyrosine kinase." Proc Natl Acad Sci U S A **100**(11): 6706-6711.
- Sommer, G., V. Agosti, I. Ehlers, F. Rossi, S. Corbacioglu, J. Farkas, M. Moore, K. Manova, C. R. Antonescu and P. Besmer (2003). "Gastrointestinal stromal tumors in a mouse model by targeted mutation of the Kit receptor tyrosine kinase." Proceedings of the National Academy of Sciences of the United States of America **100**(11): 6706-6711.
- Sowa, M. E., E. J. Bennett, S. P. Gygi and J. W. Harper (2009). "Defining the Human Deubiquitinating Enzyme Interaction Landscape." Cell **138**(2): 389-403.
- Stucky, C. C. H., K. N. Johnson, R. J. Gray, B. A. Pockaj, I. T. Ocal, P. S. Rose and N. Wasif (2012). "Malignant Peripheral Nerve Sheath Tumors (MPNST): The Mayo Clinic Experience." Annals of Surgical Oncology **19**(3): 878-885.
- Subramanian, A., P. Tamayo, V. K. Mootha, S. Mukherjee, B. L. Ebert, M. A. Gillette, A. Paulovich, S. L. Pomeroy, T. R. Golub, E. S. Lander and J. P. Mesirov (2005). "Gene set enrichment analysis: a knowledge-based approach for interpreting genome-wide expression profiles." Proc Natl Acad Sci U S A **102**(43): 15545-15550.

Subramanian, A., P. Tamayo, V. K. Mootha, S. Mukherjee, B. L. Ebert, M. A. Gillette, A. Paulovich, S. L. Pomeroy, T. R. Golub, E. S. Lander and J. P. Mesirov (2005). "Gene set enrichment analysis: A knowledge-based approach for interpreting genome-wide expression profiles." Proceedings of the National Academy of Sciences of the United States of America **102**(43): 15545-15550.

Subramanian, S., R. B. West, C. L. Corless, W. B. Ou, B. P. Rubin, K. M. Chu, S. Y. Leung, S. T. Yuen, S. Zhu, T. Hernandez-Boussard, K. Montgomery, T. O. Nielsen, R. M. Patel, J. R. Goldblum, M. C. Heinrich, J. A. Fletcher and M. van de Rijn (2004). "Gastrointestinal stromal tumors (GISTs) with KIT and PDGFRA mutations have distinct gene expression profiles." Oncogene **23**(47): 7780-7790.

Taguchi, T., H. Sonobe, S. Toyonaga, I. Yamasaki, T. Shuin, A. Takano, K. Araki, K. Akimaru and K. Yuri (2002). "Conventional and molecular cytogenetic characterization of a new human cell line, GIST-T1, established from gastrointestinal stromal tumor." Laboratory Investigation **82**(5): 663-665.

Tan, B. L., M. N. Yazicioglu, D. Ingram, J. McCarthy, J. Borneo, D. A. Williams and R. Kapur (2003). "Genetic evidence for convergence of c-Kit- and alpha4 integrin-mediated signals on class IA PI-3kinase and the Rac pathway in regulating integrin-directed migration in mast cells." Blood **101**(12): 4725-4732.

Taniguchi, M., T. Nishida, S. Hirota, K. Isozaki, T. Ito, T. Nomura, H. Matsuda and Y. Kitamura (1999). "Effect of c-kit mutation on prognosis of gastrointestinal stromal tumors." Cancer Research **59**(17): 4297-4300.

Tarn, C., L. Rink, E. Merkel, D. Flieder, H. Pathak, D. Koumbi, J. R. Testa, B. Eisenberg, M. von Mehren and A. K. Godwin (2008). "Insulin-like growth factor 1 receptor is a potential therapeutic target for gastrointestinal stromal tumors." Proceedings of the National Academy of Sciences of the United States of America **105**(24): 8387-8392.

Taylor, B. S. (2011). "Advances in sarcoma genomics and new therapeutic targets." Nat. Rev. Cancer **11**: 541-557.

Theos, A. and B. R. Korf (2006). "Pathophysiology of neurofibromatosis type 1." Annals of Internal Medicine **144**(11): 842-849.

Thway, K. and C. Fisher (2014). "Malignant peripheral nerve sheath tumor: pathology and genetics." Annals of Diagnostic Pathology **18**(2): 109-116.

Tian, Q. S., H. F. Frierson, G. W. Krystal and C. A. Moskaluk (1999). "Activating c-kit gene mutations in human germ cell tumors." American Journal of Pathology **154**(6): 1643-1647.

Tiffen, J., S. J. Gallagher and P. Hersey (2015). "EZH2: an emerging role in melanoma biology and strategies for targeted therapy." Pigment Cell & Melanoma Research **28**(1).

Timokhina, I., H. Kissel, G. Stella and P. Besmer (1998). "Kit signaling through PI 3-kinase and Src kinase pathways: an essential role for Rac1 and JNK activation in mast cell proliferation." Embo Journal **17**(21): 6250-6262.

Tomlins, S. A., B. Laxman, S. M. Dhanasekaran, B. E. Helgeson, X. H. Cao, D. S. Morris, A. Menon, X. J. Jing, Q. Cao, B. Han, J. D. Yu, L. Wang, J. E. Montie, M. A. Rubin, K. J. Pienta, D. Roulston, R. B. Shah, S. Varambally, R. Mehra and A. M. Chinnaiyan (2007). "Distinct classes of chromosomal rearrangements create oncogenic ETS gene fusions in prostate cancer." Nature **448**(7153): 595-U599.

Tomlins, S. A., D. R. Rhodes, S. Perner, S. M. Dhanasekaran, R. Mehra, X. W. Sun, S. Varambally, X. Cao, J. Tchinda, R. Kuefer, C. Lee, J. E. Montie, R. B. Shah, K. J. Pienta, M. A. Rubin and A. M. Chinnaiyan (2005). "Recurrent fusion of TMPRSS2 and ETS transcription factor genes in prostate cancer." Science **310**(5748): 644-648.

Tong, J. Y., F. Hannan, Y. H. Zhu, A. Bernardis and Y. Zhong (2002). "Neurofibromin regulates G protein-stimulated adenylyl cyclase activity." Nature Neuroscience **5**(2): 95-96.

Tos, A. P. D., M. C. Montesco, I. Hostein, L. Toffolatti, F. Chibon, D. Pissaloux, L. Alberti, E. Lazzari, D. Ranchere-Vince, C. R. Rossi, I. Ray-Coquard, J. Y. Blay and J. M. Coindre (2010). "Reproducibility of Molecular Analysis in Soft Tissue Sarcomas and GIST: A Report from CONTICANET Network of Excellence." Modern Pathology **23**: 18a-19a.

Tran, T., J. A. Davila and H. B. El-Serag (2005). "The epidemiology of malignant gastrointestinal stromal tumors: An analysis of 1,458 cases from 1992 to 2000." American Journal of Gastroenterology **100**(1): 162-168.

Tworek, J. A., H. D. Appelman, T. P. Singleton and J. K. Greenson (1997). "Stromal tumors of the jejunum and ileum." Modern Pathology **10**(3): 200-209.

Tworek, J. A., J. R. Goldblum, S. W. Weiss, J. K. Greenson and H. D. Appelman (1999). "Stromal tumors of the abdominal colon - A clinicopathologic study of 20 cases." American Journal of Surgical Pathology **23**(8): 937-945.

Tworek, J. A., J. R. Goldblum, S. W. Weiss, J. K. Greenson and H. D. Appelman (1999). "Stromal tumors of the anorectum - A clinicopathologic study of 22 cases." American Journal of Surgical Pathology **23**(8): 946-954.

Tzen, C. Y. and B. L. Mau (2005). "Analysis of CD117-negative gastrointestinal stromal tumors." World Journal of Gastroenterology **11**(7): 1052-1055.

Upadhyaya, M., S. Han, C. Consoli, E. Majounie, M. Horan, N. S. Thomas, C. Potts, S. Griffiths, M. Ruggieri, A. von Deimling and D. N. Cooper (2004). "Characterization of the somatic mutational spectrum of the neurofibromatosis type 1 (NF1) gene in neurofibromatosis patients with benign and malignant

tumors." Hum Mutat **23**(2): 134-146.

Van Glabbeke, M. and MetaGIST (2010). "Comparison of Two Doses of Imatinib for the Treatment of Unresectable or Metastatic Gastrointestinal Stromal Tumors: A Meta-Analysis of 1,640 Patients." Journal of Clinical Oncology **28**(7): 1247-1253.

Varambally, S. (2002). "The polycomb group protein EZH2 is involved in progression of prostate cancer." Nature **419**: 624-629.

Varambally, S., S. M. Dhanasekaran, M. Zhou, T. R. Barrette, C. Kumar-Sinha, M. G. Sanda, D. Ghosh, K. J. Pienta, R. G. Sewalt, A. P. Otte, M. A. Rubin and A. M. Chinnaiyan (2002). "The polycomb group protein EZH2 is involved in progression of prostate cancer." Nature **419**(6907): 624-629.

Varambally, S., S. M. Dhanasekaran, M. Zhou, T. R. Barrette, C. Kumar-Sinha, M. G. Sanda, D. Ghosh, K. J. Pienta, R. G. A. B. Sewalt, A. P. Otte, M. A. Rubin and A. M. Chinnaiyan (2002). "The polycomb group protein EZH2 is involved in progression of prostate cancer." Nature **419**(6907): 624-629.

Vauthey, J. N., J. M. Woodruff and M. F. Brennan (1995). "Extremity malignant peripheral nerve sheath tumors (neurogenic sarcomas): a 10-year experience." Ann Surg Oncol **2**(2): 126-131.

Ventura, A., D. G. Kirsch, M. E. McLaughlin, D. A. Tuveson, J. Grimm, L. Lintault, J. Newman, E. E. Reczek, R. Weissleder and T. Jacks (2007). "Restoration of p53 function leads to tumour regression in vivo." Nature **445**(7128): 661-665.

Verweij, J., P. G. Casali, J. Zalcberg, A. LeCesne, P. Reichardt, J. Y. Blay, R. Issels, A. van Oosterom, P. C. Hogendoorn, M. Van Glabbeke, R. Bertulli and I. Judson (2004). "Progression-free survival in gastrointestinal stromal tumours with high-dose imatinib: randomised trial." Lancet **364**(9440): 1127-1134.

Verweij, J., P. G. Casali, J. Zalcberg, A. LeCesne, P. Reichardt, J. Y. Blay, R. Issels, A. van Oosterom, P. C. W. Hogendoorn, M. Van Glabbeke, R. Bertulli, I. Judson, E. S. T. B. S. Grp, I. S. Grp and A. G. Tria (2004). "Progression-free survival in gastrointestinal stromal tumours with high-dose imatinib: randomised trial." Lancet **364**(9440): 1127-1134.

Vitari, A. C., K. G. Leong, K. Newton, C. Yee, K. O'Rourke, J. F. Liu, L. L. Phu, R. Vij, R. Ferrando, S. S. Couto, S. Mohan, A. Pandita, J. A. Hongo, D. Arnott, I. E. Wertz, W. Q. Gao, D. M. French and V. M. Dixit (2011). "COP1 is a tumour suppressor that causes degradation of ETS transcription factors." Nature **474**(7351): 403-+.

Walker, E., W. Y. Chang, J. Hunkapiller, G. Cagney, K. Garcha, J. Torchia, N. J. Krogan, J. F. Reiter and W. L. Stanford (2010). "Polycomb-like 2 Associates with PRC2 and Regulates Transcriptional Networks during Mouse Embryonic

Stem Cell Self-Renewal and Differentiation." Cell Stem Cell **6**(2): 153-166.

Walker, L., D. Thompson, I. M. Frayling and D. Baralle (2005). "Malignancy in neurofibromatosis type 1." Journal of Medical Genetics **42**: S48-S48.

Wardelmann, E., A. Hrychyk, S. Merkelbach-Bruse, K. Pauls, J. Goldstein, P. Hohenberger, I. Losen, C. Manegold, R. Buttner and T. Pietsch (2004). "Association of platelet-derived growth factor receptor alpha mutations with gastric primary site and epithelioid or mixed cell morphology in gastrointestinal stromal tumors." Journal of Molecular Diagnostics **6**(3): 197-204.

Wardelmann, E., I. Losen, V. Hans, I. Neidt, N. Speidel, E. Bierhoff, T. Heinicke, T. Pietsch, R. Buttner and S. Merkelbach-Bruse (2003). "Deletion of Trp-557 and Lys-558 in the juxtamembrane domain of the c-kit protooncogene is associated with metastatic behavior of gastrointestinal stromal tumors." International Journal of Cancer **106**(6): 887-895.

Wasag, B., M. Debiec-Rychter, P. Pauwels, M. Stul, H. Vranckx, A. Van Oosterom, A. Hagemeijer and R. Sciot (2004). "Differential expression of KIT/PDGFR-A mutant isoforms in epithelioid and mixed variants of gastrointestinal stromal tumors depends predominantly on the tumor site." Modern Pathology **17**(8): 889-894.

Watson, M. A., A. Perry, T. Tihan, R. A. Prayson, A. Guha, J. Bridge, R. Ferner and D. H. Gutmann (2004). "Gene expression profiling reveals unique molecular subtypes of Neurofibromatosis Type I-associated and sporadic malignant peripheral nerve sheath tumors." Brain Pathol **14**(3): 297-303.

Wei, G. H., G. Badis, M. F. Berger, T. Kivioja, K. Palin, M. Enge, M. Bonke, A. Jolma, M. Varjosalo, A. R. Gehrke, J. Yan, S. Talukder, M. Turunen, M. Taipale, H. G. Stunnenberg, E. Ukkonen, T. R. Hughes, M. L. Bulyk and J. Taipale (2010). "Genome-wide analysis of ETS-family DNA-binding in vitro and in vivo." EMBO J **29**(13): 2147-2160.

West, R. B., C. L. Corless, X. Chen, B. P. Rubin, S. Subramanian, K. Montgomery, S. Zhu, C. A. Ball, T. O. Nielsen, R. Patel, J. R. Goldblum, P. O. Brown, M. C. Heinrich and M. Van de Rijn (2004). "The novel marker, DOG1, is expressed ubiquitously in gastrointestinal stromal tumors irrespective of KIT or PDGFRA mutation status." American Journal of Pathology **165**(1): 107-113.

Willmore-Payne, C., J. A. Holden, S. Tripp and L. J. Layfield (2005). "Human malignant melanoma: detection of BRAF- and c-kit-activating mutations by high-resolution amplicon melting analysis." Human Pathology **36**(5): 486-493.

Won, H. H., S. N. Scott, A. R. Brannon, R. H. Shah and M. F. Berger (2013). "Detecting Somatic Genetic Alterations in Tumor Specimens by Exon Capture and Massively Parallel Sequencing." Jove-Journal of Visualized Experiments(80).

- Won, H. H., S. N. Scott, A. R. Brannon, R. H. Shah and M. F. Berger (2013). "Detecting somatic genetic alterations in tumor specimens by exon capture and massively parallel sequencing." J Vis Exp(80): e50710.
- Wu, J., J. P. Williams, T. A. Rizvi, J. J. Kordich, D. Witte, D. Meijer, A. O. Stemmer-Rachamimov, J. A. Cancelas and N. Ratner (2008). "Plexiform and dermal neurofibromas and pigmentation are caused by Nf1 loss in desert hedgehog-expressing cells." Cancer Cell **13**(2): 105-116.
- Xie, H., J. Xu, J. H. Hsu, M. Nguyen, Y. Fujiwara, C. Peng and S. H. Orkin (2014). "Polycomb repressive complex 2 regulates normal hematopoietic stem cell function in a developmental-stage-specific manner." Cell Stem Cell **14**(1): 68-80.
- Xu, G. F., B. Lin, K. Tanaka, D. Dunn, D. Wood, R. Gesteland, R. White, R. Weiss and F. Tamanoi (1990). "The Catalytic Domain of the Neurofibromatosis Type-1 Gene-Product Stimulates Ras Gtpase and Complements Ira Mutants of *Saccharomyces-Cerevisiae*." Cell **63**(4): 835-841.
- Xu, G. F., P. Oconnell, D. Viskochil, R. Cawthon, M. Robertson, M. Culver, D. Dunn, J. Stevens, R. Gesteland, R. White and R. Weiss (1990). "The Neurofibromatosis Type-1 Gene Encodes a Protein Related to Gap." Cell **62**(3): 599-608.
- Yang, F. C., S. Chen, T. Clegg, X. Li, T. Morgan, S. A. Estwick, J. Yuan, W. Khalaf, S. Burgin, J. Travers, L. F. Parada, D. A. Ingram and D. W. Clapp (2006). "Nf1+/- mast cells induce neurofibroma like phenotypes through secreted TGF-beta signaling." Hum Mol Genet **15**(16): 2421-2437.
- Yang, F. C., D. A. Ingram, S. Chen, Y. Zhu, J. Yuan, X. Li, X. Yang, S. Knowles, W. Horn, Y. Li, S. Zhang, Y. Yang, S. T. Vakili, M. Yu, D. Burns, K. Robertson, G. Hutchins, L. F. Parada and D. W. Clapp (2008). "Nf1-dependent tumors require a microenvironment containing Nf1+/- and c-kit-dependent bone marrow." Cell **135**(3): 437-448.
- Yang, J. L., A. Ylipaa, Y. Sun, H. Zheng, K. X. Chen, M. Nykter, J. Trent, N. Ratner, D. C. Lev and W. Zhang (2011). "Genomic and Molecular Characterization of Malignant Peripheral Nerve Sheath Tumor Identifies the IGF1R Pathway as a Primary Target for Treatment." Clinical Cancer Research **17**(24): 7563-7573.
- Yarden, Y., W. J. Kuang, T. Yangfeng, L. Coussens, S. Munemitsu, T. J. Dull, E. Chen, J. Schlessinger, U. Francke and A. Ullrich (1987). "Human Protooncogene C-Kit - a New Cell-Surface Receptor Tyrosine Kinase for an Unidentified Ligand." Embo Journal **6**(11): 3341-3351.
- Zhang, J., L. Ding, L. Holmfeldt, G. Wu, S. L. Heatley, D. Payne-Turner, J. Easton, X. Chen, J. Wang, M. Rusch, C. Lu, S. C. Chen, L. Wei, J. R. Collins-Underwood, J. Ma, K. G. Roberts, S. B. Pounds, A. Ulyanov, J. Becksfort,

P. Gupta, R. Huether, R. W. Kriwacki, M. Parker, D. J. McGoldrick, D. Zhao, D. Alford, S. Espy, K. C. Bobba, G. Song, D. Pei, C. Cheng, S. Roberts, M. I. Barbato, D. Campana, E. Coustan-Smith, S. A. Shurtleff, S. C. Raimondi, M. Kleppe, J. Cools, K. A. Shimano, M. L. Hermiston, S. Doulatov, K. Eppert, E. Laurenti, F. Notta, J. E. Dick, G. Basso, S. P. Hunger, M. L. Loh, M. Devidas, B. Wood, S. Winter, K. P. Dunsmore, R. S. Fulton, L. L. Fulton, X. Hong, C. C. Harris, D. J. Dooling, K. Ochoa, K. J. Johnson, J. C. Obenauer, W. E. Evans, C. H. Pui, C. W. Naeve, T. J. Ley, E. R. Mardis, R. K. Wilson, J. R. Downing and C. G. Mullighan (2012). "The genetic basis of early T-cell precursor acute lymphoblastic leukaemia." Nature **481**(7380): 157-163.

Zhang, M., Y. X. Wang, S. Jones, M. Sausen, K. McMahon, R. Sharma, Q. Wang, A. J. Belzberg, K. Chaichana, G. L. Gallia, Z. L. Gokaslan, G. J. Riggins, J. P. Wolinsky, L. D. Wood, E. A. Montgomery, R. H. Hruban, K. W. Kinzler, N. Papadopoulos, B. Vogelstein and C. Bettegowda (2014). "Somatic mutations of SUZ12 in malignant peripheral nerve sheath tumors." Nature Genetics **46**(11): 1170-1172.

Zhen, D. B., K. G. Rabe, S. Gallinger, S. Syngal, A. G. Schwartz, M. G. Goggins, R. H. Hruban, M. L. Cote, R. R. McWilliams, N. J. Roberts, L. A. Cannon-Albright, D. H. Li, K. Moyes, R. J. Wenstrup, A. R. Hartman, D. Seminara, A. P. Klein and G. M. Petersen (2015). "BRCA1, BRCA2, PALB2, and CDKN2A mutations in familial pancreatic cancer: a PACGENE study." Genetics in Medicine **17**(7): 569-577.

Zheng, H., L. Chang, N. Patel, J. Yang, L. Lowe, D. K. Burns and Y. Zhu (2008). "Induction of abnormal proliferation by nonmyelinating schwann cells triggers neurofibroma formation." Cancer Cell **13**(2): 117-128.

Zhu, G., G. W. Montgomery, M. R. James, J. M. Trent, N. K. Hayward, N. G. Martin and D. L. Duffy (2007). "A genome-wide scan for naevus count: linkage to CDKN2A and to other chromosome regions." Eur J Hum Genet **15**(1): 94-102.

Zhu, Y., P. Ghosh, P. Charnay, D. K. Burns and L. F. Parada (2002). "Neurofibromas in NF1: Schwann cell origin and role of tumor environment." Science **296**(5569): 920-922.

Zou, C. Y., K. D. Smith, J. Liu, G. Lahat, S. Myers, W. L. Wang, W. Zhang, I. E. McCutcheon, J. M. Slopis, A. J. Lazar, R. E. Pollock and D. Lev (2009). "Clinical, Pathological, and Molecular Variables Predictive of Malignant Peripheral Nerve Sheath Tumor Outcome." Annals of Surgery **249**(6): 1014-1022.

Zucman, J., T. Melot, C. Desmaze, J. Ghysdael, B. Plougastel, M. Peter, J. M. Zucker, T. J. Triche, D. Sheer, C. Turc-Carel and et al. (1993). "Combinatorial generation of variable fusion proteins in the Ewing family of tumours." EMBO J **12**(12): 4481-4487.